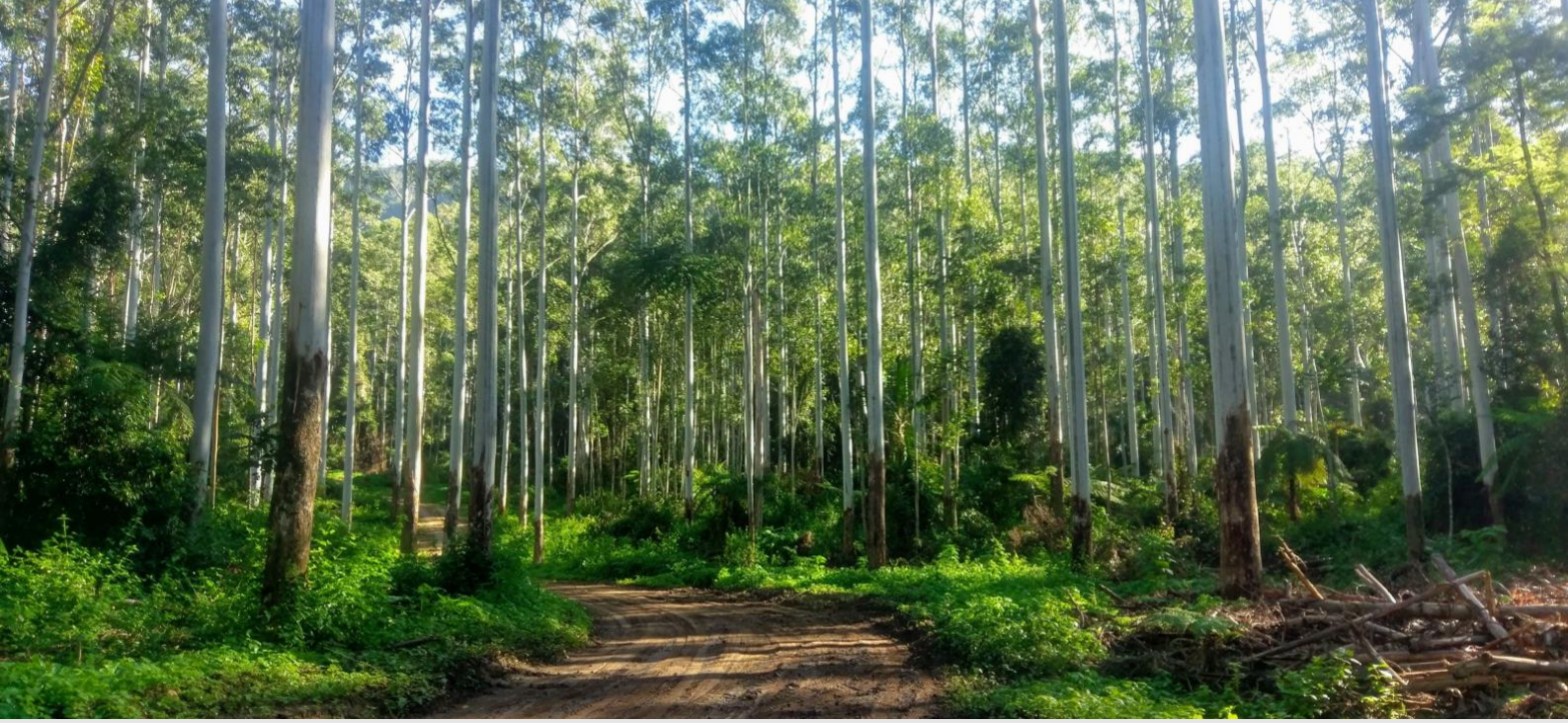

Remote sensing of NSW private native forests

Application of potential indicators

August 2024

Mullion group

FLINTpro

Disclaimer:

This report presents information based on the authors' best understanding of current technologies and approaches. To the extent permitted by law, the Mullion Group excludes all liability to any person for any consequences, including but not limited to all losses, damages, costs, expenses, and any other compensation, arising directly or indirectly from using this publication (in part or in whole) and any information or material contained in it.

Contact: info@flintpro.com

Hislop, S. & Stone, C. (2024) Remote sensing of NSW private native forests – application of potential indicators

Table of Contents

Executive Summary

The NSW Natural Resources Commission (NRC) engaged The Mullion Group to deliver a remote sensing feasibility study in relation to the Private Native Forestry Monitoring, Evaluation and Reporting framework (PNF MER), as specified in the PNF Codes of Practice (the codes). The study objectives were to:

- assess the capability of remote sensing technologies to monitor PNF code conditions and/or biophysical outcomes (noting that not all PNF code conditions or outcomes may be suitable to monitor remotely)
- consider the feasibility of each remote sensing technology, including cost effectiveness, frequency of return sampling, usefulness of data generated, and whole-of-life-cycle considerations such as data storage, processing and analysis
- propose indicators to monitor PNF code conditions and/or biophysical outcomes under the PNF codes
- analyse readily available remote sensing data to demonstrate what the data can explain in terms of outcomes and/or conditions.

This report addresses the final objective and builds on the indicators proposed in the second report. For background information, readers should consider reading the first report, which addressed the first two objectives above and is available on the NSW NRC's website[1].

In this report, worked examples and analysis of readily available remote sensing data are presented for several potential remote sensing 'indicators', as identified and workshopped in earlier stages of this feasibility study. At the site scale, these include indicators of structural complexity, an analysis of canopy gaps and area harvested, modelled volume and basal area estimates and examples based on terrain information (slopes, riparian areas, tracks and roads). These indicators are based on high resolution airborne laser scanning (ALS) data, with some field-based data provided by Forestry Corporation of NSW for the modelling work. At a bioregional scale, an assessment of forest connectivity is presented, using the National Forest and Sparse Woody Vegetation data, along with intersections with existing NSW Department of Climate Change, Energy, the Environment and Water (DCCEEW) data products, including the Statewide Landcover and Tree Study (SLATS) and the Fire Extent and Severity Mapping (FESM) products. The Biodiversity Indicator Program is also discussed, along with a summary of using satellite time-series to explore drought impacts.

In addition to the worked examples, further potential indicators are addressed via a summary of existing literature (provided as Appendix 1). These include vertical connectivity, dead tree crowns, compositional complexity and structural recovery. These indicators are currently considered low feasibility, due to high costs and technical and data limitations. However, they may warrant consideration in future. A comprehensive literature review on the application of LiDAR data for forest structure monitoring is also provided as Appendix 2.

The analysis and worked examples presented in this report offer a starting point for the potential remote sensing indicators and what they may be able to tell us about PNF areas at the site scale and within the broader landscape. However, these results should be considered preliminary, prior to the development of a comprehensive PNF MER monitoring and sampling program. The overall design of the monitoring and sampling program to support the PNF MER is not part of this remote sensing feasibility study. It is recommended that such a design include three tiers of observation: ground based, high-resolution aerial samples (ALS and imagery) and wall-to-wall moderate resolution satellite imagery, to be collected at regular and defined frequencies within a statistically defendable

[1] Hislop, S. & Stone, C. (2023) Remote sensing of NSW private native forests – options and feasibility. https://www.nrc.nsw.gov.au/publications-current

sampling strategy. This approach would facilitate the application of the indicators presented in this report.

1. Introduction

This report is the third stage in the remote sensing feasibility study and builds on the work outlined in the previous two reports. The first report presented a comprehensive review of remote sensing technologies and capabilities within the context of a Private Native Forestry Monitoring, Evaluation and Reporting Framework (PNF MER)[2]. The second report proposed potential remote sensing indicators at both site and bioregional scales, with a focus on what can realistically be achieved with current data and technology solutions within a moderate budget.

This report presents worked examples of a selection of the proposed indicators using existing datasets (where available). Where existing data was not available or the feasibility of the indicator was deemed low due to technical challenges, background information is provided, guided by existing literature (Appendix 1).

The potential remote sensing indicators addressed in this report are summarised in Table 1.

Table 1. Proposed remote sensing indicators from Report 2 and how they are addressed in this report.

Proposed Indicator [related PNF condition(s)]	**Feasibility** (from Report 2)[3]	**How it is addressed in this report**
Structural complexity [regeneration, protection of habitat and biodiversity]	High	Section 2.1. Site scale worked example based on ALS samples
Structural recovery [regeneration]	Medium	Partly addressed in Section 4.4. Drought and fire disturbance and recovery with satellite time series. Discussed further in Appendix 1.4.
Canopy gaps [regeneration, canopy openings and adjacency limits]	High	Section 2.3. Site scale worked example based on ALS samples
Spatial connectivity [regeneration, protection of habitat and biodiversity]	High	Section 4.1. Bioregional scale worked example based on forest cover data

[2] Natural Resources Commission (2023) *Approved Private Native Forestry Monitoring, Evaluation and Reporting Framework*.

[3] *Feasibility was based on technical difficulty, ability to extract meaningful information and potential costs, where high represents greatest likelihood of success.*

Proposed Indicator [related PNF condition(s)]	**Feasibility** (from Report 2)[3]	**How it is addressed in this report**
Vertical connectivity [regeneration, protection of habitat and biodiversity]	Medium	Appendix 1.1. Background only
Dead tree crowns (%) [habitat trees – dead standing trees]	Low	Appendix 1.2. Background only
Area harvested [area harvested reporting requirement]	Medium	Section 2.2. Results based on published paper (Hislop *et al.* 2024)
Basal area [minimum stand basal area]	Low	Section 2.4. Worked example based on FCNSW data over State forests
Volume harvested [volume harvested reporting requirement]	Medium	Section 2.4. Worked example based on FCNSW data over State forests
Compositional complexity [regeneration, protection of habitat and biodiversity]	Low	Appendix 1.3. Background only
Riparian exclusions (% maintained) [riparian exclusions]	Medium	Section 3.1. Individual site scale example based on ALS to demonstrate the method
Slope exclusions (% maintained) [slope exclusions]	Medium	Section 3.2. Regional scale example based on ALS derived DTM. (note this indicator was not included in the original version of Report 2)
Tracks intersecting drainage lines (count/density) [roads, tracks, crossings]	Low	Section 3.3. Brief discussion of techniques, challenges and potential solutions.
Soil erosion (minor) [minimise soil disturbance/movement, protection of dispersible or erodible soils]	Low	Discussed briefly in Section 3.3. Tracks and roads
Landscape heterogeneity	Low	Not addressed in this report

Proposed Indicator [related PNF condition(s)]	**Feasibility** (from Report 2)[3]	**How it is addressed in this report**
Disturbance (timing and magnitude)	High	Sections 4.2, 4.3 and 4.4. Explored through the intersection of PNF areas with FESM and SLATS data and outputs from Hislop *et al.* (2023)
Spectral recovery	Medium	Partly addressed in Section 4.4. Drought and fire disturbance and recovery with satellite time series. Discussed further in Appendix 1.4.
Mass soil movement	Low	Not addressed in this report. Not considered relevant for PNF monitoring
Fire severity (& recovery) modelling (e.g., FESM)	High	Section 4.3. Intersection of FESM data with PNF areas (severity only)
Statewide Landcover and Tree Study (SLATS)	High	Section 4.2. Intersection of SLATS data with PNF areas
Biodiversity Indicator Program (BIP)	High	Discussed in Section 4.1. Spatial connectivity

The terms bioregional and site are used here to refer to two distinct spatial scales, as per the language used in the PNF codes. We interpret site scale to essentially relate to a PNF plan area for an individual property, noting there are a large range of property sizes. Bioregional scale we interpret to refer to large areas and interchangeable with terms such as landscape or regional. The IBRA bioregions are one such classification used in Australia, which could be used as both reporting units and sampling strata (not used here).

The proposed indicators at the site scale rely heavily on airborne laser scanning (ALS), which, under the funding assumptions applied in this study and current technological constraints, will need to be collected as samples (e.g., transects). Samples collected within a robust sampling framework (e.g., a design-based stratified sample) would satisfy monitoring requirements, being the basis of traditional plot-based forest monitoring used throughout the world for decades. Note that in future, there may be opportunities to use new technologies such as Geiger-mode LiDAR which can collect data at higher altitudes and thus cover much greater areas. With traditional ALS, as with satellite imagery, there is typically a trade-off between spatial resolution and coverage extent.

Indicators at bioregional scales lend themselves more to using moderate resolution satellite imagery, which offers wall-to-wall coverage at regular time steps. Note that moderate resolution imagery can also provide accurate estimates when used in a sampling framework rather than wall-to-wall, which would significantly reduce storage and processing times and costs. Bioregional indicators may not have the required precision for many site scale assessments. However, they can be used to make broad comparisons across tenures and to compare areas with PNF plans to the rest of the private forest estate. While these indicators can, as demonstrated later in this report, be intersected with PNF plan areas to create local summary statistics, an understanding of the spatial limitations of each product is essential before doing so. It is possible for a remote sensing product to produce broadly accurate results at a landscape scale, while at the same time, lack the precision to be reliable at a local scale.

2. Remote sensing LiDAR indicators

In this section, worked examples of several of the proposed remote sensing forest structure indicators are presented, using a format of introduction, methods, results and discussion for each. These indicators principally use LiDAR data collected from aircraft (airborne laser scanning or ALS). Note that the primary purpose of these examples is to demonstrate the processing steps required using existing data. Although we have attempted to relate these to PNF, results from the analysis should be considered preliminary and have not been validated.

2.1. Structural complexity

Introduction

Forest structural complexity (or diversity) is considered important for habitat and biodiversity. Therefore, maintaining or protecting structural complexity may be an objective in sustainable forest management. LiDAR technology allows for an accurate and comprehensive representation of forest structure. LiDAR can be collected from the ground (e.g., terrestrial/mobile laser scanning; TLS, MLS), from aircraft (ALS) or satellites (e.g., GEDI). Each platform has its pros and cons – generally there is a trade-off between detail and spatial coverage. In this indicator, we focus on ALS from a fixed wing aircraft (flying height ~1000m), with point densities in the range of 30 p/m^2.

In the example here we demonstrate the use of airborne LiDAR-derived height measures, specifically: top height, mean height, canopy cover, skewness, standard deviation and the coefficient of variation. While there are many more complex LiDAR-derived structural metrics, the suite chosen here are simple metrics that have proven useful elsewhere in representing forest structure and serve to demonstrate the required processing steps. These six metrics should not be assumed to represent all elements of forest structure, which is a complex topic with many unknowns.

In addition, relating these metrics to on-ground canopy structure and management practices requires additional location specific interpretation. Haywood & Stone (2011a), for example, interpreted that positive skewness values were associated with sparse canopies and negative values with closed canopies, when using ALS data to estimate structural attributes of mountain ash (*Eucalyptus regnans*) forests in Victoria. Further background information, including a discussion on more complex metrics, is available in Appendix 2.

Methods

LiDAR height metrics are based on the vertical distribution of points in a defined spatial area. Figure 1 shows an example LiDAR point cloud for a 'plot' and the corresponding histogram of heights (i.e., the number of points in each height bin). From this histogram (vertical profile), summary statistics can be extracted, which we refer to as LiDAR metrics. For example: top height, mean height, standard deviation, canopy cover (i.e., the proportion of points above a height threshold).

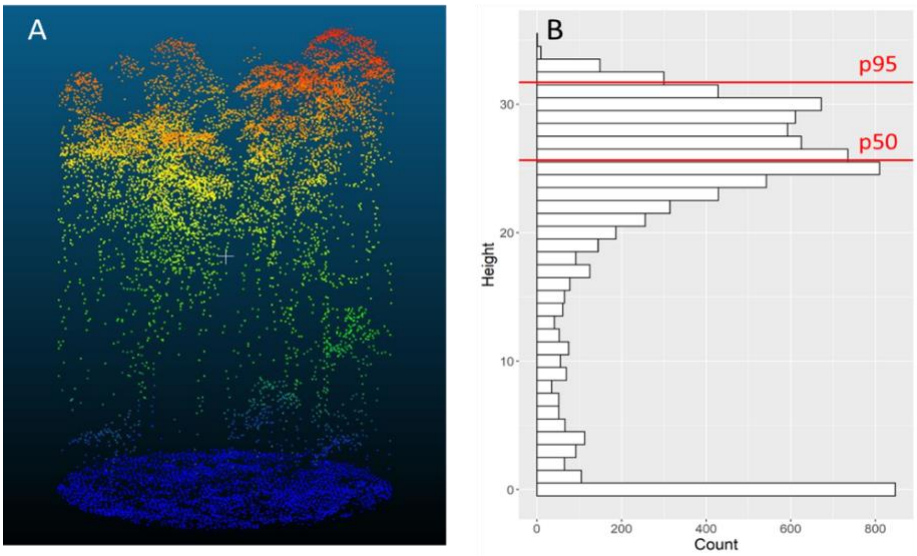

Figure 1. Example of a LiDAR point cloud over a plot (A) and the resulting distribution of height values (B), with the 50th and 95th percentiles shown in red.

To create a 2-dimensional surface (map) of a particular LiDAR metric, a grid of a defined pixel size (e.g., 30m) is placed over the point cloud and the vertical profile of points in each pixel is used to compute the metric of interest (Figure 2).

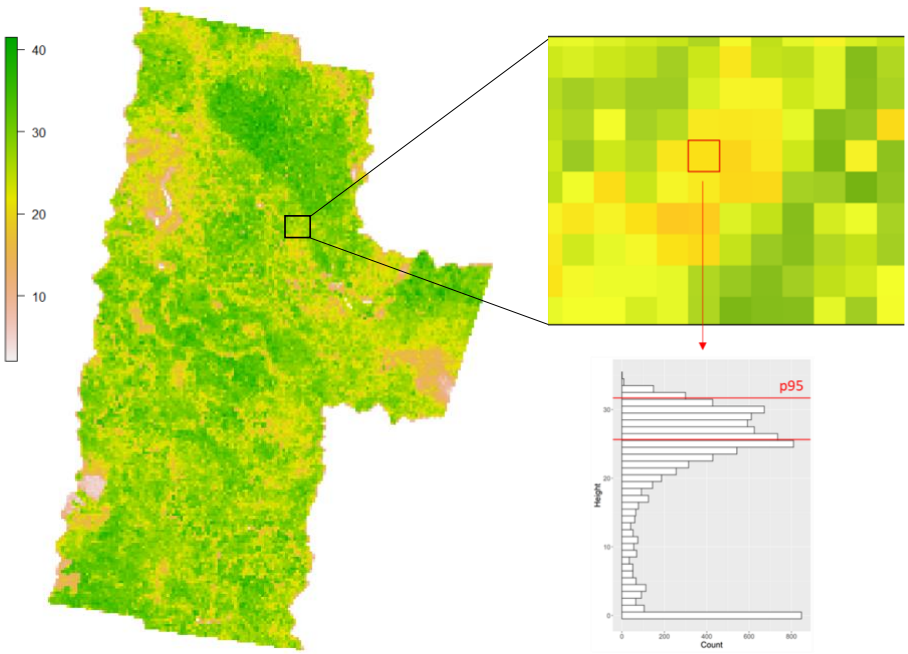

Figure 2. Example of a LiDAR metric (p95) calculated from the height distribution of points in each grid cell (pixel) across a LiDAR extent.

In this indicator, LiDAR metrics representing height (95th percentile, average), vertical variation (standard deviation, skewness) and canopy cover were calculated using only the first returns from the normalized point clouds from ALS data, using a grid size of 30 × 30 m. In addition, the coefficient of variation (CV) was calculated from the average height and standard deviation layers ($CV = \frac{\sigma}{\mu}$).

The derived LiDAR metrics in themselves do not produce insights without performing additional analysis in line with specific monitoring questions. For example, we may wish to look at whether structure is any different in areas where harvesting is permitted compared with non-harvesting areas. Alternatively, if multi-date LiDAR exists, we can compare the two dates in time.

Here, we used the multi-date NSW Department of Primary Industries (DPI) PNF R&D program ALS to compare derived LiDAR metrics both temporally (2020 to 2021) and spatially (PNF areas to non PNF areas of forest from the ALS spill-over areas), as indicated in Figure 3. The entire workflow for the processing and analysis is shown in Figure 4.

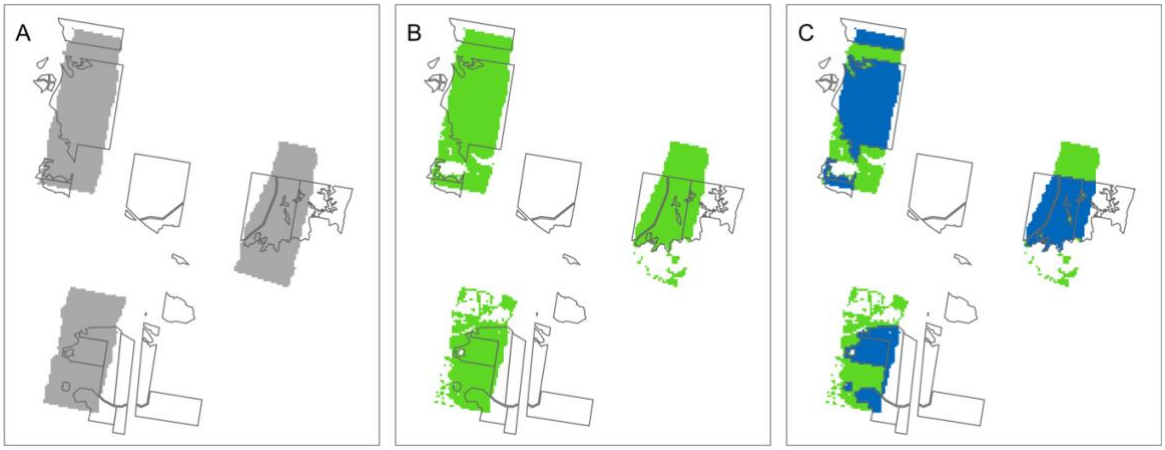

Figure 3. (A) Areas of overlapping ALS capture from 2020 and 2021, (B) Areas of forest in either 2020 or 2021 according to the ALS data (green) and (C) Areas of forest inside PNF plan areas (blue) and outside (green). Grey lines indicate PNF plan area boundaries.

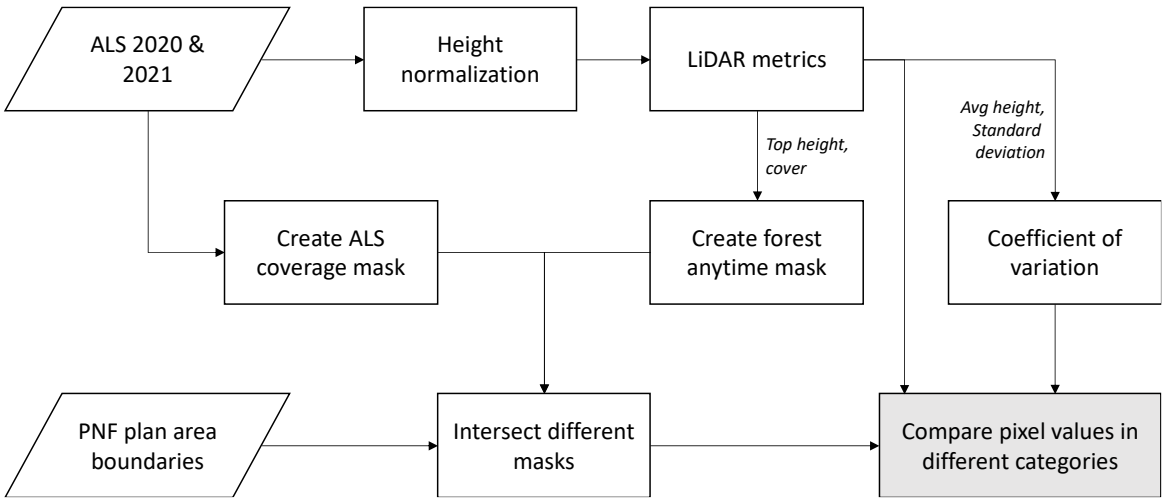

Figure 4. Structural complexity processing and analysis workflow.

The DPI PNF R&D program ALS consists of LiDAR samples (transects) collected over 253 properties with live PNF plans (as of March 2020) in the NSW northeast (Figure 5). Two acquisitions covering the same areas were collected in April 2020 and April 2021 (i.e., one-year apart).

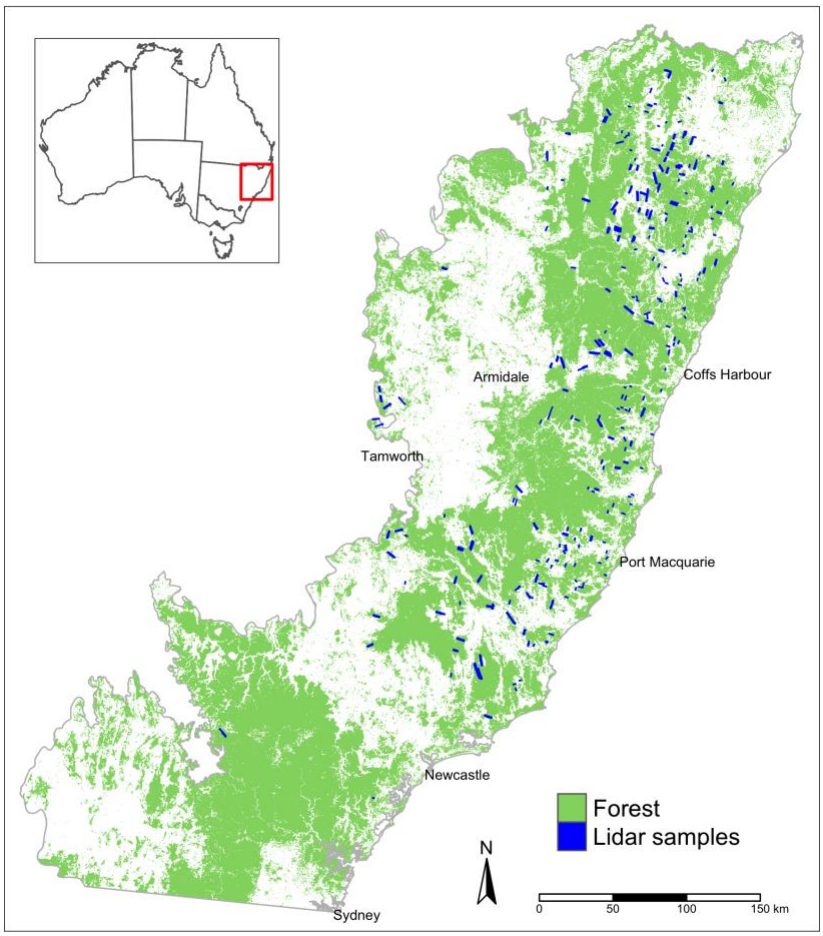

Figure 5. Location of LiDAR samples collected under the PNF R&D program (Hislop *et al.* 2024).

The raster layers for each of the LiDAR metrics were intersected with the forest mask and PNF plan areas to create four different categories for comparison: PNF 2020, PNF 2021, Not PNF 2020 and Not PNF 2021. The forest mask used here was computed from the LiDAR-derived top-height and cover metrics using thresholds of above 2m in height and 20% canopy cover, as per the Australian definition of forest. To enable the same areas to be compared temporally, a forest layer from both 2020 and 2021 was computed and if a pixel was forest in either of these years it was considered forest. Pixel values for each category were then extracted and summarised. All processing steps were performed in R, using the *lidR*, *sf* and *terra* packages.

Results & discussion

Figure 6 shows an example of how two structural metrics (average height and skewness) change following selective harvesting. In this example, there is a clear decrease in average height and an increase in the skewness, which means that there are more LiDAR returns in the lower vegetation strata (i.e., the upper canopy is sparser). This agrees with previous findings (e.g., Haywood & Stone 2011a).

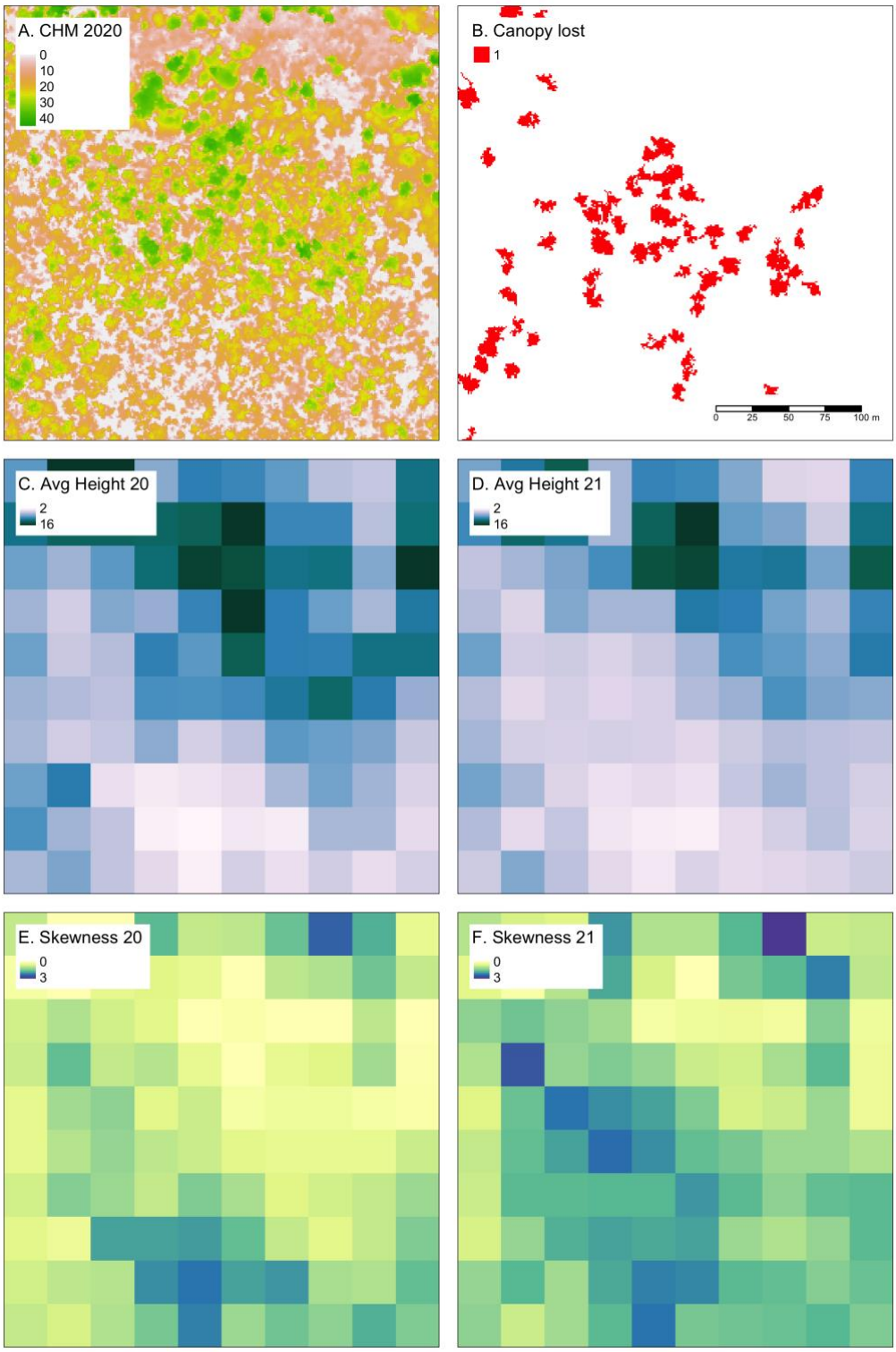

Figure 6. Example of how two structural metrics change following harvesting. The CHM from 2020 is shown for reference (A), panel (B) shows the canopy lost between 2020 and 2021, (C) the average height in 2020, (D) the average height in 2021, (E) the skewness in 2020 and (F) the skewness in 2021.

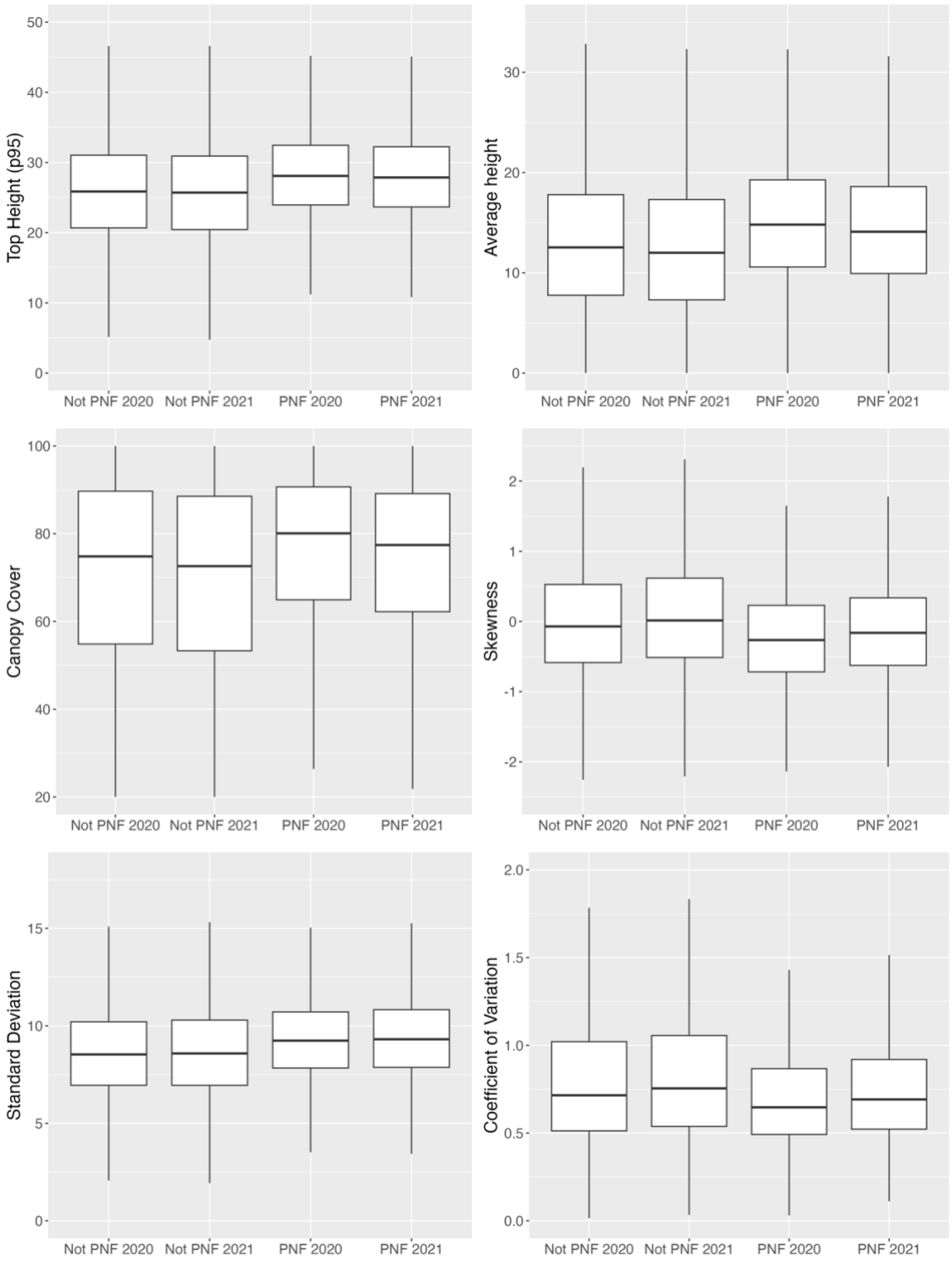

Figure 7. Boxplots of all pixel values in the various categories for each of the structural metrics.

Results from each metric are summarised across the entire region in Table 2 and Figure 7. The results indicate that, in general, the non-PNF areas have a slightly greater range in values across all metrics compared with the PNF areas. There appears to be a greater variation between non-PNF and PNF areas (spatial) than between 2020 and 2021 (temporal). It is also notable that the top height is around 2m higher in PNF areas compared to surrounding non-PNF areas. The areas of forest outside of PNF areas may be in National Parks, State Forests or parts of private properties without active PNF plans. The results here may indicate that forests inside the PNF plan areas are perhaps of higher quality, with slightly higher tree heights and canopy cover percentage (on-ground observations would be required to confirm this). The skewness is also slightly negative, which means the point-cloud has more points in the upper canopy. Note that only the first returns were used to calculate the different metrics, so the denser the canopy the more biased towards the top of the canopy the point-cloud is. Although using all returns would contain more points in the mid and lower vegetation strata, in order to produce meaningful results using all points, an appropriate height cut-off value needs to be used. Otherwise, the ground and surface vegetation returns tend to dominate the height distributions. It would also be possible to use a range of different height thresholds to create multiple versions of each metric, which could be tailored towards habitat requirements for different fauna.

Table 2. Median values for each metric and category.

	Median values			
Metric	**Not PNF 2020**	**Not PNF 2021**	**PNF 2020**	**PNF 2021**
Top height (p95)	25.91	25.75	28.11	27.88
Average height	12.57	12.03	14.81	14.10
Cover	74.49	72.14	79.99	77.33
Standard deviation	8.54	8.59	9.24	9.31
Coefficient of variation	0.73	0.77	0.65	0.69
Skewness	-0.06	0.03	-0.26	-0.16

The workflow presented here demonstrates how LiDAR structural metrics can be produced, analysed and summarised to produce insights across a large region (northeast NSW). Further location specific interpretation would be required to relate metric values to on-ground structure, vegetation types and management actions. For example, in general, the metric standard deviation tends to be smaller in more uniform or single-storey forest stands compared to stands with a complex, multistorey structure, while sparser canopies may show positive skewness and a higher coefficient of variation.

Note also that here we made a general assumption that the ALS samples are representative of the region as a whole. However, the samples were collected in a stratified random sampling framework which was biased towards recently approved PNF plans. Therefore, for statistically defendable estimates, further work to create stratum level estimates would be required.

An alternative use for LiDAR metrics is to use them in modelling applications, either as training data for satellite-based models to create wall-to-wall maps or as covariates in models of field measured variables (discussed in Section 2.4). Therefore, these metrics may be more useful to be thought of as

interim products which can provide valuable inputs to other models and applications, including habitat modelling scenarios.

Key takeaways

ALS derived LiDAR metrics offer a means to characterise and summarise forest structure across large areas. The metrics presented here have been shown elsewhere to represent different aspects of forest structure and its response to disturbances. Together, they describe the basic forest structure of a site.

It is not possible, however, to say 'this value is good, this value is bad' because values depend on forest type, region, etc. All we can say without further investigation and interpretation is 'this area is different to this area, or this area is different now to what it was previously'.

Opportunities for further work

The ALS derived metrics could be intersected with other spatial layers (e.g., bioregions, tenure, forest type, etc.) to increase understanding of their behaviour in different environments.

More complex metrics may offer a more complete picture of forest structure (see Appendix 2).

Further work is required to relate metrics to on-ground information of importance.

2.2. Area harvested

Introduction

The area of forest impacted by harvesting has been the focus of many research studies worldwide. Many of these have used satellite time-series (particularly Landsat) to attempt to automatically detect harvesting events. Most satellite-based techniques have demonstrated reasonable capabilities with respect to detecting clear-fell events. However, the abilities of these methods diminish rapidly with detecting more subtle events such as selective harvesting. Hislop *et al.* (2024) assessed the sensitivities of Landsat and Sentinel-2 to PNF harvesting events in northern NSW and found individual events were only visually apparent in a Sentinel-2 monthly time-series around half of the time. In a Landsat seasonal time-series, it was closer to a quarter. It is likely that automated approaches would fare even worse than the visual assessment. Harvesting events may be more apparent in commercial high-resolution satellite imagery (e.g., Planet Skysat). However, high-resolution imagery does not lend itself to automated time-series approaches in the same way as Landsat/Sentinel-2 does currently (and has costs involved). This is due to radiometric and geolocation inconsistencies through time, along with several practical limitations (e.g., data access, data volumes, temporal frequency).

An alternative approach using multi-date ALS was developed by DPI Forest Science as part of the DPI R&D program and is documented in Hislop *et al.* (2024). These techniques and results are summarised here.

Methods

The workflow developed to estimate the extent of harvesting across a one-year period from multitemporal ALS is outlined in Figure 8. The methods are principally based on using the difference between two canopy height models (CHMs) to identify tree canopy loss (Figure 9). To remove noise, the difference layer was filtered to only include patch sizes greater than 50 m^2 and height differences greater than 10 m. With this tree-loss raster, a rolling average of density at a 1-ha scale was created. To distinguish harvesting from 'natural' loss (e.g., trees that had fallen over), the density layer was filtered using a threshold value of 0.043 ha^{-1}. That is, anything with a density of

tree-loss greater than 0.043 ha^{-1} was considered harvesting, whereas other areas of loss were considered natural tree loss. The threshold value was calculated using a reference dataset based on a human interpretation of 406 sample patches. While using a single threshold value will result in some misclassifications, in this work it was shown to have a high accuracy (97%).

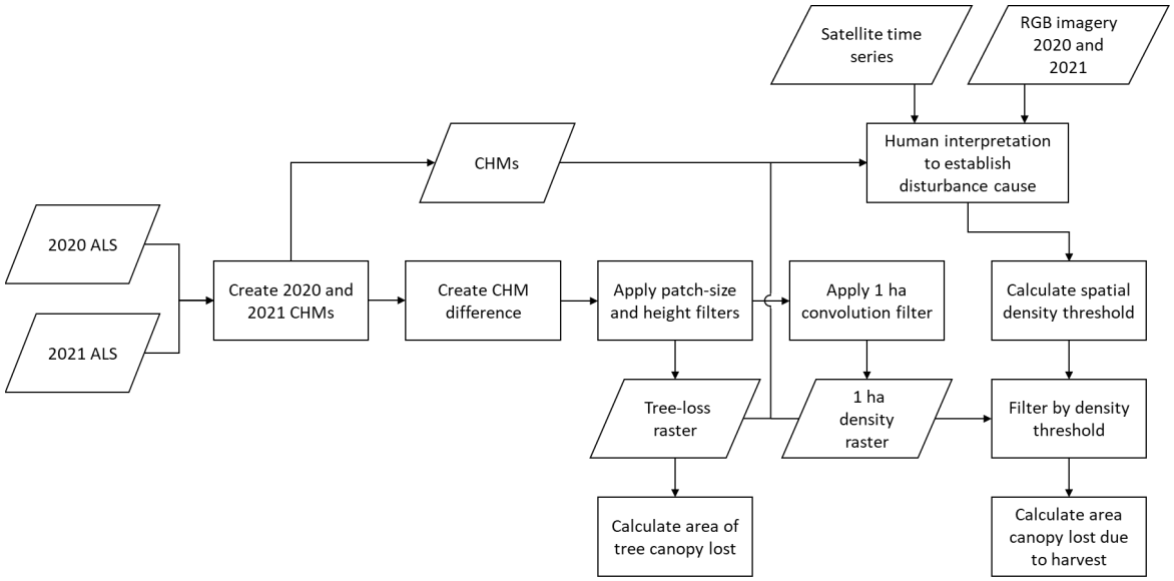

Figure 8. Workflow for processing the LiDAR to estimate canopy loss due to harvesting (Hislop *et al.* 2024).

The workflow summarised here was repeated for each of the 253 PNF properties where ALS was collected in both 2020 and 2021. The final harvesting layers (presence/absence) were summarised to calculate the area impacted. Because the selection of properties was based on a stratified random sample, reliable estimates and confidence intervals across the entire NSW northeast could be derived. Note that this would not be possible without a robust sampling framework (Kathuria 2023).

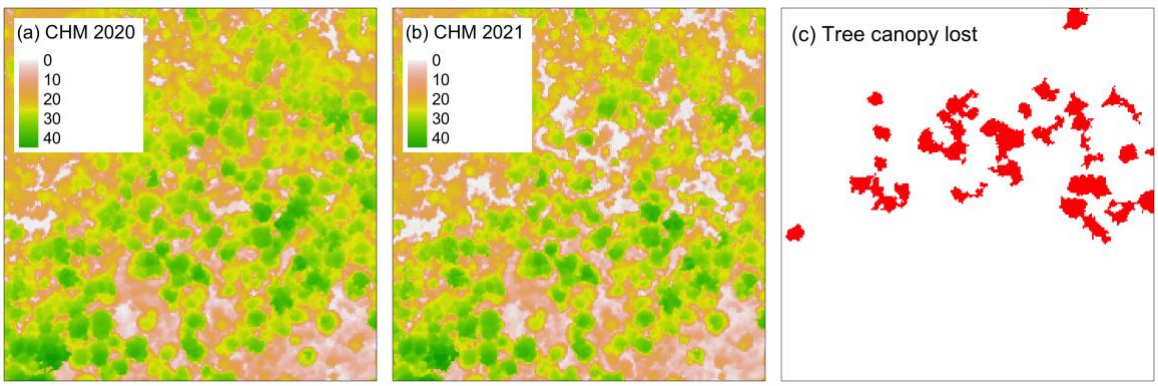

Figure 9. Example of the output from the CHM differencing method (Hislop *et al.* 2024).

Results & discussion

The area of private native forests impacted by harvesting across the one-year period (2020-2021) was estimated to be 1665 ha (± 492 ha at the 95% confidence level) or 0.37% (± 0.11%) across 455,000 ha (total area with an approved PNF plan as of March 2020). The results for each stratum are shown in Table 3. Note that the standard errors and thus the 95% confidence interval may at first glance seem high, however this is because the area impacted by harvesting is comparably low

(0.37%). In addition, many properties recorded no harvesting at all within the one-year period. The sampling design also allowed for a comparison based on different property size classes and time since plan approval. The results suggested that harvesting is more likely to occur soon after plan approval and was slightly greater in percentage terms for plan areas < 200 ha. The authors also attempted to investigate broad patterns of harvesting by aggregating results to a 10km grid and looking at the average height loss and density (Figure 10). No clear patterns were observed, based on the limited dataset.

Also of note, 30% of the tree-loss identified was considered natural loss (e.g., trees falling over on their own accord). It is not known whether this is a 'normal' rate of attrition or was exacerbated by the 2019-20 drought and wildfires. As mentioned above, satellite imagery is likely to miss many harvesting events, particularly those of low intensity. However, low intensity events also contribute less to the overall area harvested, so the omissions may be largely negligible for estate-level monitoring and reporting purposes. Further assessment and discussion on using satellite imagery to estimate forest harvesting through the Statewide Landcover and Tree Study (SLATS) program is provided in Section 4.2.

Table 3. Stratum level estimations of all canopy loss and that due to harvesting based on the spatial density threshold (Hislop *et al.* 2024).

Year stratum (PNF plan approval)	Area Stratum	Population Area (ha)	Estimated Canopy Loss (ha)	Percent Canopy Loss	Estimated Harvesting Loss (ha)	Standard Error (ha)	Percent Harvesting
Pre-2016	< 50 ha	28,111	198.9	0.71	171.3	117.9	0.61
Pre-2016	50 to 200 ha	71,227	178.8	0.25	72.9	39.2	0.10
Pre-2016	200 to 500 ha	86,476	296.7	0.34	151.0	67.7	0.17
Pre-2016	> 500 ha	169,090	755.6	0.45	458.7	178.3	0.27
2016-2019	< 50 ha	9,801	38.0	0.39	18.3	11.3	0.19
2016-2019	50 to 200 ha	22,309	196.6	0.88	153.6	64.9	0.69
2016-2019	200 to 500 ha	26,546	219.4	0.83	183.7	60.3	0.69
2016-2019	> 500 ha	22,895	134.9	0.59	99.5	39.3	0.43
2019-2020	< 50 ha	2,731	100.0	3.66	92.5	15.5	3.39
2019-2020	50 to 200 ha	4,715	161.7	3.43	149.0	37.6	3.16
2019-2020	200 to 500 ha	6,035	123.1	2.04	112.9	0.0*	1.87
2019-2020	> 500 ha	4,829	7.7	0.16	1.8	0.0*	0.04
Total		454,764	2411	0.53	1665	251	0.37

*the standard error for these strata is 0 because all properties in the population were included

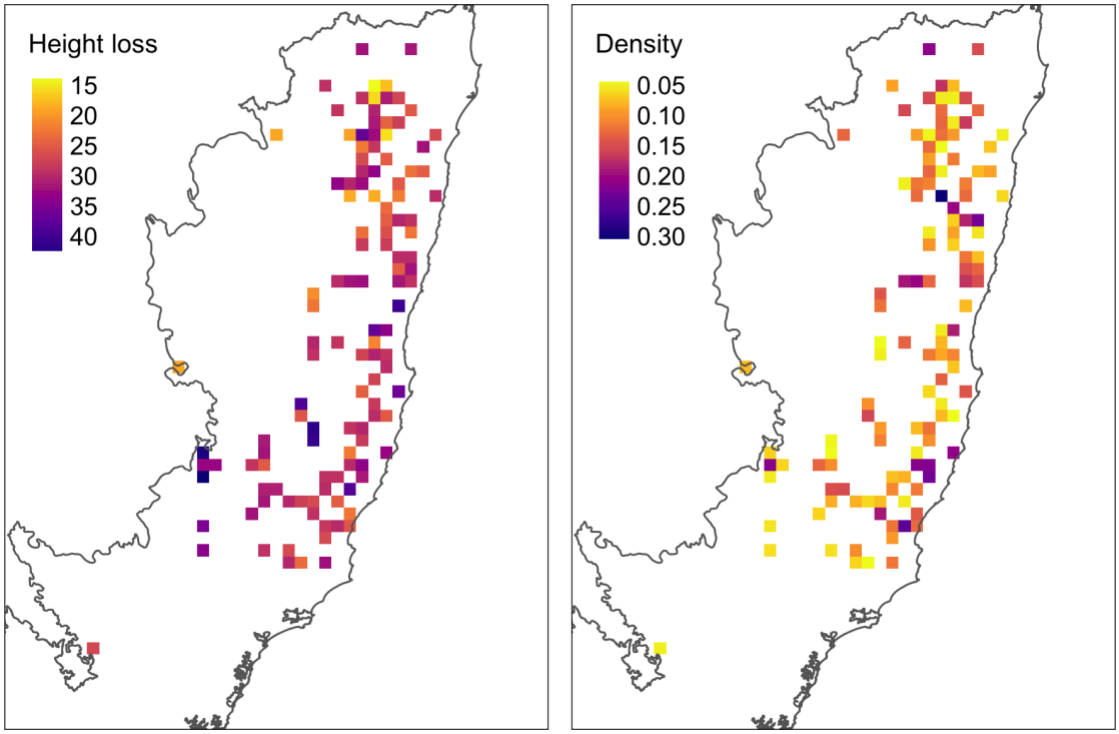

Figure 10. Average height loss and spatial density, aggregated to a 10 km grid (Hislop et al. 2024).

Key takeaways

Monitoring area harvested over time can help us understand, in part, production trends over time, which relates to the PNF outcome 'maintain the productive capacity' and also has links to 'maintain forest health and regeneration' and 'maintain the persistence of native species'.

Key to the above work was the capture of ALS samples across two time-steps one year apart. Because the ALS samples were collected in a design-based sampling framework, the harvested area across the whole region could be estimated, along with statistically derived confidence intervals.

This study represents what is possibly the most comprehensive and accurate assessment of PNF harvesting impacts to date. It is not known whether the figures for 2020-2021 represent a typical year, however, the results are a baseline that future monitoring can be compared against. Although multi-date ALS provides comprehensive and highly accurate information, the cost of repeat acquisitions can be an inhibiting factor. Therefore, lower accuracy satellite imagery may be a preferred approach for monitoring area harvested (see Section 4.2).

Opportunities for further work

Areas harvested could be intersected with forest type mapping (e.g., Yield Association Groups or Plant Community Types) to explore species specific patterns and trends. Data collected for this indicator could also be used for the riparian, slope and track related indicators discussed in Section 3.

2.3. Canopy gaps

Introduction

Gaps in the forest canopy can be both desirable and undesirable. From a regeneration perspective, canopy gaps are important so that shade intolerant species can access sunlight. On the other hand, canopy gaps are a form of fragmentation and may inhibit some fauna species' ability to move throughout an area. Canopy gaps may also change habitat conditions by drying out the forest floor. Repeat measurements over time could be used to understand canopy gap dynamics (rate and extent of closure) as the forest regenerates. Here, we present an aggregated assessment of canopy gaps across the properties where recent ALS data was collected.

It is important to note that spatial scale has a direct influence on how gaps are represented. Gaps may be evident in high-resolution products such as LiDAR derived canopy height models (CHMs) but not in satellite derived forest cover maps. It is unlikely that Sentinel-2 satellite imagery (10m pixel resolution), for example, would be able to provide an accurate assessment of canopy gaps for monitoring PNF at the site scale.

In this section, a process for extracting canopy gaps from a 1m canopy height model (CHM) is presented. A summary of a selection of PNF plan areas in northeast NSW is provided, using the DPI R&D program ALS from 2021 only.

Methods

LiDAR derived canopy height models (CHMs) from only the 2021 DPI R&D program LiDAR were processed into binary canopy gaps products using a 2m height threshold (i.e., every pixel below 2m is given a value of 1, all other pixels are set to 0). These products were intersected with the PNF plan areas and filtered to include only patches with greater than 50 connected pixels (50 m^2; Figure 11). These derived layers were then used to calculate landscape statistics for each property, including the number of individual gaps and percent area covered by gaps.

Results & discussion

The number of canopy gaps and area percentage using a patch size greater than 0.005 ha were calculated for each of the 253 properties, using the ALS data from 2021. The properties were split into three categories based on the area impacted by harvesting between 2020 and 2021, according to work undertaken by Hislop *et al.* (2024) (see Section 2.2). The classes used were: Recent harvesting (total area in the property greater than 1.5 ha), Limited recent harvesting (area between 0 and 1.5 ha) and, No recent harvesting. This enabled a class comparison for the purposes of this report (Figures 12 – 14). However, we have not verified that the individual canopy gaps identified here are related to harvesting. It is possible that many gaps are natural persistent landscape features and were also present in the 2020 data (not tested here). Verifying if gaps are related to harvesting would require additional information, such as on-ground validation or a cross-reference with area harvested maps (e.g., Section 2.2) or landholder post-harvest reporting, which is now required under the PNF codes of practice released in May 2022. In summary, the methods and results for this indicator are based on a single ALS capture and not intended to represent area harvested, which was addressed in the previous indicator (Section 2.2).

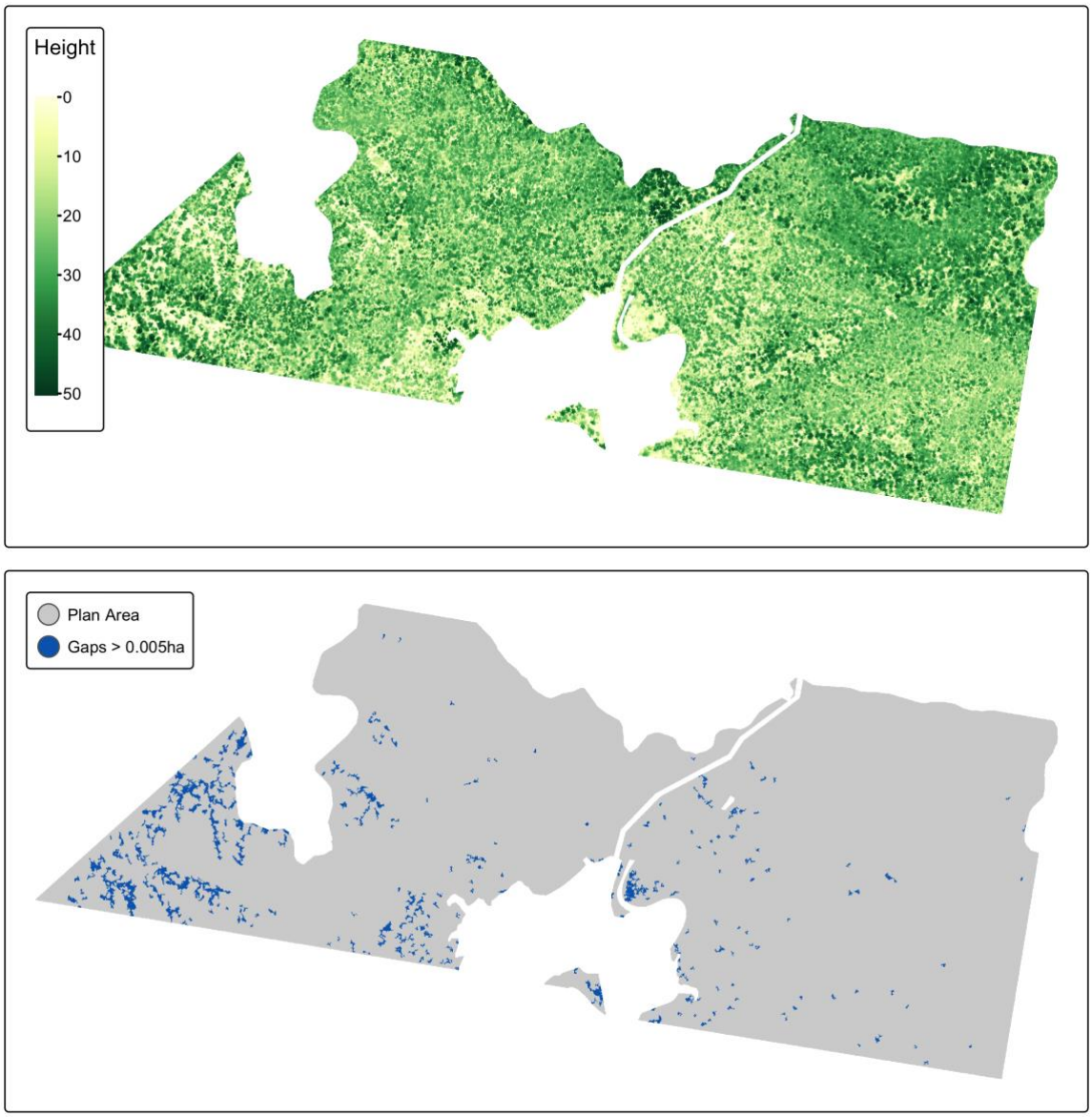

Figure 11. Example canopy height model (top) and canopy gaps greater than 0.005 ha (bottom).

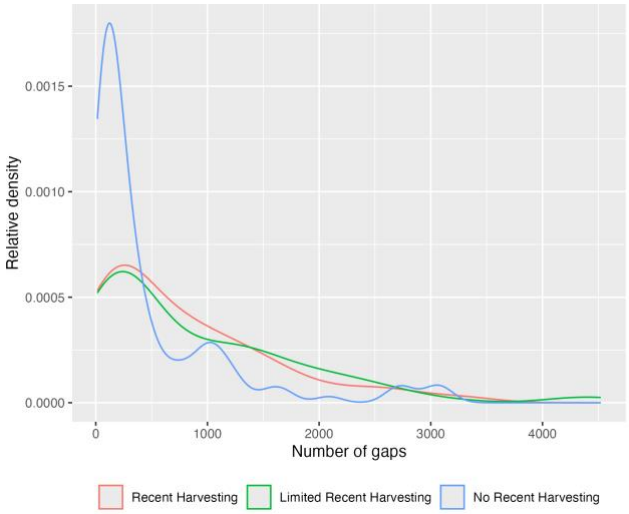

Figure 12. Relative density of the number of gaps per PNF plan for gaps greater than 0.005 ha.

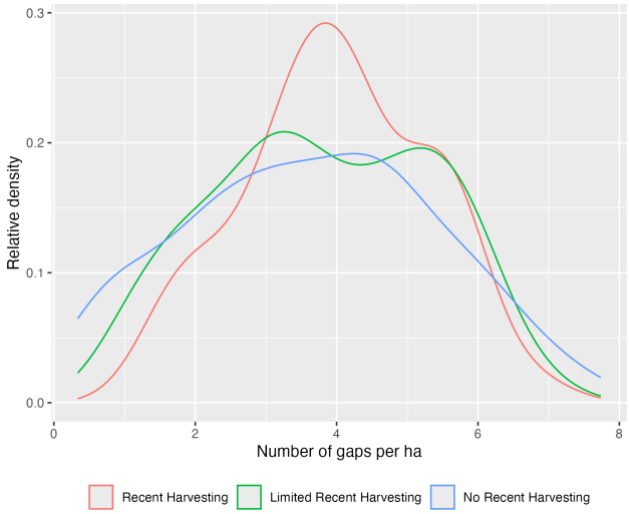

Figure 13. Relative density of the number of gaps per hectare per PNF plan for gaps greater than 0.005 ha.

The median number of canopy gaps greater than 0.005 ha for properties with recent harvesting was 582, while for properties with no recent harvesting, the median number of gaps was 193 (Table 4). However, if we convert these counts to a per hectare value, the median number of gaps is much the same for all three classes (3.6 – 3.9). This likely reflects the fact that most recent harvesting (in area terms) occurred in larger properties.

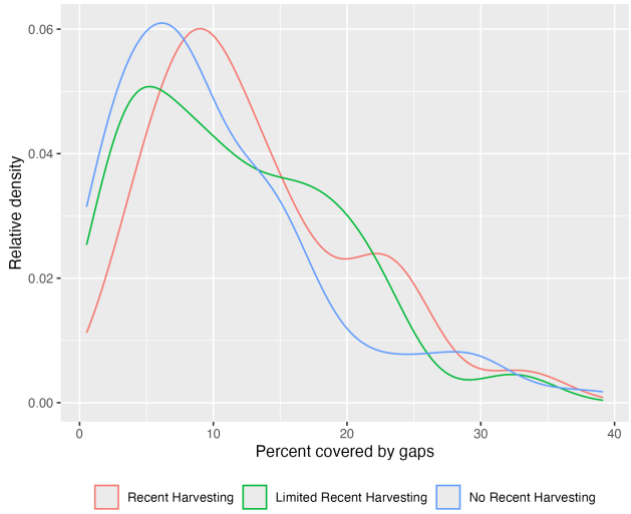

Figure 14. Relative density of the area percentage covered by gaps per PNF plan for gaps greater than 0.005 ha.

Table 4. Median number of gaps > 0.005 ha, gaps per ha and area covered by gaps (per property – 2021 ALS only).

	Number of gaps	Number of gaps per ha	Area covered by gaps
Recent Harvesting	582	3.9	11.08
Limited Recent Harvesting	521	3.8	10.39
No Recent Harvesting	193	3.6	8.53

Key takeaways

The analysis presented here suggests that more gaps exist in recently harvested areas compared with the other areas under PNF plans. However, it is expected that the majority of these will close as the forest regenerates and the crowns of neighbouring trees expand. This could be confirmed with future ALS acquisitions.

Although ALS data provides a precise method of mapping and quantifying canopy gaps, the expense of acquisition means that the data may be best collected as samples. A robust sampling framework allows inferences to be made about the population as a whole.

Opportunities for further work

The gap analysis could be undertaken with different height thresholds and different gap sizes to cater to the requirements of different fauna species.

Comparisons across bioregions, tenures etc. may also be worthwhile avenues for future research.

2.4. Volume and basal area

Introduction

Inventory attributes such as volume and basal area have traditionally been collected on the ground in sample plots. If the plot data is collected in an appropriate design-based sampling framework, inferences about the whole area in question can be made. An alternative/complementary approach to estimate inventory attributes is to combine field measurements with ALS data, which has been referred to as the 'area-based approach' (White *et al.* 2013). In the area-based approach, forest inventory attributes are predicted across the extent of the ALS coverage by setting up statistical dependencies between ALS derived predictor variables and ground-based response variables. The main advantages of the area-based approach are full spatial knowledge of the predicted attributes and more precise estimates of certain variables. It also somewhat circumvents the need for a pure design-based statistical sampling framework, opening the door to alternatives such as hybrid or model-assisted sampling strategies.

Methods

The general workflow for the area-based approach is to, firstly, extract the relevant LiDAR point-clouds for sample plots which have measured values of the response variables in question (e.g., volume or basal area). A model is then created to determine the statistical relationships between the response variables and the LiDAR metrics. This model is then used to predict the response variables across the broader ALS extent using the grid-based wall-to-wall LiDAR metrics (Figure 15).

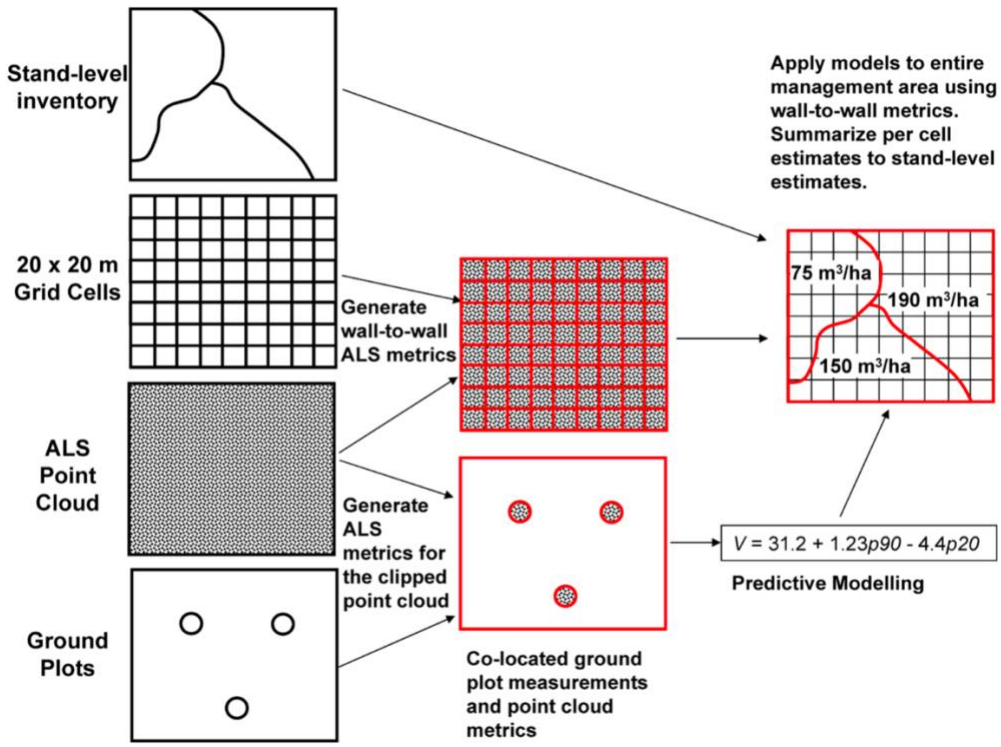

Figure 15. Schematic of the area-based approach (from White *et al.* 2013)

We demonstrate the process here using plot and ALS data from Forestry Corporation of NSW (FCNSW) because of the limited plot data availability in PNF areas. FCNSW provided plot level

information for volume and basal area for 1739 plots. These were cross-referenced with available ALS data and filtered to include only those with a close temporal match (within 3 years) and no harvesting event between the ALS capture and the plot measurement. This left 227 plot measurements that were considered reliable for modelling purposes. Two separate Random Forests models were constructed: one for basal area and one for volume. Random Forests is an ensemble learning algorithm for classification and regression, which is based on a series of decision trees. Each tree is made up of a random subset of the available data and variables. The final model outcome is essentially based on an average of all the trees (i.e., the forest). Here, because the desired output values were continuous variables, the Random Forests algorithm was used in regression mode. Random Forests is popular in remote sensing spatial models due to its robustness to over-fitting, outliers and class imbalance (Mellor *et al.* 2015).

The same LiDAR metrics used earlier for the structural complexity indicator were used here as predictor variables (top height, average height, skewness, standard deviation and canopy cover).

Results & discussion

The model for volume was able to explain 65% of the variance in the data, according to the Random Forests in-built out-of-bag assessment, while the model for basal area was able to explain 55%. These models could likely be improved with more high-quality training data and additional predictor variables, however, the results here are satisfactory to demonstrate the potential of the process.

The models were then used to predict volume and basal area across the PNF ALS transects from 2020 and 2021 (Figure 16). Note, we do not recommend using a model created in State forests to predict into private forests, due to differences in forest management practices. It was used here to demonstrate a process in the absence of specific PNF plot data, and the results may provide a broad estimate of these metrics. Field-based validation for accuracy assessment would be required before having confidence in the results.

Average values were computed by intersecting the modelled surfaces with the PNF plan areas. The average volume across the predicted PNF plan areas with ALS in 2021 was 207 m^3/ha. The average basal area was 24 m^2/ha. If we consider only those properties where recent harvesting had occurred (see Section 2.2), the average volume was actually slightly greater (210 m^3/ha) while the average basal area was essentially the same. This suggests that the intensity of harvesting on PNF has limited impact on these metrics and the remaining basal area appears well above the threshold value of 14 m^2/ha specified in the PNF codes. Further investigation would be required to confirm this.

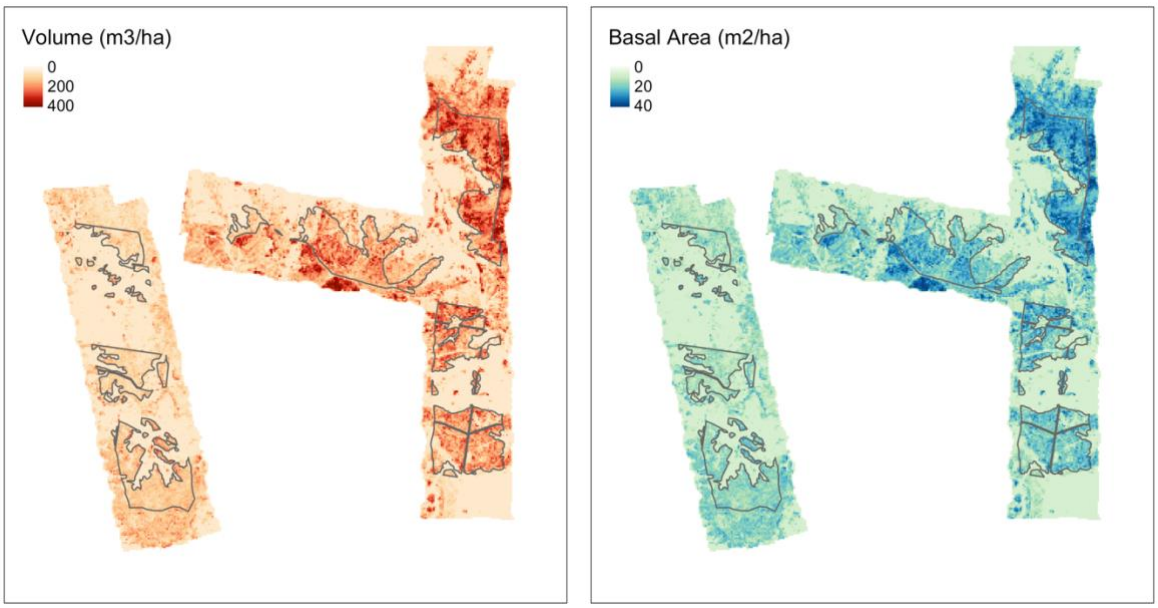

Figure 16. Examples of modelled volume and basal area across a sub-sample of PNF plan areas.

Key takeaways

Spatial modelling as demonstrated above is a tried and tested method to produce maps of variables of interest which cannot be measured directly with remote sensing.

The accuracy of the modelled products is dependent on the quality of the training data along with the ability of the predictor variables in capturing the variation in the training data.

Field validation in PNF areas would be required before having confidence in these results.

Opportunities for further work

The above output maps could be validated with PNF specific field data to provide an understanding of whether the models are broadly transferrable from State forests to private forests.

The accuracy of the models used here could potentially be improved with more training data and a larger number of predictor variables, including non-ALS data (e.g., satellite imagery, terrain, climate, etc.).

3. Remote sensing terrain indicators

This section presents examples of potential remote sensing indicators related to forest terrain (or the ground surface under the trees). Monitoring the ground surface, including aspects of soil erosion, drainage features and forest infrastructure (e.g., roads and tracks), is an important consideration for a forest monitoring program, as these are related to habitat, water quality and the forest's ability to regenerate. Note that these indicators overlap with compliance functions, which would need to be considered prior to application in a monitoring program.

3.1. Slope exclusion areas

Introduction

It is generally accepted that harvesting should not occur on steep slopes. Not only is it potentially dangerous for the operators, it can have adverse impacts on soil erosion and flow-on negative impacts to water quality and stream condition. The PNF codes specify that harvesting should not occur on slopes greater than 30 degrees.

The slope of the terrain can be calculated from a digital terrain model (DTM or digital elevation model – DEM). This is achieved by considering each pixel in relation to its surrounding 8 pixels. There are automatic functions in most GIS software to calculate slope from a DTM. Here, the *terrain* function in the R package *terra* was used.

An example of a 1m DTM and 30m DTM for the same area is shown in Figure 17. Figure 18 shows the slope layer computed from the 1m DTM and a derived slope exclusion layer, with slopes above 30 degrees highlighted.

Note that LLS has existing slope data that it uses for PNF purposes. The information presented here is provided to demonstrate a method rather than as a suggested replacement for existing datasets.

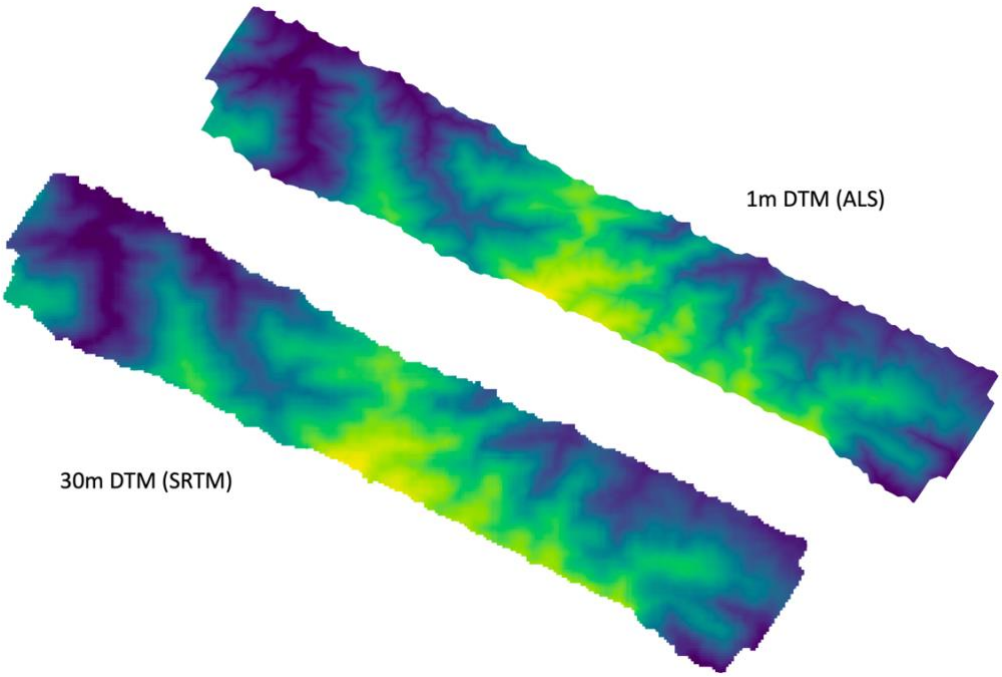

Figure 17. Example of a 30m DTM from the Shuttle Radar Topography Mission (SRTM), which is available globally, and a 1m DTM generated from ALS.

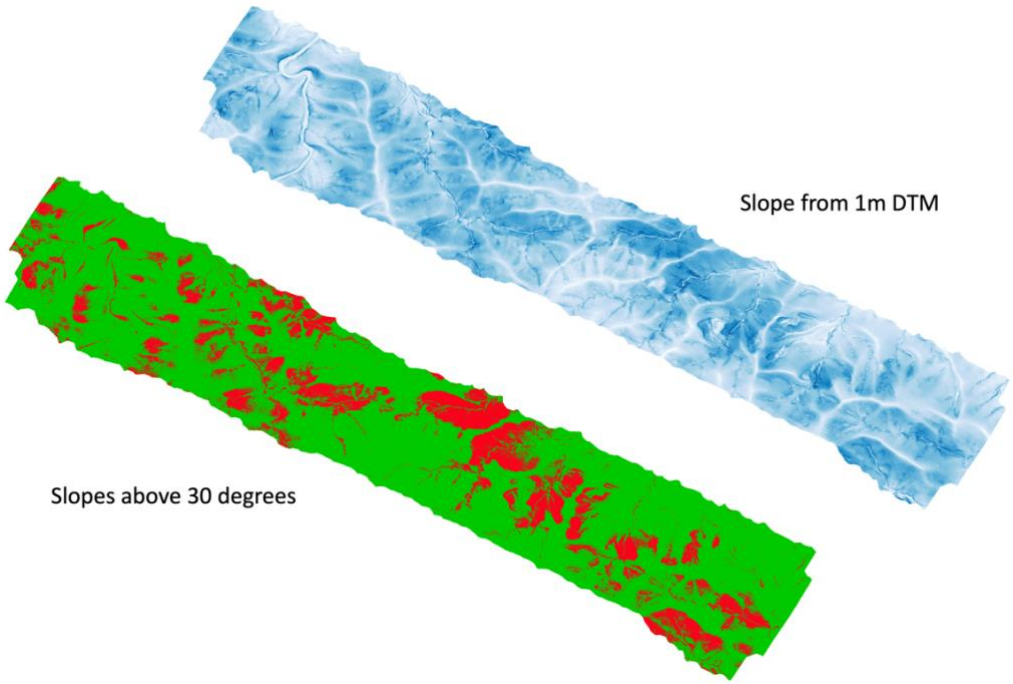

Figure 18. Example of a slope layer generated from 1m DTM and a slope exclusion layer with slopes above 30 degrees (red).

Methods

A simple analysis was undertaken here to provide a general summary with respect to PNF plan areas and their intersection with various slope classes. Here, we used a slope layer generated from NSW Spatial Services ALS data across northeast NSW (Figure 19). This layer overlaps with over 70% of the area of PNF plan approvals in NSW. The slope layer was first classified into 10-degree slope classes (0-10, 10-20, 20-30, 30-40, >50) and intersected with PNF plan areas to derive summary statistics.

Results & discussion

The intersection of the slope class layer with the PNF plan area boundaries in northeast NSW indicates that most (93%) of the forest areas in the northeast with PNF plans have slopes below 30 degrees (Table 5). Approximately 7% of the total PNF area was found to have a slope greater than 30 degrees, which should be excluded from harvesting. Note that approved areas in a PNF plan do not represent the net harvestable area and may include exclusion areas where harvesting operations are prohibited (e.g., steep slopes, riparian buffers).

Table 5. Area (ha) and percent of PNF plan approved areas in each slope class in northeast NSW according to NSW Spatial Services ALS data.

Slope class	Area (ha)	Percent
0-10	172,055	36.3
10-20	155,454	32.8
20-30	114,268	24.1
30-40	30,506	6.4

40-50	2,141	0.5
> 50	200	0.04

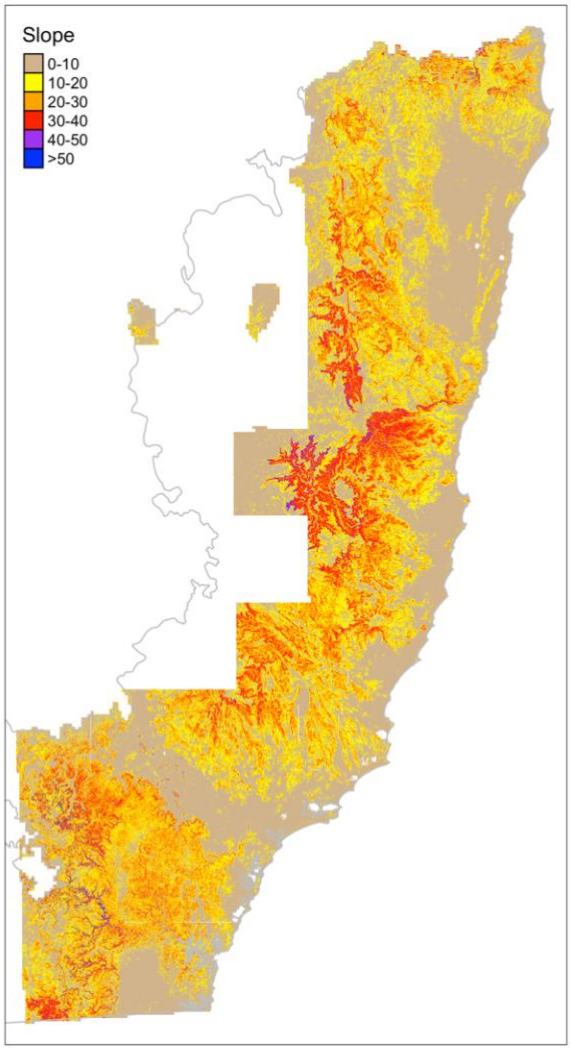

Figure 19. Slope class layer derived from NSW Spatial Services ALS data

Key takeaways

Calculating slopes from a DTM is a reasonably straightforward process. Results can vary depending on the quality and resolution of the DTM so it should not be assumed that the slope layer is 100% accurate.

Opportunities for further work

Noting the overlap with compliance functions, consider if this indicator may be more appropriate to use as a compliance tool.

The slope exclusion areas (greater than 30 degrees) could be cross-referenced with known harvest areas (e.g., from Section 2.2) to calculate the percentage that are maintained.

3.2. Riparian exclusion areas

Introduction

Harvesting operations are prohibited in areas close to streams, which protects the riparian areas from erosion and debris entering the waterways. Existing stream order data exists across NSW[4], where stream order refers to the number of upstream tributaries each stream has. This dataset is not 100% accurate and therefore if high-resolution ALS data exists, it may be preferable to use it to produce a more accurate map of riparian exclusion areas.

Here, we demonstrate the processing steps required to create a stream order dataset from a digital terrain model (DTM). There are a range of algorithms in different software packages available for extracting streams from a DTM (e.g., hydrology toolsets in ArcGIS, watershed functions in GRASS GIS, flow accumulation tools from Whitebox Geospatial). The standard process used by the algorithms is calculate the flow direction of each pixel in relation to its neighbours and use this information to calculate the flow accumulation across multiple pixels (Figure 20). By setting relevant minimum accumulation thresholds a representation of the stream network can be generated.

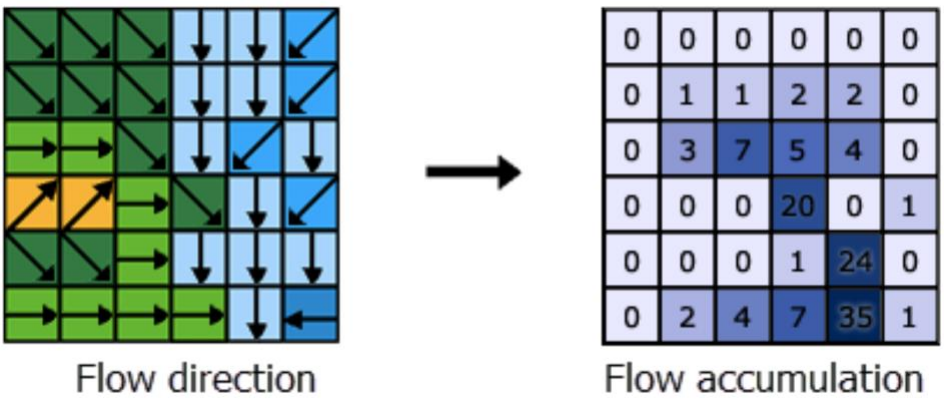

Figure 20. Example of flow direction and its relationship to flow accumulation. *Source:* *ESRI ArcGIS Pro help*

Methods

A worked example of the required process is presented here, using a combination of Whitebox tools, GRASS GIS functions and R (Figure 21). Firstly, the flow accumulation and direction were calculated using a DTM (here a high-resolution 1m DTM was used). Following this process, the streams were extracted using the *extract_streams* Whitebox function. In this function, a threshold value needs to be defined, which refers to the minimum value in the flow accumulation raster that is accepted as a stream. Here, a value of 2000 was used, which was chosen using trial and error. Following the stream extraction process, the streams were ordered according to the Strahler stream ordering method (specified in the PNF codes). This ordering system means that streams with no others flowing into them are termed 1st order, streams with one other flowing into them are 2nd order and so on. Generally, the higher the order, the larger the stream will be. Note that the threshold flow accumulation value will also influence the stream ordering. If a higher threshold value is used, then streams may end up with a lower stream order value.

The stream order raster was converted to a vector dataset using GRASS GIS, as this function appeared to produce a superior output than the Whitebox equivalent. The streams were then

[4] https://spatial.industry.nsw.gov.au/arcgis/rest/services/PUBLIC/StreamOrder/MapServer

smoothed to remove jagged artifacts before buffers were applied using the R package *sf*. As specified in the codes, 1st order streams were given a 10m buffer, 2nd order 20m and 3rd order or higher 30m. These buffered areas represent riparian exclusion zones.

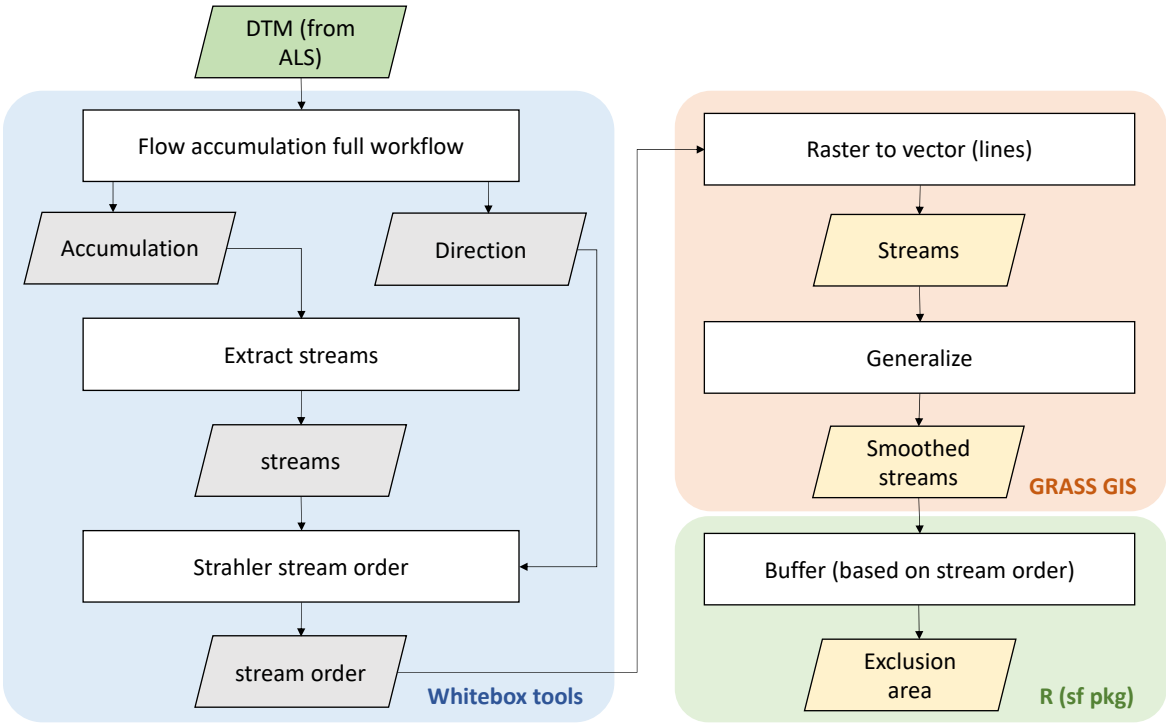

Figure 21. Workflow for creating the riparian exclusion areas from a LiDAR derived DTM.

Results & discussion

Example results from four of the steps in the workflow are shown in Figure 22. A comparison between the streams generated through this process and those in an existing state-wide dataset are shown in Figure 23. This highlights that, depending on the base product and processing decisions made, results can vary significantly. This is important from the perspective of exclusion areas being accurately monitored, as there may be discrepancies between on-ground harvesting operations and mapped streams.

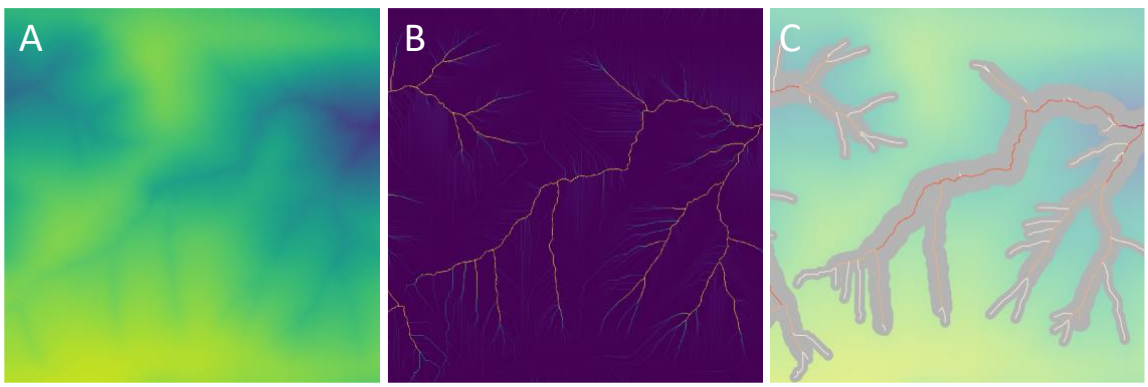

Figure 22. Example of a 1m DTM (A), flow accumulation raster (B), and derived stream order and exclusion areas based on specified buffer distances (C).

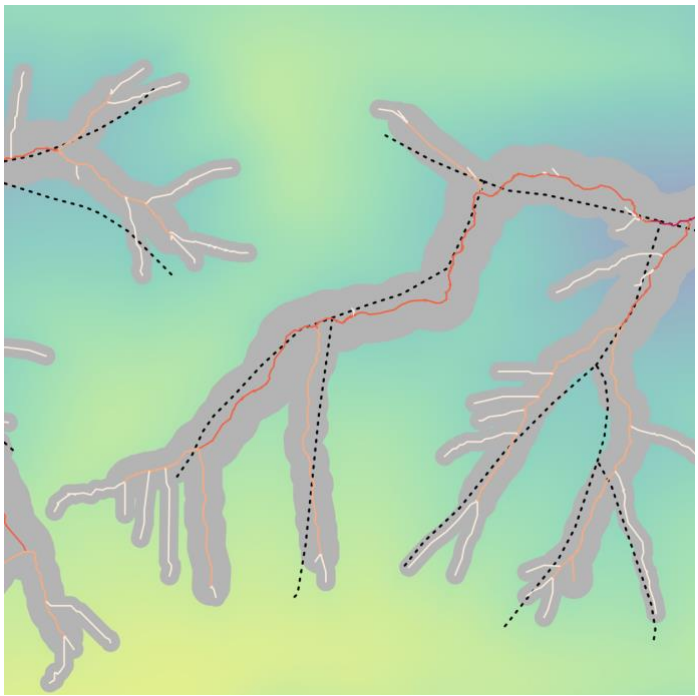

Figure 23. Comparison of the streams generated from the 1m DTM and an existing state-wide stream order dataset (dashed black lines)

Key takeaways

An accurate DTM derived from high resolution ALS is likely to produce the most accurate stream network. However, if this is not available, existing stream order data could be used.

Opportunities for further work

Noting the overlap with compliance functions, consider if this indicator may be more appropriate to use as a compliance tool.

The buffered stream order data could be cross-referenced with known harvest areas (e.g., from Section 2.2) to calculate the percentage of riparian exclusion areas that are maintained.

3.3. Roads and tracks

Farm and forest tracks crossing ephemeral and perennial streams, particularly those that are poorly designed and constructed, may cause a reduction in the water quality of NSW's headwater streams. Roads and tracks are a cumulative problem for water quality – once they are constructed, they are very rarely removed. Lidar data offers a way of assessing whether this problem is significant in PNF and whether or not the problem is increasing. Airborne LiDAR has the ability to penetrate the forest canopy and provide an accurate model of the ground (i.e., a DTM). With high density ALS, tracks can be identified, including temporary tracks made for harvesting operations. With two ALS captures (e.g., pre- and post-harvest), the difference between too DTMs can be undertaken, in a similar vein to the difference in CHMs discussed previously (Section 2.2). Differences could be quantified as a means of monitoring ground-based disturbance, where removals may equal new tracks or other types of soil erosion and additions could be from debris build-up. However, manual interpretation would be needed to assign a causal agent to these disturbances. Also note that differences may not

be true change, as there will always be a small amount of noise in the data, due to sensor scan angles, positional inaccuracies etc.

While automated methods for extracting streams from DTMs (Section 3.2) are reasonably well established and conceptually simple, methods for extracting roads or tracks are far less advanced. Here, we provide examples of the information available in DTMs for highlighting areas of change and indicating forest tracks which are often not visible in aerial imagery (i.e., shaded by tree canopies). Figure 24 shows DTMs from the 2020 and 2021 ALS data. To the naked eye, there is no discernible difference, however if we subtract one raster from the other, differences (in the range of 1-2m) are apparent (Figure 24-C).

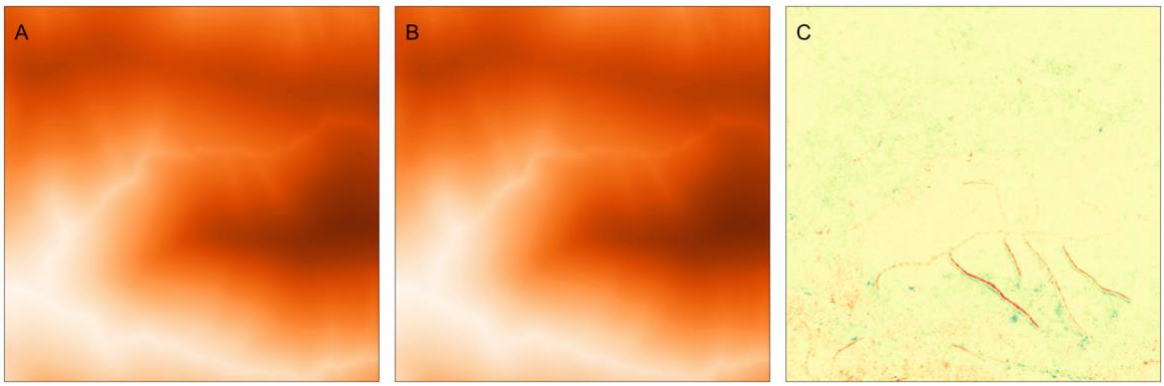

Figure 24. DTM from 2020 (A), DTM from 2021 (B), difference between DTMs (C), where red is a negative change and green is a positive change

To more easily visualise features in DTMs, hillshade rasters can be created (Figure 25). This method uses the slope and aspect layers (derived from DTMs) and a hypothetical sun angle to assign a shade value to each pixel. In Figure 25, example hillshade rasters in a harvesting area for 2020 and 2021 are shown. These indicate that the main tracks run along ridge lines, with some smaller tracks and drainage features also apparent. The tracks in these examples do not appear to intersect drainage lines (i.e., the gullies).

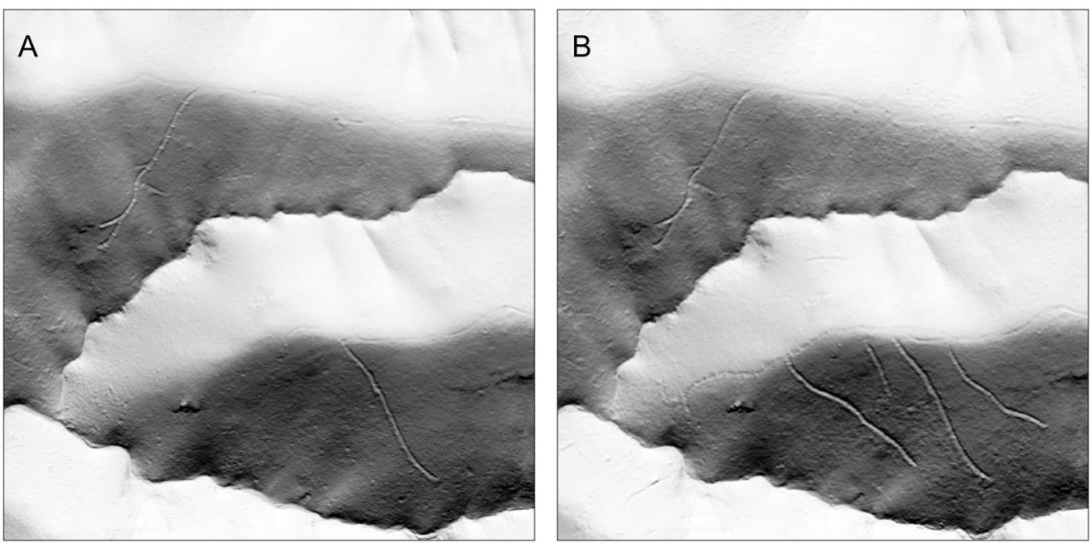

Figure 25. Hillshade images derived from the DTMs for 2020 (A) and 2021 (B)

As mentioned above, automated methods for extracting roads and tracks from LiDAR DTMs are not readily available. Therefore, it is recommended that monitoring tracks in relation to drainage

features is undertaken through a manual image interpretation exercise. It is not feasible to do this across all properties (or areas), therefore a random sample of locations should be selected for interpretation. A well-designed sampling framework should satisfy the requirements of a monitoring program, as the samples will be representative of the population as a whole.

Key takeaways

ALS data can highlight tracks under the forest canopy, however automatically extracting these is challenging.

Manual interpretation methods may be the most pragmatic and accurate means for determining tracks with ALS data. A random sample (e.g., 30-50 properties) may be sufficient for monitoring purposes.

Opportunities for further work

Noting the potential overlap with compliance functions, consider if this indicator may be more appropriate to use as a compliance tool.

To utilise ALS in the context of forest tracks and their impact on monitoring outcomes around water quality, an appropriate 'indicator' needs to be determined. For example, the number or percentage of tracks intersection drainage lines.

4. Remote sensing satellite indicators

In this section, bioregional scale indicators are presented using satellite derived information, including existing data products from the Australian government and the NSW Department of Climate Change, Energy, the Environment and Water (DCCEEW; formerly DPE) and NSW Department of Primary Industries.

Bioregional scale indicators provide contextual information relating to landscape scale forest conditions and trends. PNF occurs within this broad context and bioregional indicators can support interpretation of monitoring program results.

4.1. Spatial connectivity using the National Forest and Sparse Woody Vegetation data

The National Forest and Sparse Woody Vegetation data is an annual Australia wide forest and sparse woody extent product produced by the Australian Government Department of Climate Change, Energy, the Environment and Water (DCCEEW)[5]. The product is based on Landsat data (~25m resolution) and contains 3 classes representing forest (> 20% canopy cover and >2m in height), sparse woody vegetation (canopy cover between 5% and 19%) and non-forest. Here, we used only the forest class to create a binary forest/non-forest cover product.

A simple workflow is presented here to demonstrate how a forest extent layer can be used to represent forest connectivity. Note that connectivity is difficult to define and dependent on the data's spatial resolution and scale of interest. Originally, we planned to use LiDAR derived CHMs at a 1m resolution to look at connectivity at the site scale. However, because PNF plans only cover forested areas, the whole area within plan boundaries is more-or-less connected at that scale, with

[5] https://data.gov.au/dataset/ds-dga-b0d6b762-fe24-4873-91bd-ae0a8bbb452e

only small gaps, as shown in Section 2.3. Hence a regional representation of the northeast NSW is demonstrated here. We stress that the analysis presented is not intended to be an ecologically appropriate connectivity calculation, just a way to illustrate a process, the types of decisions and assumptions that could be applied in the analysis, and to illustrate how the results could be presented. The northeast region (also used in the earlier ALS examples) is 12.3 million hectares in area, of which approximately 60% is forest.

Connectivity, as used here, is the inverse of fragmentation. Fragmentation in turn can be represented by the number and size of forest 'patches'. Using the R package *landscapemetrics* (based on the FRAGSTATS program), the forest extent layers from 1988-2022 were converted into layers where each discrete patch of connected pixels is given a unique value. The number of discrete patches of forest across the region can then be counted (Figure 26). Here, we have discarded patches less than 1 ha in size, as these were considered irrelevant for the purpose of this exercise. The number of forest patches in northeast NSW was found to be around 62,000 and has remained fairly stable across the last three decades.

Each unique forest patch can then be given a value equal to total area of the connected pixels in the patch. We then need to define a minimum area of forest to label as 'connected' forest (Figure 27). Here, a value of 1,000 ha was used as an example, but this value is arbitrary and is context dependent. Different fauna species would have different requirements with respect to forest connectivity and their ability to move throughout the landscape. Note that an enormous expanse of forest in this region (over 4.3 Mha) is connected based on the assumptions applied, despite it containing plenty of gaps. This broad assessment should not be used to consider species specific habitat requirements.

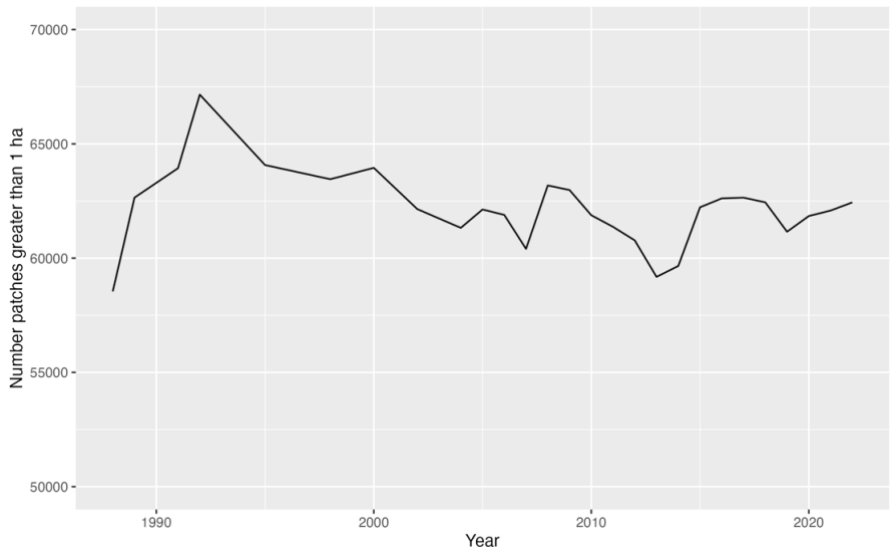

Figure 26. Number of forest patches greater than 1 ha in northeast NSW between 1988 and 2022, according to the National Forest and Sparse Woody Vegetation data

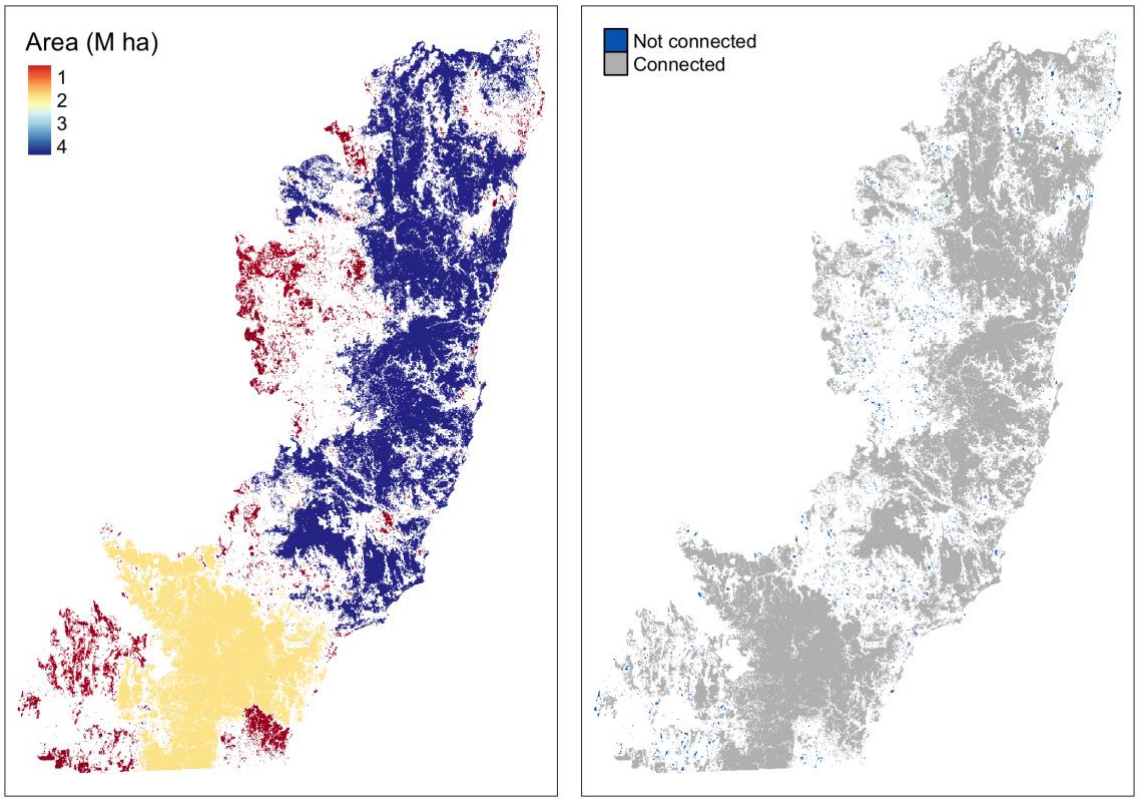

Figure 27. Area of forest patches in northeast NSW with connected pixels (left) and a representation of connected and disconnected forest patches using a 1000 ha threshold value (right)

By intersecting the connected forest layer with the PNF plan areas, we can quantify the proportion of these forests that are connected to the surrounding environment. Using the connectivity layer from 2022, around 98% of the forest within PNF plan areas in northeast NSW was considered connected. The connectivity assessment undertaken here is a simplistic representation of connectivity to demonstrate a process. In the Biodiversity Indicator Program (BIP), connectivity/fragmentation is addressed more holistically in NSW through the indicators Ecological Connectivity of Terrestrial Habitat and Ecological Carrying Capacity of Terrestrial Habitat[6]. The datasets supporting these indicators are available on SEED[7]. An example is given in Figure 28. At this stage, these products are only available at a single time step. If more time steps become available, the products will be able to be used to look at changes through time and potentially used for monitoring purposes.

[6] https://www.environment.nsw.gov.au/-/media/OEH/Corporate-Site/Documents/Animals-and-plants/Biodiversity/Biodiversity-Indicator-Program/biodiversity-outlook-report-first-assessment-200621.pdf
[7] https://datasets.seed.nsw.gov.au/dataset/biodiversity-indicator-program-data-packages

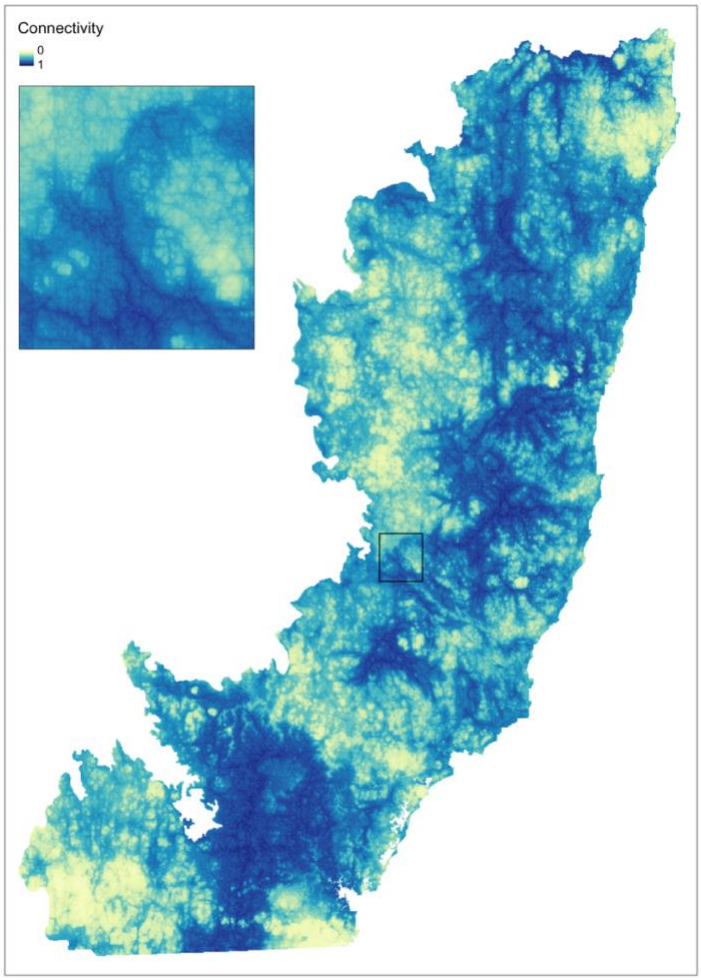

Figure 28. Ecological Connectivity of Terrestrial Habitat from the Biodiversity Indicator Program

Key takeaways

PNF harvesting is unlikely to lead to large changes in forest connectivity. Although canopy gaps are temporarily created, large scale fragmentation would only occur if the PNF codes are not being followed.

The BIP indicators and derived products should be considered moving forward, particularly if these products will be produced at regular time-steps.

4.2. Satellite derived tree loss using the Statewide Landcover and Tree Study (SLATS) data

The main objective of the Statewide Landcover and Tree Study (SLATS) Woody Vegetation Change is to map the location and extent of woody vegetation clearing each year across NSW[8]. This has been achieved over the last three decades using various satellite imagery sources (Landsat, SPOT and more recently Sentinel-2). In the SLATS data, woody vegetation loss is classified into four categories: natural, agricultural, infrastructure and forestry. As indicated in the SLATS documentation,

[8] https://www.environment.nsw.gov.au/topics/animals-and-plants/native-vegetation/landcover-science/2021-nsw-vegetation-clearing-report

"assignment of these classes is primarily based on visual interpretation of the location and the pattern of the clearing with reference to supporting data sources such as tenure." SLATS data from 1988–2020 is currently publicly available. The dataset for 2021 is not yet publicly available but was provided for this analysis.

Here, we spatially intersected the SLATS data from 2017–2021 (which is based on 10m Sentinel-2 satellite imagery) with the PNF plan boundaries provided by Local Land Services (LLS). An area of loss was calculated for each class and year by summing the pixels. Figure 29 shows an example of SLATS tree-loss data compared with ALS-derived tree-loss data (see Section 2.2) for an area of private forest where recent harvesting has occurred.

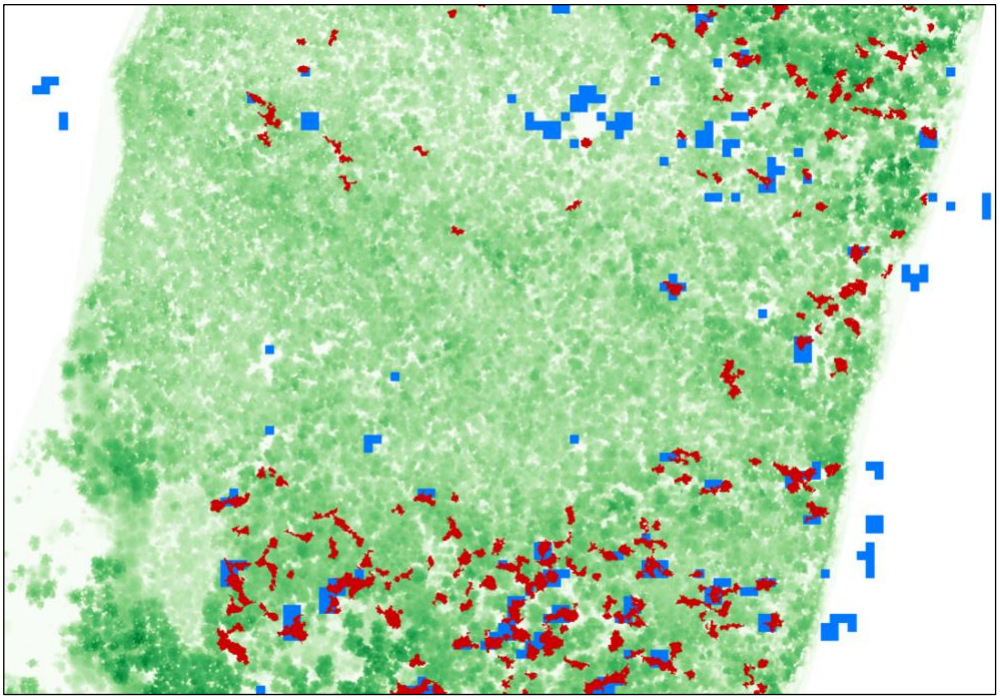

Figure 29. Example of SLATS tree loss data (blue) compared with the ALS-derived tree loss (red) on an example PNF property, with the CHM from 2020 shown in green. Note that the pre- and post-dates for both datasets do not perfectly align.

Results from intersecting the SLATS data with the PNF plan areas are shown in Table 6 (whole of NSW) and Table 7 (northeast NSW). Note that northeast NSW contains a large proportion of the approved PNF plan areas, which is reflected in the values in Table 7 making up a considerable proportion of the state-wide values.

The SLATS area value for the forest class for northeast NSW for 2020 (1264 ha) is not too dissimilar to that estimated by Hislop *et al.* (2024) using the multi-date ALS samples, which was 1665 ha (± 492). Note that a direct comparison cannot be made due to the time period not aligning exactly (the ALS was from April 2020 and April 2021), while SLATS is nominally based on a calendar year (this is not exact and depends on image availability). Based on the limited assessment undertaken here, SLATS appears to be picking up a reasonable amount of the higher intensity harvesting events. Detecting low intensity harvesting with moderate resolution satellites like Sentinel-2 is likely not possible. Hislop *et al.* (2024) indicated that many of the lighter harvesting events were not even visually apparent in Sentinel-2 data.

Table 6. Area (ha) of tree loss in PNF plan areas across NSW according to SLATS data

Year	Natural	Agricultural	Infrastructure	Forestry	Total
2017	335	80	94	885	1,393
2018	76	119	115	757	1,067
2019	30,072	116	155	592	30,935
2020	4,462	35	122	1,550	6,170
2021*	1	30	75	1,346	1,452

*provided by NSW DCCEEW for use in this project

Table 7. Area (ha) of tree loss in PNF plan areas in northeast NSW according to SLATS data

Year	Natural	Agricultural	Infrastructure	Forestry	Total
2017	334	72	77	806	1,290
2018	58	88	70	603	819
2019	29,789	89	126	439	30,444
2020	3,385	19	62	1,264	4,730
2021	1	27	62	942	1,032

Key takeaways

The SLATS Woody Vegetation Change product based on 10m Sentinel-2 satellite imagery appears to capture a reasonable proportion of PNF harvesting and is likely more effective for higher intensity harvesting. SLATS data will not be able to accurately capture small scale or low intensity harvesting.

Intersecting the yearly SLATS products with active PNF plan areas is a straightforward exercise to provide rough estimates of area harvested, however an understanding of capabilities and limitations is necessary.

Opportunities for further work

SLATS could potentially be extended (or calibrated) to focus more directly on PNF harvesting related woody change. Regardless of whether this occurs, using SLATS in conjunction with ALS data, collected within a statistically robust sampling design, will likely yield more reliable results.

4.3. Fire disturbance using the Fire Extent and Severity Mapping (FESM) data

The NSW Fire Extent and Severity Mapping (FESM) program provides annual maps of fire extent and severity across NSW at 10m spatial resolution[9]. It is based on a machine learning model that uses Sentinel-2 imagery trained with manually interpreted high-resolution aerial imagery (Gibson *et al.* 2020). The fire severity classes are outlined in Table 8. FESM products are available from 2016/17 onwards (note that 2016/17 is based on Landsat-8 data).

Table 8. Description of the five fire severity classes presented in the FESM products

Severity class	Description
Unburnt	Unburnt surface with green canopy
Low	Burnt surface with unburnt canopy
Moderate	Partial canopy scorch
High	Full canopy scorch (± partial canopy consumption)
Extreme	Full canopy consumption

Here, we intersected the FESM data layers from the 2018/19 fire season onwards with the current PNF plan area boundaries (~650,000 ha) to provide an estimate of the area of forest within the relevant properties that was disturbed by fire over the last five years (Table 9).

Table 9. Area (ha) of PNF plan areas (state-wide) disturbed by fire in each FESM severity class

Year	Low	Moderate	High	Extreme	Total
2018-19	8,499	9,960	3,040	354	21,853
2019-20	47,558	67,593	44,618	29,750	189,520
2020-21	504	569	146	13	1,232
2021-22	348	300	61	3	713
2022-23	336	220	53	6	615

Due largely to the extreme fire season of 2019-20, the area of PNF forest impacted by fire in recent years is substantial (~40%). Note that subsequent analysis of post-fire recovery with satellite-derived spectral indices has indicated much of the coastal northeast in particular has shown strong spectral recovery (e.g., Gibson and Hislop 2022; Gibson *et al.* 2022; Hislop *et al.* 2023).

Key takeaways

The FESM products offer a means of assessing fire severity across broad areas. It is important to recognise that, as a modelled product primarily based on Sentinel-2 imagery, it is not 100% accurate and may not be appropriate for site scale monitoring.

Since the focus of FESM is to map wildfires, it is unlikely to be suitable for characterising sub-canopy fuel reduction burns.

[9] https://datasets.seed.nsw.gov.au/dataset/fire-extent-and-severity-mapping-fesm

4.4. Drought and fire disturbance and recovery using satellite time-series

The 2018–2019 drought in southeast Australia led to the unprecedented wildfires during the second half of 2019 and into 2020. In addition to the large areas of forest that burned, there was significant canopy collapse from the drought itself, leading to dieback and some tree mortality. Using Sentinel-2 satellite imagery, Hislop *et al.* (2023) attempted to map the location areas of forest that were impacted by the drought, including areas which were later burnt by wildfire.

Monitoring forest disturbance and recovery across broad areas using satellite time series is now well established, with several time series change detection algorithms in existence (e.g., Hermosilla *et al.* 2015, White *et al.* 2017). However, many of these algorithms are based on an annual time series with a focus on longer historical time-frames (and therefore use Landsat data). Because Hislop *et al.* (2023) aimed to map multiple disturbances (e.g., drought and fire) in a short time-period, a higher frequency time series was required. The authors therefore developed a method which used a monthly time series of Sentinel-2 satellite imagery. A brief summary is given here and the outputs are intersected with PNF plan areas to provide summary statistics. More information on using satellite time series to investigate structural recovery is provided in Appendix 1.4.

Figure 30 indicates the approach that was applied to each individual pixel. Firstly, baseline pre-drought conditions were established, based on the mean and standard deviation of the Normalized Burn Ratio (NBR) index from 2016–2018. Following this, monthly median values for each month from August 2019 onwards were calculated. These were then converted into z-values (secondary y-axis in Figure 30) based on the formula $z = \frac{x - \mu}{\sigma}$.

Bioregion specific thresholds were used to determine if and when the pixel first became 'disturbed', and this was cross-referenced with known fire locations and timings to indicate whether the disturbance was due to drought or fire (or both drought and fire). The resultant map of disturbed areas is shown in Figure 31. This figure also indicates the time-frame that disturbed areas spent under the threshold at different latitude slices. This visual shows that areas in the north were impacted earlier and spent slightly less time under the threshold than areas in the south.

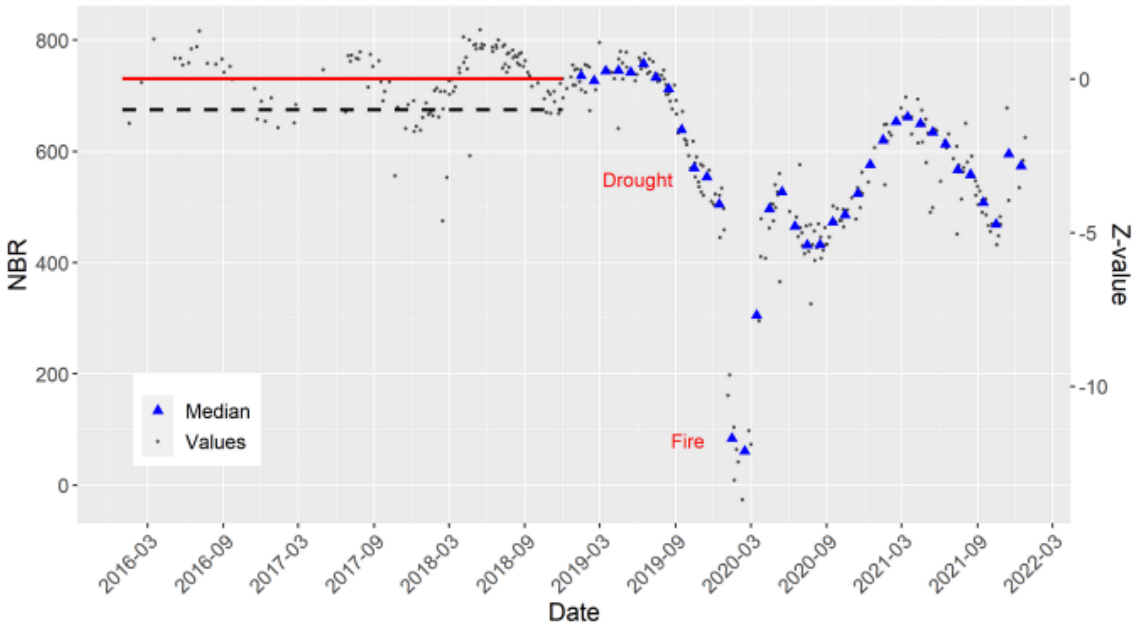

Figure 30. Example of an individual pixel through time. Sentinel-2 NBR values are shown in grey and the monthly median values for 2019 onward in blue. The horizontal lines are the mean and standard deviation for the stable period (2016-2018), used to calculate the z-scores (from Hislop *et al.* 2023).

The intersection of the drought extent map with PNF plan areas showed that a significant proportion of PNF plan areas were affected by either drought or fire or both during 2019 and early 2020, with only 24% classified as not disturbed (Table 10).

Table 10. Area and percentage of PNF plan areas disturbed in the 2019–2020 drought and wildfires, according to Hislop *et al.* (2023). Note that this covers over 90% of PNF plan areas.

Disturbance class	Area (ha)	Percent
Not disturbed	144,322	24.2
Fire only	152,658	25.6
Drought only	216,515	36.3
Drought and fire	75,767	12.7
Fire (previous year)	6,472	1.1

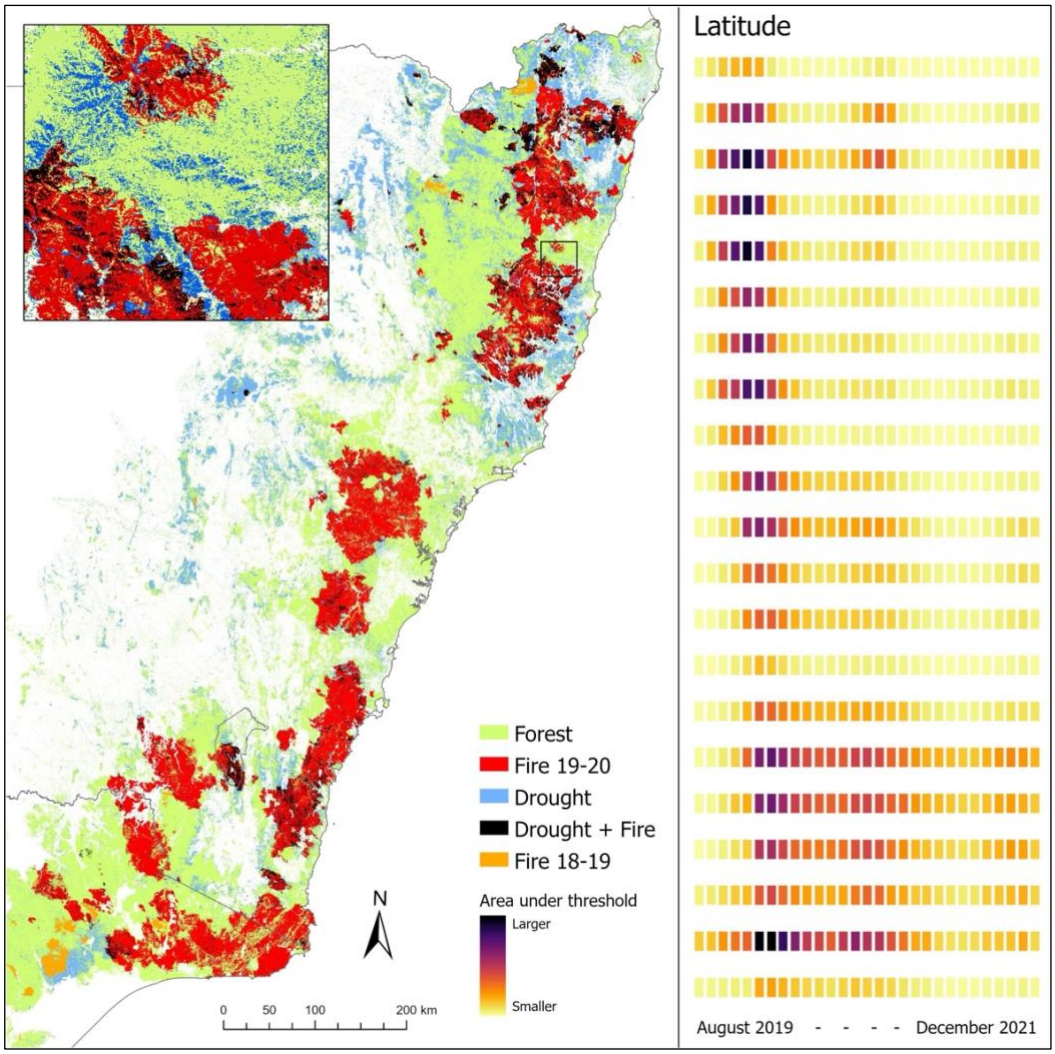

Figure 31. Map of disturbed areas in each class and the corresponding aggregated areas of disturbance across 50 km slices of latitude, where the darker colours indicate a greater area under the threshold. A zoomed in map of a small area is also shown (from Hislop *et al.* 2023).

In Hislop *et al.* (2023), forest recovery was explored further by extracting 50,000 random pixel samples in five classes and comparing the z-values across three different years – the year of disturbance, 1-year post-disturbance and 2-years post disturbance (Figure 32). This analysis suggested that most areas had substantially recovered spectrally from both the drought and fires after two years, a finding that was echoed by Gibson and Hislop (2022) in their initial assessment of forest recovery in wildfire impacted areas. Note that spectral recovery (that is, what satellites such as Landsat and Sentinel-2 remotely sense) does not equal structural or functional recovery. However, it has been shown to act as a reasonable proxy (e.g., White *et al.* 2019), and in the absence of other information may be suitable for broadscale assessments.

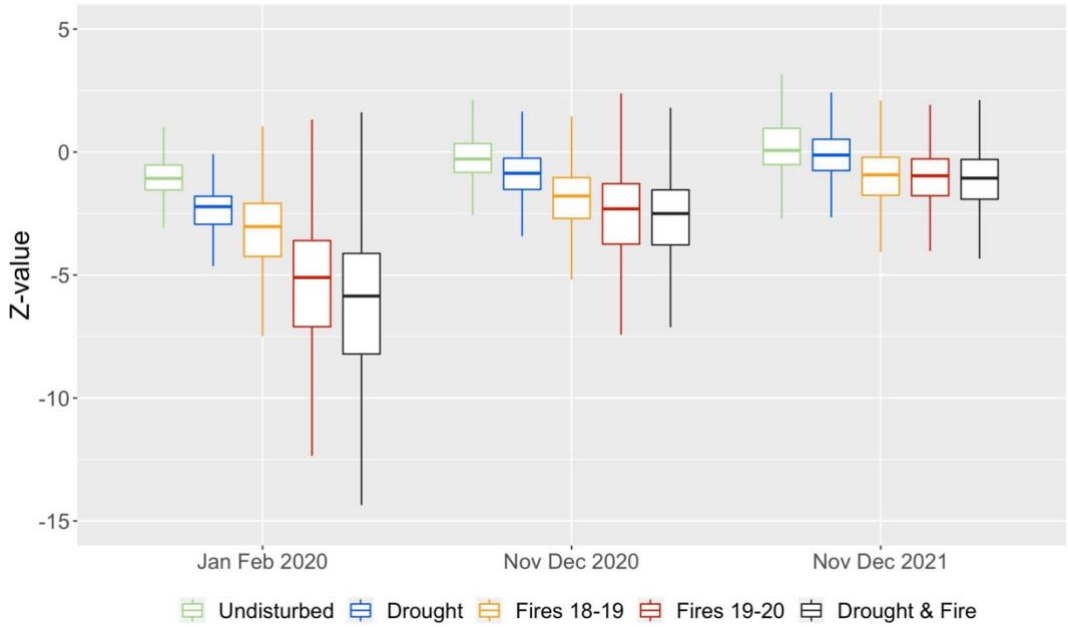

Figure 32. Boxplots showing z-values of 50,000 samples for the four disturbed categories and an undisturbed category in January–February 2020, November–December 2020 (~1 year recovery) and November–December 2021 (~2 years recovery) (from Hislop *et al.* 2023).

Key takeaways

Spectral time series with moderate resolution satellites (e.g., Landsat, Sentinel-2) has an established track record in broadscale forest monitoring, particularly with respect to characterising large abrupt disturbances such as wildfire and clear-fell harvesting. Techniques to track post-disturbance recovery are advancing but still developing.

The methods outlined here (Hislop *et al.* 2032) represent a new approach for investigating large scale drought impacts. Further research is required in this domain.

Moderate resolution spectral time series is limited in its ability to accurately represent forest regeneration after selective harvesting.

Opportunities for further research

There are many avenues for ongoing research in this domain. One obvious area is to look at ways to link structural recovery from multi-date LiDAR with the spectral recovery from satellites.

5. Conclusion

This report shows that a multitude of remote sensing systems exist, which can provide data that can be analysed to provide results related to the structure and condition of native forests. However, no single system can provide all the necessary data suitable for the multi-scale spatial requirements being considered for the PNF MER (i.e., at both site and bioregional scales). Appropriate coverage at all the necessary spatial scales requires the acquisition of data from multiple platforms (including field data), collected within a statistically defendable sampling strategy.

This report has also demonstrated that numerous data workflows are available to derive a large suite of potential indicators. However, while it is now possible to generate these results, it is also

important that the interpretation of results is linked to forest management. This requires knowledge of the temporal behaviour of forests at both site and bioregional scales, and how various attributes are reflected in specific indicators at a given point in time.

The use of remote sensing for forest monitoring is increasingly being used across the world to compliment traditional field-based inventory plots. While sensors and systems are continuously improving, there will always be limitations in what can be reliably measured and the accuracy of such measurements.

The worked examples and potential indicators presented in this report should act as a starting point for further development and analysis in the context of PNF monitoring with remote sensing. The techniques and data presented offer many opportunities for further research questions to be explored. However, this would likely require more open data policies, additional funding and scientific curiosity.

Appendix 1. Low feasibility indicators: background information

In this section, background information based on existing literature for an additional four potential remote sensing indicators is presented. These indicators are seen as low feasibility, due to high costs, difficulties in implementation and the use of emerging technologies. These indicators may be valuable to consider in future, as technology and knowledge advances.

1.1. Vertical connectivity

The vertical connectivity of vegetation is an integral component of forest structure and includes both canopy and understorey structure. Understorey structure has major implication for stand regeneration and wildlife habitat selection. Several of the LiDAR metrics identified as useful in describing structural complexity (Section 2.1) can also be applied in the evaluation of vertical connectivity, including metrics derived from LiDAR height profiling based on a series of percentile heights and a suite of structural complexity metrics (see Appendix 2 for further information). LiDAR height profiling can directly quantify vertical foliage distribution, which includes the forest subcanopy elements. Listopad *et al.* (2015) argues that height profiles derived from high resolution LiDAR have a variety of ecological applications, including characterising successional stages and predicting species richness.

Note, however, that the relationship between vertical profiles of LiDAR returns and vertical canopy profiles is complex and governed by factors like scan angle, leaf angle distribution, presence of non-photosynthetic vegetation, foliar clumping and stand structure. Hence the preference of some researchers for working with Leaf Area Density (LAD) profiles (or Plant Area Density (PAD) profiles; Figure A1).

The creation of LAD profiles is now a common approach to characterize the vertical distribution patterns of vegetation captured by ALS data (Bouvier *et al.* 2015). The LAD at a given height (z) is related to the ratio between the number returns below z and the total number of returns. The LAD values can be viewed as the decomposition of the Leaf Area Index (LAI) among the vertical strata so the LAI can be calculated as the LAD values obtained along the vertical profile. This standardized approach, however, is reliant on a uniform distribution of the LiDAR point cloud. De Almeida *et al.* (2020), for example, calculated LiDAR LAD profiles using 4 m^3 voxels (2 x 2m horizontal resolution and 1m vertical resolution) using only 1^{st} returns within 5^0 of scan nadir view angle. Fortunately, improving the homogeneity of point clouds can be achieved through various methods (see Appendix 2).

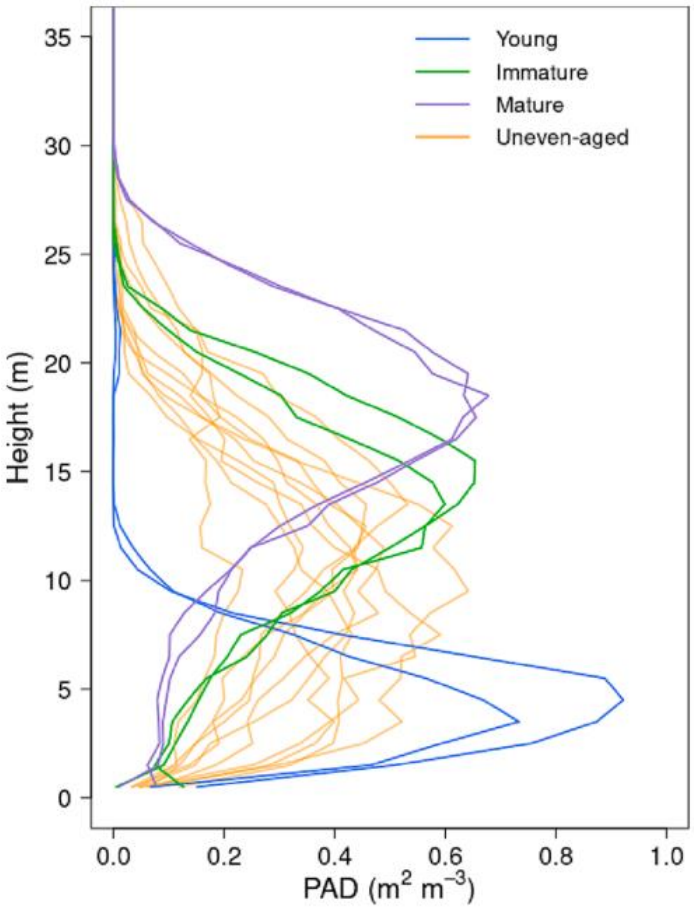

Figure A1. Illustrating Plant Area Density (PAD) profiles of different forest management types, from Aalto et al. (2023)

Jiang (2020) extracted height percentiles and the density of points within height classes to provide canopy profile models for a comparison of eucalypt forest structure in the Central Highlands of Victoria. The density of points was assumed to represent foliage density in different height strata and used to examine the connectivity between vertical layers. In another study, Jiang (in Stone & Hislop 2022) presented a new canopy profile model to characterize vertical structure. Instead of using gap fraction at given height (z), she directly used the projection coverage of point clouds to represent the foliage density for that height level (z), called foliage coverage profile. The projection coverage of points at given height (z) can be adjusted by the voxel size of point clouds.

Using a voxel-based approach of dense Mobile Laser Scanning (MLS) data, Puletti *et al.* (2021) derived several LiDAR metrics to estimate vegetation presence or absence in four different forest strata ranging from 0.5m to 10m from the ground in order to characterise four spatial density and inhomogeneity of understorey forest structure at these four horizontal height classes. The acquired MLS point clouds were first normalized using the TLSNormalize function in the TreesLS R package (deConto *et al.* 2017). From these results a Plant Vegetation Index (PVI) was then computed as the sum of vegetated voxels over their total number. The PVIs were then used to derive strata Plant Density Indices (PDI) at a broader scale following the defined understorey height classes. In a similar study mapping understorey vegetation in an Italian native forest, Ferrara *et al.* (2023) acquired MLS LiDAR data and used the *TreeLS* R package to voxelise and compute vegetation presence-absence and detailed vertical density profiles from which he aggregated into PDI values per strata forest floor (0.5–1m), shrubs (1–2m), lower understorey (2–5m), upper understorey (5–10m) and subcanopy (> 10m).

Some authors (e.g., Ehbrecht *et al.* 2016) advocate for the value of a single descriptor of vertical structure as opposed to profiles describing foliage distribution. For example, the structural indicator Foliage Height Diversity (FHD), which is based on the Shannon diversity index but instead of species and their abundances, it uses foliage height profiles and the proportions of plant material in the profiles, i.e.,

$$FHD = -\sum_{i} p_i \times \log p_i$$

Where p_i is the proportion of total foliage, or LiDAR returns, in the vertical layer *i.* Alternatively it can be calculated as the proportion of the PAD in the *i*th vertical layer to the total PAD. To address some of the challenges with interpreting FHD, Ehbrecht *et al.* (2016) proposed an index called the Effective of Number of Layers (ENL) (Appendix 2).

In addition, Listopad *et al.* (2015) also proposed two vertical structural indices based on a modified Shannon diversity index and modified Evenness index which describe vertical height diversity. When comparing forest stands with differing fire frequencies, they observed an increase in both indices with a decrease in fire frequency.

Table A1. A list of LiDAR derived indicators which have been considered useful indicators for monitoring the vertical structure of forests. Details are provided in Appendix 2.

LiDAR indicators
Height profiles of height percentiles
Height profiles of LAD/PAD (or LAI/PAI)
SD & CoV of height percentiles
SD & CoV of LAD/PAD vertical distributions
Kurtosis & Skewness of height percentiles
Kurtosis & Skewness LAD/PAD of vertical distributions
Canopy Relief Ratio
Foliage Height Diversity (= Height Evenness Index)
Effective Number of Layers

Fire fuel estimates

Assessment of vertical connectivity is also an important of fire fuel load estimates. Hillman *et al.* (2021) used Remotely Piloted Airborne Systems (RPAS, also referred to as UAVs or drones) LiDAR point clouds acquired over a dry sclerophyll forest to relate the arrangement of fuel over the vertical profile to fuel properties in all strata. They also developed a method that identifies vegetation connectivity. They initially normalised the point cloud density using a 2cm binary voxel space indicating the presence or absence of vegetation before applying a vertical layer pouring algorithm. The vertical layer pouring algorithm was then used to identify the connection between different vegetation layers, which considers any element that is directly adjacent or overlapping with a higher strata layer to be a part of that layer. Each voxel is assigned a unique identifier depending on its

connectiveness to neighbouring voxels, both horizontally and vertically and the procedure is repeated from the top down. Each voxel is then assigned to a strata class based on the Victorian Overall Fuel Hazard Assessment Guide (OFHAG; Victorian Department of Sustainability & Environment, 2010) height thresholds.

Application of Radar to estimate vertical structure

While LiDAR allows for the characterization of vegetation structure in the vertical profile, the limited temporal availability of ALS data prevents its routine use for analysis of post disturbance recovery trajectories. On the other hand, satellite Synthetic Aperture Radar (SAR) backscatter data is readily available from several satellite platforms including Sentinel-1. Depending on the wavelength of the instrument, the SAR signal can penetrate and interact with forest canopy components to characterise forest structure.

Fernandez-Guisuraga *et al.* (2022) monitored the vertical structural diversity (VSD, based on the proportion of vegetation cover in various height strata) within a fire-affected native forest in Spain. Through the fusion of C-band SAR data (from Sentinel-1) and multispectral data (from Sentinel-2), the authors modelled VSD using Random Forests. The best performing model accurately explained VSD in unburned control plots (R^2 = 87 and RSME = 0.16) and burned plots 1 year after fire (R^2 = 80 and RMSE = 0.13). However, the authors acknowledged that for forests with higher canopy closure and biomass, the use of SAR sensors with longer wavelengths such as PALSAR-2 L-band onboard the ALOS-2 satellite would be able to better penetrate forest canopies.

Application of GEDI to estimate vertical structure

Finally, numerous studies have used data from the Global Ecosystem Dynamics Investigation (GEDI) instrument onboard the International Space Station (ISS) for assessing canopy height, profile metrics and biomass. An r package 'rGEDI' is now available for visualizating and processing GEDI Level1B, Level2A and Level2B data (Silva *et al.* 2021). Hirschmugl *et al.* (2023), for example, assessed vertical forest structure in the Austrian Alps using both ALS and GEDI data. They used the GEDI waveform data (L2B) (25 m) to derive Foliage Height Diversity (FHD) (Clawges *et al.* 2008) and the effective Number of Layers (ENL) (Ehbrecht *et al.* 2016) metrics. They concluded that while GEDI data are suitable for deriving vertical forest structure, there are limitations due to the limited resolution (each pulse sample has a footprint of ~25 m). They recommend that the full potential of GEDI waveform data for vertical forest structure assessments has not yet been realised.

In another study evaluating GEDI data for estimating vertical connectivity in forests, Huettermann in Stone & Hislop (2022) utilised simulated GEDI observations to compare height characteristics between 3 classes of fire severity, one year after the 2019-20 wildfires in coastal NSW forests based on different Relative Height metrics. Examination of the Relative Height profiles indicated that initial recovery following the wildfire (i.e., the first few months) may have been more pronounced in the upper canopy, which was then followed by more regrowth in the lower and mid-stories as stand recovery progressed.

1.2. Dead tree crowns

Standing dead trees have a unique ecological role, contributing directly to forest biodiversity through, for example, the provision of fauna habitat (Owens *et al.* 2014, Miltiadou *et al.* 2018). Of particular interest is the location of habitat trees, including old, dying, or dead trees with hollows. Currently, it is not possible to use remote sensing to directly map tree hollows with confidence. However, partial success has been achieved using modelling approaches that model 'probability' of tree hollows. Direct detection can potentially be achieved with high-resolution LiDAR or cameras and advanced machine-learning modelling

approaches, but this research is in its infancy and requires further validation in eucalypt forests.

Figure A2. Aerial photograph over a stand of dead and dying trees affected by Bell Miner Associated Dieback (Silver & Carnegie 2017)

Aerial interpretation

Traditionally, qualitative assessment of tree mortality has been achieved through aerial reconnaissance. This requires expert visual interpretation of forest canopy decline from the aircraft, often associated with sketch mapping of the extent of impacts. The sketches are then digitised and entered into a GIS (A. Carnegie, NSW DPI Forest Science, *pers. comm*.). A well-established alternative has been the manual interpretation (Aerial Photographic Interpretation; API) of imagery acquired by piloted aircraft. Trained interpreters can accurately identify and map individual dead tree crowns, however, this requires the expertise and specialist photogrammetric software and hardware.

Mapping tree mortality using multispectral data

Airborne digital multispectral imagery has been used to detect and classify canopy damage using machine learning approaches, including the detection of dead and dying trees in plantations or homogeneous native forests. For example, Windrim *et al.* (2020) demonstrated the benefits of combining multiple data formats based on airborne multi-spectral photogrammetry, including photogrammetric point clouds and rasterised canopy height information, for detecting dead trees in a *Pinus radiata* plantation.

Canopy dieback in native forests has also been mapped using spectral satellite imagery, with better results achieved with high spatial resolution data. Murfitt *et al.* (2016), for example, used the object-based software eCognition and a watershed crown delineation algorithm to

segment individual native ash tree crowns in WorldView-2 (4 band, 2 m) imagery before applying a series of vegetation indices to each segmented tree crown.

It is possible to utilise lower spatial resolution satellite imagery to detect and map canopy dieback, but these datasets are often augmented with other sources of spatial information. For example, Haywood & Stone (2011) were successful in modelling and mapping dead and dying trees in areas affected by Bell Miner Associated Dieback (Figure A2), using predictors derived from 10m multispectral SPOT5 imagery and co-incident ALS data and topographic derived variables. The most influential predictor variables included an image textural statistic based on the SWIR band and the ALS derived Coefficient of Variation, Skewness, and the 10th and 90th height percentiles.

Use of RPAS imagery to detect individual dead and dying trees

Recently, Remotely Piloted Aircraft Systems (RPAS) have been evaluated for small-scale forest health assessments (Ecke *et al*. 2022, Estrada *et al*. 2023). Both aircraft and RPAS operate at much lower altitudes than satellites and so can provide very high spatial resolution (< 10 cm). This more easily permits tree level detection and segmentation to classify the health of individual tree crowns. This object-based approach reduces spectral noise from non-tree crown elements such as understorey vegetation. Importantly, very high resolution imagery acquired by RPAS or aircraft is now often used as a source of reference (training/calibration/validation) data for scaling up modelled parameters based on regional scale satellite imagery (e.g., Abdollahnejad *et al.* 2021).

Significant advances have been made in the automatic detection and modelling of dead standing trees in high resolution imagery (Sylvain *et al.* 2019). The application of deep learning applications is revolutionizing object detection and classification in high resolution imagery (e.g., Zhao *et al.* 2023, Appendix 2). These deep learning approaches have proven to be more robust to occlusion and complex scenes than traditional machine learning modelling such as Random Forests.

Jiang *et al.* (2023), for example, successfully applied a customised Faster-RCNN framework to detect dead standing trees in UAV imagery acquired over dense native forest in China, achieving an overall accuracy of 95.5%. In a similar study, Sani-Mohammed *et al.* (2022) applied a Mask R-CNN deep learning approach to 20 cm airborne imagery to locate standing dead trees in a dense native forest in Germany, achieving accuracy of over 85%.

While deep learning models are improving our ability to automatically detect old, dying, and dead trees in complex forested scenes, they are very data 'hungry' and require a significant amount of image annotation to calibrate the models, which is labour intensive. Fortunately, there are now approaches to help with this process – for example, through leveraging of pre-trained deep learning models, data augmentation or the application of synthetic imagery (Grondin *et al.* 2022, Zhao *et al.* 2023).

Application of LiDAR data to detect dead and dying trees

In recent years, studies have evaluated the use of ALS data in relation to detecting dead or dying trees for applications such as the estimation of dead biomass, forest health assessment and wildlife habitat studies (Casas *et al.* 2016). However, due to irregular patterns and distribution of dead and dying trees, traditional area-based approaches often

result in inaccurate density estimates, therefore tree-based approaches have been preferred (Jutras-Perreault *et al.* 2023).

Traditional tree crown delineation approaches such as local maxima filtering are often inaccurate due to the irregular tree shapes presented by dead standing trees (Miltiadou *et al.* 2018). However, the 3D information obtained from LiDAR has proven to be more successful. Miltiadou *et al.* (2020), for example, investigated the possibility of detecting dead eucalypt trees from voxelised LiDAR through the extraction of features from cylindrical 3D windows using field data for training and the k-NN classifier.

By comparing the tree-level plant area density profiles between foliage only (PAD_f) and stem only (PAD_s) point clouds, Ruizhu (in Stone & Hislop 2022) found that standing stag or dead-top trees could be identified. For the PAD_s of stag trees, there is no clear height break in PAD_s but there is a clear height break in PAD_f. In addition, for stags, the total PAD above half the tree height is higher for the stem only than the foliage only. In contrast, for healthy live trees, the opposite behaviour is observed (Figure A3).

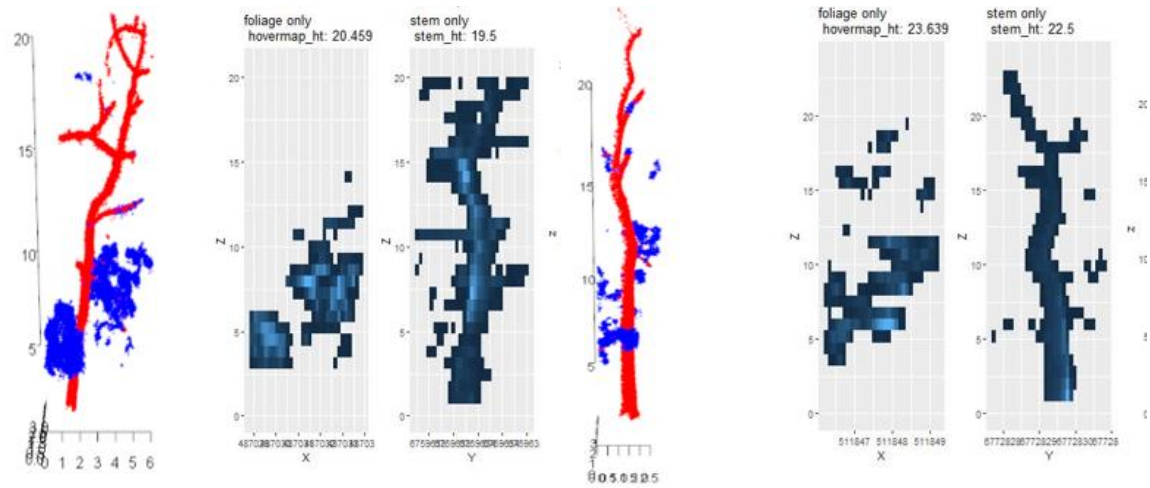

Figure A3. Examples of tree-scale PAD profiles derived from FSCT segmented foliage only and stem only of dying trees in a coastal NSW forest (Jiang in Stone & Hislop 2022).

In another study in New Zealand, Meiforth *et al.* (2020) investigated the use of pan-sharpened WorldView-2 satellite imagery (1.8 m) and LiDAR data for detecting damage symptoms, individual kauri trees affected by the disease *Pytophthora agathidicida*. They concluded that notwithstanding issues related to misalignment between WV2 and the LiDAR, the combination of both datasets improved damaged crown detection compared to only WV2 attributes for all tested use cases.

Owens *et al.* (2014) also evaluated the combination of multispectral aerial imagery and ALS data, in a study looking at detecting hollow bearing trees in eucalypt forests. They manually delineated individual tree crowns and applied maximum-likelihood classification on spectral values for classifying tree senescence levels while tree crown density estimates were obtained from a 10m height threshold ALS-derived CHM. This was because the strong correlation with hollow-bearing potential was the stage of tree senescence. Both the imagery and ALS demonstrated capabilities in separating mature trees into five senescence classes.

1.3. Compositional complexity

Forest composition refers to the different species of plants that make up a forest. As a gross generalization, we could say that greater composition complexity is desirable. However, this is site dependent and certainly weeds and non-native species are undesirable.

NSW DPE continues to update its State Vegetation Type Mapping (SVTM). This program provides current maps of the three levels of vegetation classification hierarchy: Plant Community Type, Vegetation Class and Vegetation Formation. Another approach to mapping the composition of forests is focused on classifying the dominant canopy (i.e., the assemblages of mature trees) into principal forest types (Baur 1965). Based on the Baur's description of forest types, aerial photo interpretation (API) has been used to map these tree assemblages across some NSW forests. A subsequent process has been used to classify the forest types into groupings called Yield Association Groups (YAGs). YAGs are defined by the tree canopy species mix, elevation above sea level, site wetness and canopy height of mature trees (A. Kathuria, Biometrician, NSW DPI, *pers comm*.). A report on the YAG classification across all forest tenures for the NSW north coast was made available on-line by NSW DPI in 2018. This modelling approach is currently being replicated for the NSW south coast. Another valuable source on tree species is the NSW BioNet Vegetation Information System. For example, tree species records extracted from BioNet have been used for the predictive modelling of koala tree species, a key parameter for koala habitat information.

Traditionally, the mapping of forest composition has been undertaken at the stand scale using stereo aerial photography and manual API. Skilled API operators can accurately map forest types, especially when presented with unclear boundaries. Unfortunately, at present in NSW, neither stereo aerial photography nor ALS data are supported by a systematic acquisition program.

The application of satellite spectral data for mapping tree species over regional forests has been successfully demonstrated overseas. For example, Melnky *et al.* (2023) successfully developed classifiers of forest species using Sentinel-2 images in north-western Ukraine. Ferreira *et al.* (2019) used high resolution imagery acquired by WorldView-3 and applied an individual tree crown-based approach to classify large, distinct tree crowns in a tropical forest in south-eastern Brazil. They demonstrated that in addition to the spectral information, texture analysis of the panchromatic band was useful for distinguishing species-specific differences in crown structure.

Closed-canopy, sclerophyll forests in eastern NSW are dominated by eucalypts, with the species within subgenus groupings being taxonomically and structurally very similar. Under these circumstances the mapping of eucalypt tree species is possible but requires very high spectral and spatial resolution data, in particular hyperspectral data. For example, Shang & Chisholm (2013) successfully applied airborne hyperspectral imagery and machine learning to classify seven eucalypt species in a native forest near Jervis Bay, achieving a classification accuracy of 94.7%. While not yet considered operationally feasible in Australia, recent studies overseas have achieved accurate tree species classification using hyperspectral data (Yel & Gormus 2023).

In Germany, Shi *et al.* (2018) evaluated a large suite of LiDAR metrics derived from ALS data for mapping tree species. Interestingly they found that radiometric features such as return

intensity were more influential than the geometric features. They also suggested that a higher point density would provide more species-specific structural information.

Several studies have also successfully classified tree species through the fusion of hyperspectral data and 3D data (either LiDAR or stereo photogrammetry) (Mäyra *et al.* 2021) and the application of machine deep learning models (Sothe *et al.* 2020). Mäyra *et al.* (2021), for example, presented a workflow for tree species classification from high resolution hyperspectral and LiDAR imagery to produce accurate tree species maps. In particular, they demonstrated that the deep learning CNN models outperformed the traditional machine learning methods. Their best performing 3D-CNN model achieved an F1-score of 0.86.

Finally, in addition to the species identification and mapping of individual trees, several approaches have emerged to assess plant biodiversity more generically via remote sensing. One approach is often related to the Spectral Variability Hypothesis (SVH) (Fassnacht *et al.* 2022). The general tenet of the SVH is that the biodiversity of a given area is positively related to the spectral variation of the same area. The R package 'biodivMapR', for example, is designed to compute a selection of α- and β-diversity indicators from optical imagery (airborne and satellite), based on the SVH (Feret & Boissieu 2019).

It is now acknowledged, however, that the SVH does not hold true across all spatial scales and ecosystems. Seasonal phenotypic variation can challenge a stable link between spectral variation and biodiversity. Nevertheless, if repeatable, standardised spectral variation metrics are identified, it is a concept worth evaluating in Australian native forests.

1.4. Structural recovery

Forest recovery is a process not a state, with the recovery of structure, composition and function manifesting gradually through successional stages following disturbance. The nature and rate of forest recovery can relate to several factors including the type and severity of disturbance and the inherent productivity of the site. Definitions of forest recovery often involve the use of terms such as regeneration and regrowth, including the re-establishment of forest biomass and canopy structure (Bartels 2016). In an ecological or silvicultural context, this often implies the re-establishment of forests over time, and can be quantified by measurements of canopy cover, height, basal area, and stem density. Undertaking manual ground-based recovery measurements over large areas is not a feasible option, however time series analysis of multi-spectral satellite imagery provides a viable and cost-effective solution for capturing broad-scale observations of forest disturbance and recovery.

Monitoring forest disturbance and recovery using satellite time series is now well established, with several time series change detection algorithms in existence. The algorithms attempt to examine individual pixels through time and use statistical techniques to extract changes and trends, including recovery from disturbance (e.g., Hermosilla *et al.* 2015, White *et al.* 2017, Hislop *et al.* 2023). Several approaches have been developed including threshold-based change detection and trajectory segmentation. Threshold-based change detection requires a prerequisite threshold value to determine forest disturbances while trajectory-segmentation based approaches capture the trend based on information derived from the time series without the need for estimating thresholds. Two well established trajectory segmentation methods include LandTrendr (Kennedy *et al.* 2020) and

BFAST (Verbesselt *et al.* 2010). Both these algorithms distil often noisy time series into a simplified series of segments and provide a number of metrics that provide information on disturbance magnitude and regeneration (Banskota *et al.* 2014).

Numerous spectral indices and metrics have been proposed for use in these time series methods, including for assessment of post-disturbance vegetation recovery. While greenness indices such as NDVI can characterize the initial pulse of vegetation recovery, these indices saturate rapidly. In contrast, indices using the shortwave infrared (SWIR) bands, such as NBR, are more strongly linked to vegetation structure and hence provide an indication of increasing forest structural complexity associated with regenerating stands (White *et al.* 2017). Note that most high spatial resolution satellites do not contain SWIR bands, which gives satellites such as Landsat and Sentinel an advantage in this respect.

While spectral recovery is somewhat limited in its ability to represent structural recovery, studies have demonstrated it can act as a reasonable surrogate (White *et al.* 2019, 2022). White *et al*. (2019) characterized spectral trends using NBR and the Years to Recover (Y2R) metric to measure post-harvest forest recovery in southern Finland. The Y2R metric characterizes long-term forest regeneration and is defined as the number of years for a pixel to return to 80% of its pre-disturbance value. The authors found that the Y2R metric correlated strongly with forest structure and composition attributes measured in the field.

As presented in Section 3.4, Hislop *et al.* (2023) analysed a monthly time series of Sentinel-2 imagery to identify areas of eucalypt forest disturbed by drought and/or fire in NSW in 2019-20. They identified areas of forest where the NBR was significantly below a pre-disturbance 'stable' period. The stable period was defined as the 3 years prior to 2019 and the disturbance thresholds were based on bioregion specific number of standard deviations below the pre-disturbance mean (Figure 26, body of report). In both Hislop *et al.* (2023) and Gibson & Hislop (2022), it was shown that some NSW forest types could recover very quickly from fire and drought, especially after above average rainfall, while other forests recovered much more slowly (e.g., Alpine forests).

Chirici *et al* (2020) also demonstrated that Landsat NBR spectral trajectories could be used to assess forest recovery after timber harvesting in an Italian native forest. They applied the LandTrendr algorithm and defined Y2R as the number of years required for a pixel to attain 90% of its pre-disturbance fitted trend NBR value.

As an alternative to using a pre-disturbance baseline, Gibson *et al.* (2022) presented a method that looks at the rate of change of a spectral index post disturbance (the 'post-fire stability index'). Where the year-on-year change in the spectral signal is high, the forest is still considered to be recovering, whereas when the rate slows, the forest can be thought of as 'recovered'. Outputs from this method are now presented as yearly operational products in NSW, alongside the Fire Severity and Extent Mapping (FESM).

In addition to time series analysis using moderate spatial resolution imagery, Ireland *et al.* (2021) demonstrated the benefits of using higher spatial resolution imagery for monitoring targeted areas of forest recovery. They acquired imagery from Maxar's WorldView-2 and WorldView3 satellites over a 3-year period (2m multispectral bands pan sharpened to 0.5m). They reported that integrating spectral data with texture indices produced the best correlations with structural features like tree height and density.

Finally, to reiterate, spectral recovery as measured with a time series of optical satellite imagery is not a direct measure of forest recovery, whereas structural indicators of recovery such as height and density can be directly measured using ALS data. Bolton *et al.* (2015) recommended that using samples of ALS data is desirable to confirm the interpretation of spectral trends.

Appendix 2. Application of LiDAR data for assessing forest structure at the stand and tree level

This review highlights recent advances in analysing LiDAR data acquired from a range of platforms and processed to derive information that contributes to the characterisation of native forest structure at the stand and tree level.

2.1 Introduction

Successful native forest management requires information on forest structure and composition. A variety of connections exist between structure and ecosystem traits including biodiversity, habitat, previous disturbance, successional trajectories, water interception, carbon storage and productivity (Moran *et al*. 2018). This includes the structure of canopies as well as sub-canopy structure which can encompass suppressed mature trees, regenerating tree saplings, and understorey shrubs and small trees, herbs/grasses and CWD.

Forest structural elements have traditionally been assessed by manual field inventories. While tree stem measurements can reliably be obtained by field crew, estimates of plot/stand level attributes such as understorey density and cover, are often inaccurate, imprecise, and time-consuming. However, over the past 20 years, LiDAR systems, including LiDAR sensors on airborne (ALS), Remotely Piloted Airborne Systems (RPAS, also referred to as UAVs), mobile terrestrial (MLS) and static terrestrial (TLS) platforms, have been applied for the assessment of both stand-level and tree-level attributes.

2.2 Approaches to working with dense point cloud data

A key challenge of working with LiDAR data is that there often a large amount of spatial heterogeneity in the density of points over space and time. These density variations can directly impact on the of derived products (Petras *et al.* 2023). Point density variations arise from differing characteristics of the LiDAR sensor, observation geometry and vegetation properties. LiDAR sensors are continuously improving in performance often resulting in higher pulse densities arising from changes to the sensor specifications such as laser power level and laser pulse repetition rate. For example, the latest Emesent Hovermap unit, ST-X offers high density point clouds with improved range reaching to top of most forest canopies. However, in dense vegetation, issues with IMU drift still need to be addressed.

During data acquisition the density of LiDAR point clouds relates to the distance from the LiDAR sensors which leads to a different average density of points at different positions. Variations in sensor height, scan angle and platform movement can also influence the density and uniformity of the point cloud (e.g., Petras *et al.* 2023). Interestingly, van Lier *et al.* (2021) reported contrasting results with respect to the effect of ALS scan angle and specific ALS metrics and in fact the actual effects were more strongly influenced by specific forest structure. For example, occlusion from dense understorey has a major influence on LiDAR performance.

The requirement to consider these differences is even more challenging when comparing datasets acquired by very different platforms. For example, the study presented by Stone & Hislop (2022) showed that ALS and MLS (Hovermap) point clouds acquired in native

eucalypt forest are complimentary, due to one system operating from above and one from below, however merging the datasets was not attempted.

Point cloud co-registration is important for analysing multi-temporal data, especially for datasets acquired by different sensors and acquisition parameters. The use of ground control points (GCPs) is recommended. Additionally, co-registration of multiple point cloud datasets can be undertaken in a semi-automatic approach using the open-source software CloudCompare. It is also possible to align spatially co-incident LiDAR point clouds acquired by different platforms using the iterative closest point (ICP) algorithm which can be accessed in the software CloudCompare (Besl & McKay, 1992, Lee *et al.,* 2022, Arkin *et al.,* 2023).

There are, however, several approaches aimed at homogenization of the point densities and harmonizing point densities across a time series or spatially adjacent datasets. One approach is decimation which is a reduction in the number of points in a point cloud that preserves selected properties of the point cloud (Petras *et al.* 2023).

Another common approach aimed at homogenization of the point density is the application of voxels (=3D rasters, also referred to as binning) (Mathes *et al.* 2023).

2.3 Using voxels

LiDAR point clouds can be processed using area-based (pixels) approaches, (e.g., Canopy Height Model), voxel-based approaches or object-based approaches (Figure A4) (Bakx *et al.* 2019).

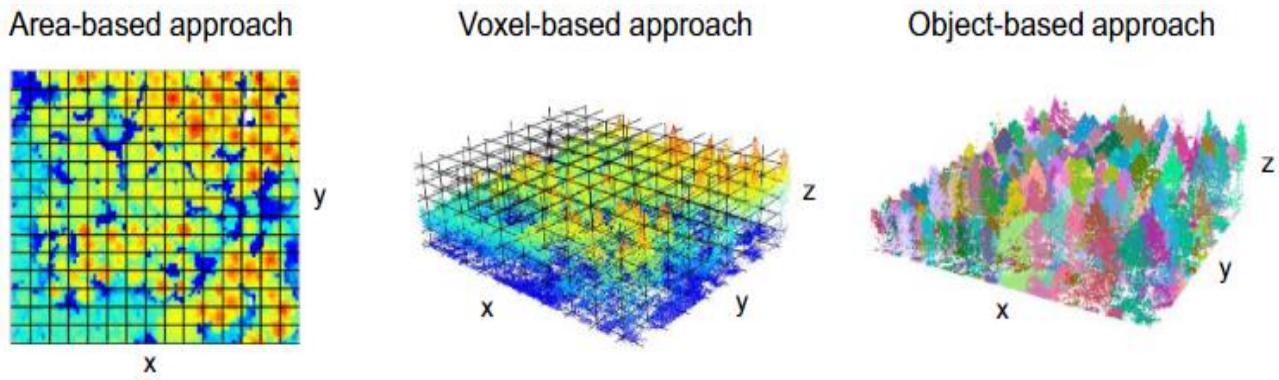

Figure A4. LiDAR point clouds can be processed using area-based approaches (i.e., rasterization into grid cell, voxel-based approaches (i.e., voxelization into 3-D voxels) or object-based approaches (e.g., segmentation into objects such as trees (from Bakx *et al.* 2019)

Voxels are commonly applied to reduce data density, as well as filtering the returns by selecting only the first or last returns. It is also possible to reduce point density through a decimate (thinning) function. Voxelization can also help address of occlusion. Mathes *et al.* (2023) concluded that voxelization of point clouds prior to the extraction of stand or tree measurements with a voxel size of a least 20cm was appropriate to reduce occlusion effects while still providing a high level of detail. Voxels are applied in the derivation of a large suite of LiDAR metrics. These voxel-based metrics are based on summarizing the LiDAR points that fall within each voxel and are directly influenced by the chosen voxel dimensions.

2.4 LiDAR metrics

Quantifying forest canopy structure as it varies in space and time requires metrics that capture both horizontal and vertical complexity. LiDAR-derived metrics are now recommended for the assessment of forest structure within multi-value forest management monitoring programs (Moudry *et al*. 2023). Vogeler *et al*. (2014), for example, demonstrated the relative importance of including LiDAR-derived metrics of vertical and horizontal structure in predicting bird species richness in two mixed conifer forests in Idaho, USA.

Numerous metrics have now been developed and applied to describe forest structure. These metrics can be categorised as being related to canopy cover, canopy height, height and density profiles and compound structural metrics (e.g., Figure A5). In general, relative measures of vegetation density or cover, where the number of returns in a vertical stratum are scaled to some measure of sampling density provide better estimates of both canopy and understorey vegetation than absolute values.

Below is a description of some of the LiDAR metrics that have been applied to characterise forest structure. They have been grouped into four categories: Canopy/stratum cover; Canopy height; Height and density profile metrics and stand structural complexity metrics.

Canopy/Stratum cover (or closure) metrics

Percentage canopy cover can be calculated based on the height (e.g., full profile or canopy stratum) and type of return for a specified ground cell size. For example, as the number of 1st returns above a certain height threshold (e.g., 2m) divided by all (or only 1st) returns x 100. Similarly, an understorey ratio is the total returns below a specified height threshold, that are not classified as ground, divided by all returns, including ground returns. Of note, van Lier *et al.* (2021) report that that these 2 metrics become unstable with increasing ALS scan angles.

Canopy height metrics

Common LiDAR height metrics include the canopy top height (=the 95th percentile height of 1st returns) and average canopy height (= average height of 1st returns). The 95th percentile height measurement is the height at which 95% of LiDAR returns fall below for each specified ground cell and is less sensitive to anomalously high points.

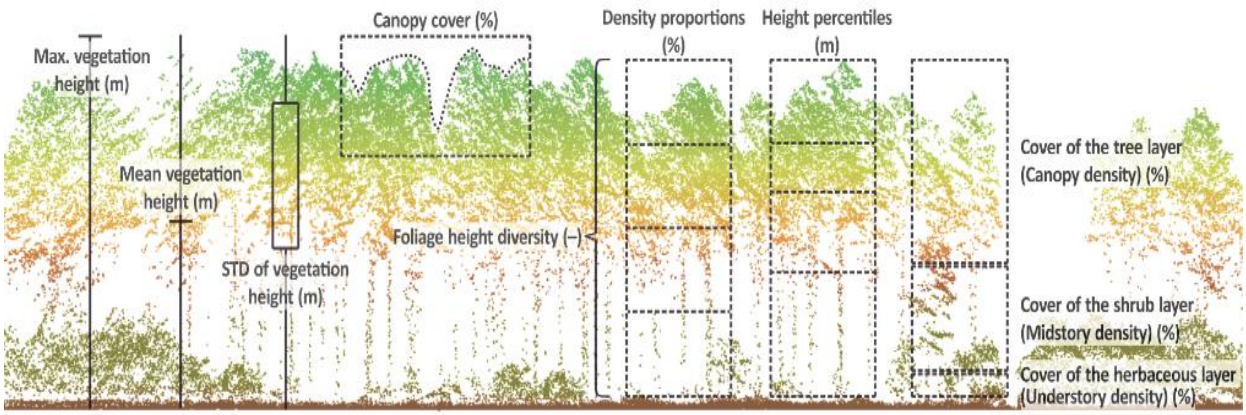

Figure A5. Illustration of some of the structural elements of forests that can be derived from LiDAR point cloud data (from Moudry *et al.* 2023).

Height and density vertical profile metrics

Canopy vertical profiles are curves of forest structural components as a function of height above ground and are considered important descriptors of forest structure. For example, vertical canopy strata density can be calculated as the % of LiDAR points between two heights, for example % of all returns between heights 5 – 10m.

Other height profile metrics

The Canopy Relief Ratio: This metric is the ratio of the difference between the mean and the minimum of LiDAR heights intersecting plot over the difference between the maximum and the minimum of LiDAR heights intersecting the plot (Gelabert *et al.* 2020). It describes the degree to which canopy surfaces are in the upper (> 0.5) or in the lower (< 0.5) portions of the height range (Torresan *et al.* 2016). Low values reflect canopy surfaces that are characterized by isolated relief features standing above extensive level surfaces, whereas higher values describe broad, somewhat level surfaces broken by occasional depressions. Karna *et al.* (2020) observed changes in the canopy relief ratio and rumple index (described below) consistent with a dominant stratum becoming more heterogeneous and fragmented after a severe fire in a native forest in the Central Highlands of south-eastern Victoria.

Weibull fitting approach: Several authors have applied distribution models to represent the vertical profile of vegetation structure in LiDAR data, such as the Weibull distribution function (Zhang *et al.* 2017). Distribution functions provide a mechanism to summarise complex canopy attributes into a short list of parameters that can be empirically analysed against stand characteristics. Jaskierniak *et al.* (2011) applied mixture models having a range of distribution functions to LiDAR height distributions to estimate plot level stand characteristics such as basal area and stand volume. Wilkes *et al.* (2016) proposed a mathematical approach that did not require some initial *a priori* knowledge. They applied vertically resolved gap probability that was aggregated over a plot that had been generalized with a nonparametric cubic spline regression for identifying the number of strata in within the height profile of native eucalypt forests.

Density profile metrics

Forest structure also directly relates to vertical dynamics of leaf density including tree canopy density metrics such as foliage projective cover (FPC) which is the proportion of horizontal area covered by the vertical projection of photosynthetic foliage for all vegetation taller than 2 m. FPC is closely related to Leaf Area Index (LAI) but can differ due to foliage clumping and leaf orientation. Fisher *et al.* (2020) using ALS data acquired over multiple Australian forests and woodlands and identified two ALS data metrics suitable for estimating FPC and the crown projective cover (CFC).

Another two ecologically important forest structural attributes that can be derived from LiDAR data include plant (or leaf) area index (PAI, LAI) (m^2/m^2) and plant (or leaf) density index (PAD, LAD) (m^2/m^3). The PAI and PAD consist of both woody and leaf materials while the LAI and LDI comprises only the foliar components. In general, it is more difficult to distinguish between leaf and woody components from ALS compared to TLS and MLS data (but refer to discussion below on new deep learning segmentation models). These two LiDAR derived attributes are now commonly used to characterize the vertical heterogeneity

of forest stands and have related to other aspects of forests. Carrasco *et al.* (2019), for example, demonstrated that ALS metrics based on LAD measurements had better explanatory power (43% of variance explained) than those based on the variation of canopy heights (32% of variance explained) when modelling bird species richness in native forests in northeast USA.

LAD profiles provide detailed information of forest canopy, subcanopy elements and individual trees. The leaf area density (LAD) metric estimates total leaf area per unit volume and requires the sampled space to be divided into voxels with a specified height (Δz) (Carrasco *et al.* 2019, de Almeida *et al.* 2019). The LAD is in fact the decomposition of the LAI among the vertical strata of the forest canopy.

The method commonly presented for deriving LAD profiles, commences with the first-return point cloud binned into voxels and the number of first returns within each voxel calculated. A vertical resolution of 1m is recommended to maximize the potential to derive vertical forest structure information (de Almeida *et al.* 2019). The MacArthur and Horn method relates the gap fraction (GF) to LAD (or LAI) and is applied to the voxelised columns of LiDAR returns (Kamoske *et al.* 2019). The GF is estimated by counting the number of returns above and below the target voxel *i* in a vertical column.

$$GF_i = -(N_{be}/(N_{tot}\ N_{ab}) \text{ and LAD for the voxel } I = LAD_i = -(\ln(GF_i)/k\ \Delta z$$

where N_{ab}=number of LiDAR returns above the voxel, N_{be} = number of returns below the voxel, N_{tot} = the total number of returns in the vertical column; k= coefficient of extinction (or sometimes referred to as the Beer-Lambert coefficient) and can vary between 0.28 to 0.67, and is often approximated as 0.5. (Carrasco *et al.* 2019, Kamoske *et al.* 2019, Roussel *et al.* 2020).

A value of 0.5 for k is commonly used in closed-canopy forest ecosystems (Kamoske *et al*. 2019). If k= 1 then it contributes to the estimation of 'effective LAD' (and 'effective LAI'). Occluded voxels are treated as no-data (where pulses out = 0 or pulses in = 0) and are not considered when calculating the mean LAD of a stratum (de Almeida *et al.* 2019). For the method presented by Kamoske *et al.* (2019), if there is not a ground return present, a NA value is assigned, and this column is not used in used in subsequent analysis. They conclude with the sum of LAD values in a column of voxels with a ground return is equal to the LAI of that vertical column. Values of strata LAD (or PAD) can then be compared over time by calculating the normalized Z-scores on a per pixel basis.

Importantly, these profile metrics can be estimated from ALS point clouds with R packages available on Github: akamoske/canopyLazR and DRAAlmeida/leafR (Table A2).

A salient assumption when deriving LAD profiles is that the ALS is acquired at a narrow off-nadir view angle and so each LiDAR pulse is vertically incident in order to calculate the pulses entering the tops of voxels and the pulses leaving the bottoms of voxels. When operating an MLS, it needs to maintain a vertical upward aim. All entering pulses not detected as returns from a voxel are assumed to pass through and enter the next voxel in a column. However, when appropriately calibrated with vegetation coefficients for a given LiDAR pulse density and for a particular grid size, LAD can provide reliable measurements of plant densities for all layers of the canopy.

De Almeida *et al*. (2019) evaluated the effects of LiDAR pulse density and horizontal grain (sampling) size of voxels on the estimation of LAD profiles and their associated LAIs over

tropical rainforest with destructive sampling, ground based LiDAR and ALS data. They reported that LAD profiles from ALS were concordant with destructive field sampling and MLS data when grain size < 10 m and pulse density > 15 pulses m^{-2}.

Other density related LiDAR metrics

Normalized relative point density: Another stratum-based density metric, also referred to as the normalized relative point density (NRD), was shown by Campbell *et al.* (2018) to be able to characterize understorey density. NRD characterizes point density as compared only to the number of points within a given height range and below.

Foliage Coverage Profile: To improve the accuracy of vertical profiles obtained from MLS datasets, Jiang in Stone & Hislop (2022), applied a new canopy profile model called the Foliage Coverage Profile to characterise the vertical structure. Instead of using Gap fraction at a given height (*z*), her approach used the projection coverage of point clouds to represent the foliage density for the height level (*z*), based on 10cm voxels. This is achieved by projecting the 3D points onto a 2D plane and then measuring the area covered by these projections. For a 10cm voxel, then each point represents a 10cm cube. At a given height (z), all point clouds within the vertical range between z and z+1 are considered.

Canopy rugosity: This metric represents the horizontal and vertical variance of leaf (or plant) density throughout the canopy (Atkins *et al.* 2018). It can be estimated using the R packages *canopyLazR* and *Forestr* (Table A2).

Clumping index: This metric is calculated as the effective Leaf Area Index over Leaf Area Index. It is considered a key variable for describing clumped spatial patterns within a canopy, with 1 indicating completely random distribution of crown returns down the profile or canopy stratum, and 0 indicating a high degree of aggregation. It could be assumed that the presence of epicormic foliage after a fire in native eucalypt forests would result in increasing values of this Clumping Index (Karna *et al.* 2020).

Stand structural complexity metrics

Numerous metrics have been derived that provide information related to the 3D structure of all strata present in a forest stand. The inclusion of height-based, cover-based and these compound structural metrics into predictive models of forest attributes such as habitat suitability have now been demonstrated. For example, in addition to the calculation of ALS metrics that describe forest height, height variability and cover, Jarron *et al.* (2020) also included more complex LiDAR metrics related to stand structural complexity into a regression model that classified sub-canopy components. Included for consideration in their modelling were the vertical complexity index (van Ewijk *et al.* 2011) and the vertical rumple index (Tompalski *et al.* 2015). Below is a brief description of some LiDAR-derived compound structural metrics that have been developed.

Skewness (asymmetry of distribution) & Kurtosis (peakedness of distribution): Metrics derived from height profiles such as skewness and kurtosis are commonly estimated for evaluating forest stand structure. Haywood & Stone (2011a) interpreted that positive skewness values were associated with sparse canopies and negative values with closed canopies when using ALS data to estimate structural attributes of mountain ash (*Eucalyptus regnans*) forests in Victoria. Bolton *et al.* (2015) applied ALS skewness and kurtosis to monitor forest recovery following wildfire disturbance in the western boreal region of

Canada. They reported that the presence of a few tall trees among a stand dominated by shorter, regenerating trees would have a positively skewed distribution. Alternatively, a dense, regenerating stand at a uniform height would display high kurtosis while a stand of trees with a mixed range of heights would have lower kurtosis.

Standard variation (SD) and Coefficient of variation (CV) of LAD/PAD (or LAI/PAI): where CV_{LAD} is the ratio of standard deviation of the LAD from the canopy profile over the LAD mean, with values between 0 and 1. The CoV indicates variability in the density distribution or volumetric packing of canopy components down the full canopy profile or canopy stratum per unit area (Karna *et al.* 2020). Lower values of CoV_{LAD} indicating less variability and greater evenness of density. For the standard deviation, small values arise from areas with homogenous vegetation, while high values reflect vertically heterogeneous vegetation (Moudry *et al.* (2022).

Rumple Index: This is the ratio of the three-dimensional canopy surface area to its projected ground area using all 1st returns per LiDAR plot. Provides an indication of vertical and horizontal variation in canopy structure that increases with roughness of the canopy surface and with structural heterogeneity (Kane *et al.* 2010, Roussel & Auty 2018).

Vertical Rumple Index: The vertical Rumple Index is based on the same principle as the Rumple Index however, it measures the complexity of the vertical structure of the stand, not the top of the canopy. Formula presented in Tompalski *et al.* (2015)

Vertical complexity index: This index describes the evenness of the vertical distribution of the points across the canopy layers (van Ewijk *et al.* 2011, Pearse *et al.* 2018). The VCI has a range of 0 – 1 where VCI = 0 signifies an even distribution of points across the canopy height and decreasing values state an increasingly uneven distribution. Jarron *et al.* (2020) calculated the VCI as the distribution of abundance of returns in 1 m height voxels.

Effective mean number of layers (ENL): This index describes the vertical structure based on the occupation of different vertical layers in relation to total space occupation of a stand. The point cloud is divided into different voxel layers and then each voxel layer is assessed based on the presence of points within them (Ehbrecht *et al.* 2016). For the ENL, increasing stand height and a more even occupation along the vertical profile result in higher values.

Foliage Height Diversity (FHD) (=Height Evenness index): This is a modified Shannon-Weiner diversity index (H') which is estimated from H = -SUM [(pi) * ln(pi)], where pi is the proportion of the total LiDAR returns that fall within a given height voxel. It is a measure of the vertical complexity of the canopy that describes how evenly the canopy is vertically distributed. Values close to 1 indicate completely even distribution of returns down the height profile (Clawges *et al.* 2008, Listopad *et al.* 2015). Using ALS data acquired over a Swiss native forest, Froideveaux *et al.* (2016) used the FHD to describe the degree of scatter of vegetation elements along the vertical forest profile. Of note is that both FHD and ENL metrics at 25m resolution can be derived from the L2B data acquired by the GEDI LiDAR sensor on board the International Space Station (e.g., Hirschmugl *et al.* 2023).

FCNSW Forest Structure Index: The Forestry Corporation of NSW has developed an in-house 'forest structure index' which resamples a 1m CHM to produce a surface representing canopy volume across a broader landscape. They have shown that this index in turn, can relate to sawlog grade volumes (T. Brown, *pers. comm*., FCNSW).

Table A2. List of software programs available for extracting forest structural metrics from LiDAR data

Package	Functions	Reference
lidR (R)	For ALS data manipulation and visualisation, e.g. • Computing canopy height models • Individual tree segmentation (raster-based watershed methods and from point cloud data)	Roussel *et al.* (2020)
forestr (R)	Deriving canopy structural metrics from ALS & MLS LiDAR data. e.g. • Leaf area index (LAD) • Rugosity • Rumple • Effective number of layers	Aikens *et al.* (2018)
leafR (R)	Estimates LAD and LAI from ALS data	De Almeida *et al.* (2019)
canopyLazR (R)	Estimates leaf area density (LAD) and leaf area index (LAI)	Kamoske *et al.* 2019)
TreesLS (R)	Uses dense point cloud data for automated tree stem detection and tree inventory parameters	De Conto *et al.* (2017 & 2019)
TREETOP (R)	Has functions that smooth, detect and delineate individual trees on a LiDAR-derived CHM and compute LiDAR metrics at plot and crown scales (Archived by CRAN but available in GitHub carlos-alberto-silva/rLiDAR	Silva *et al.* (2021)
FUSION/LDV	Open-source program for visualizing and analysis of LiDAR data including a function for watershed crown delineation	McGaughey (2021)
LAStools	Efficient tools for LiDAR processing	Isenburg (2013)

2.5 Use of high-resolution spatial data for stand and tree-level detection, segmentation and classification

The high density, point clouds acquired by LiDAR sensors and cameras attached to ground-based platforms, RPAS platforms and high-resolution systems on aircraft are suitable for object-based image analysis, in particular, the segmentation and characterization of individual tree stems which are then can be included in forest inventories (e.g., Hyyppä *et al.* 2020, Iqbal *et al.* (2021).

Individual tree detection (ITD) methods using LiDAR data can be grouped into two major types based on the input data they use: raster-based and point-cloud based. Raster-based ITD methods rely on gridded data, that provide summary information extracted from ALS points, such as minimum and maximum height of all returns within a cell. Point-cloud-based approaches identify individual trees using a variety of methods that take advantage of tree crown shape and spacing, and vertical and horizontal return density changes in the ALS point cloud (Sparks *et al.* 2022).

In addition, many of the LiDAR metrics mentioned above, that relate to the horizontal and vertical structure of forests at the stand level can also be applied to individual trees having been identified through tree crown segmentation. Karna *et al.* 2019, for example, calculated LiDAR metrics such as LAD profiles and the Height Evenness Index for individual trees.

Tree crown segmentation

As mentioned, a large array of methods has been developed for tree crown detection and delineation (Ke & Quackenbush 2011). For raster canopy surfaces (e.g., the CHM) this commonly includes applying a local maxima filter within a user-defined search window, followed by a region-growing algorithm to delineate tree crowns packaged as an algorithm such as the marker-control watershed tree delineation algorithm. This methodology has yielded favourable results for regular crown shapes (e.g., Chen *et al.* 2004). However, accuracies in tree crown segmentation can be improved when based on the point-cloud data rather than a pixel CHM (Iqbal *et al.* 2021). Both these approaches, however, are challenged with the presence of suppressed or young trees overtopped by dominant, mature trees. Several of these ITD methods have now been incorporated into open-source software including the R packages LidR and TREETOP, and the open source LiDAR processing and visualization software FUSION/LDV (Roussel *et al.* 2020, McGaughey 2021, Silva *et al.* 2021 (Table 11).

More recently, the introduction of data-driven, deep learning neural networks (a subclass of machine learning) has greatly enhanced the performance of remote sensing solutions for detecting and classifying objects in geospatial images. This includes the application of deep learning models to both high resolution 2D and 3D datasets for detecting, segmenting, and classifying individual tree crowns. These deep learning models use a series of hierarchical layers to learn directly from training data instead of using expert designed features (e.g., Weinstein *et al.* 2020). Numerous studies have demonstrated that they can have superior performance to traditional machine learning methods such as RandomForest or SVM, including the detection and delineation of tree crowns using wither 2D and 3D high resolution data (e.g., Straker, *et al.* 2023).

Unlike traditional ITC algorithms, these deep learning models do not rely on *a-priori* knowledge of the spatial distribution or crown size to parameterize the initial local maxima search. For 2D images such as a LiDAR CHM or multi-spectral imagery, CNN frameworks can be applied as either two-stage detectors (e.g., region-based convolutional neural networks) or one-stage detectors (e.g., You Only Look Once, YOLO). Straker *et al.* (2023) claim that deep learning models are highly adaptive and allow for the detection of trees independently of their spatial distribution and size. Hao *et al.* (2021), for example, included a NDVI-CHM combination into their Mask R-CNN workflow aimed at delineating tree-crowns and estimating associated heights of Chinese fir trees using UAV multispectral imagery. They

achieved an IoU = 91.3% for tree crown delineation and a R^2 = 0.87 for tree height assessment. In another study, applying Mask R-CNN to delineate tree crowns in a Brazilian forest, Braga *et al.* (2020) used WorldView-2 satellite imagery with 0.5m spatial resolution. They reported an average bounding box precision of 91% and a recall of 81%.

Tree stem segmentation

With the application of LiDAR Simultaneous Localization and Mapping (SLAM) technology, the detection and segmentation of individual tree stems in stands with dense canopy cover has rapidly advanced (Tang *et al.* 2015, Zhao *et al.* 2023). Accompanying the acquisition of dense point cloud data has been the automated processing techniques for determining stem points and measuring stem parameters. This has included circle-fitting algorithms such as the Hough Transform and RANdom SAmple Consensus (RANSAC) (Olofsson *et al.* 2014). The RANSAC algorithm assumes that points belonging to the same stem appear in the point cloud as arcs. It iteratively fits horizontal circles to a given set of points and chooses the best fit. These arcs and circles are then vertically aggregated to build the tree stems (de Paula Pires *et al.* 2022).

The R package 'TreesLS v2.0' has functions for both stem detection and segmentation (de Conto *et al.* 2019) based on the Hough Transform algorithm. For example, using LiDAR acquired by a GeoSLAM Zeb-Horizon in a Türkiye national park, Vatandaslar *et al.* (2023) processed their data in used the r packages lidR and TreesLS to detect and segment tree stems and they found no significant differences between inventory attributes obtained by conventional manual methods and the MLS-derived estimates, although estimation errors increased with stand dominated by smaller trees or dense understorey.

Another approach to the automatic segmentation of tree stems and branches based on dense point cloud data involves the application of Quantitative Structural Models (QSMs) (Raumonen *et al.* 2013). Although effective in many situations, both the circle-fitting algorithms and QSMs require significant effort in parameter tuning when applying the data across varying resolutions and forest types (Bryson *et al.* 2023).

However, supervised, deep learning models are becoming increasingly popular in the analysis of dense (3D) point clouds for segmenting and classifying 3D objects (e.g., Zhang *et al*. 2019). Semantic segmentation treats multiple objects within a single category as one entity whereas instance segmentation identifies individual objects within these categories. Numerous recent studies now present deep learning models that can automatically classify nontree points and segment points classified as trees or common elements such as separating tree foliage from tree woody biomass within a forest stand (referred to as semantic segmentation) and/or their respective individual structures, condition or composition (referred to as instance segmentation) from dense LiDAR and photogrammetric point clouds (e.g., Chang *et al.* 2022, Windrim & Bryson 2020, Figure A6).

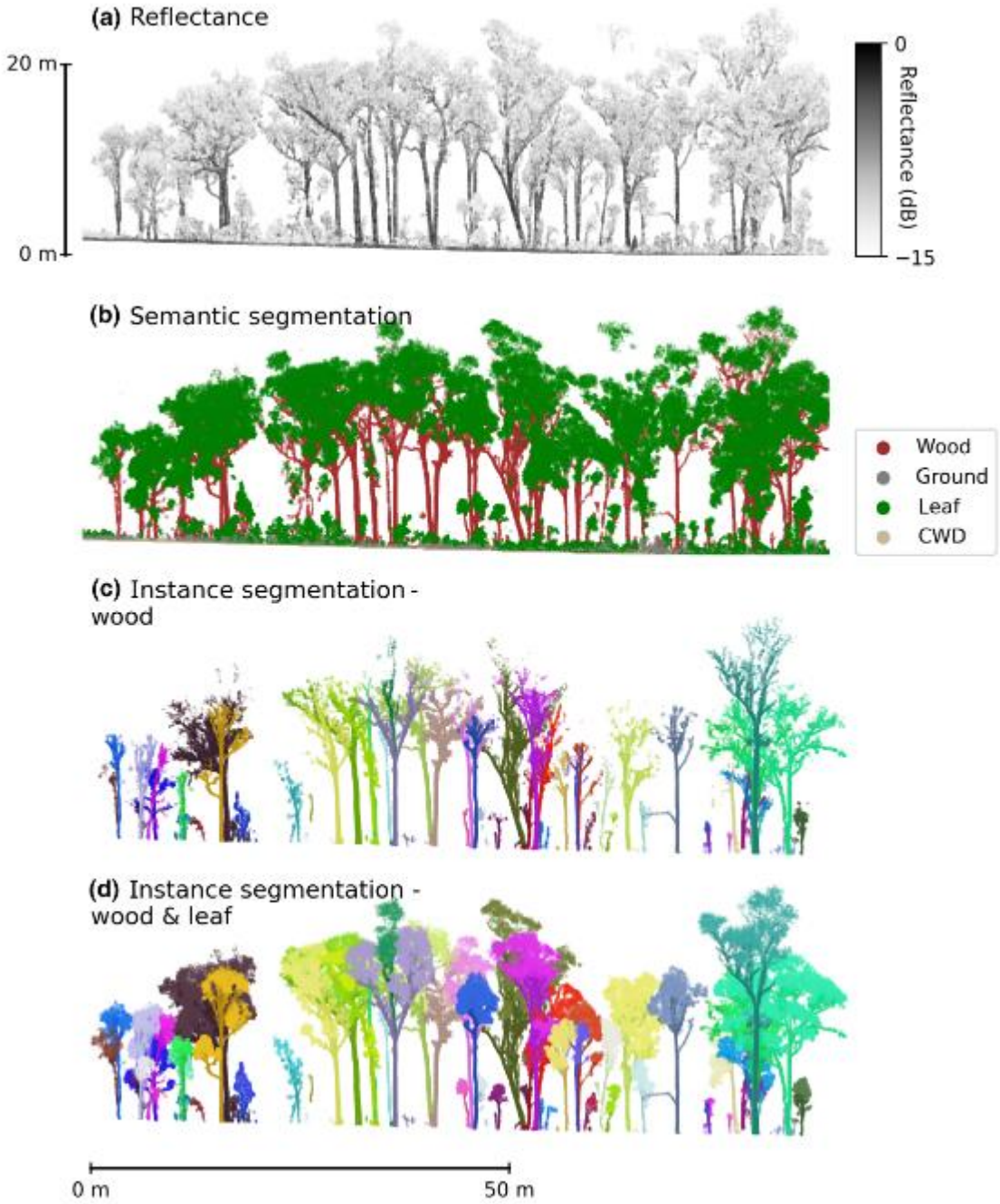

Figure A6. Illustrating semantic and instance segmentation of structures in a forest stand (Wilkes *et al.* 2023)

Recently, whole-tree segmentation workflows have been developed and provided as open-source software that present a two-stage pipeline for estimating tree inventory (e.g., Krisanski *et al.* 2021a & 2021b, Wilkes *et al*. 2023, Wielgosz *et al*. 2023). Krisanski *et al*. (2021a & 2021b) published a fully automated forest point cloud software program called the Forest Structural Complexity Tool (FSCT) aimed at extracting tree structural information from TLS, MLS and high-resolution ALS (https://github.com/SKrisanski/FSCT). This program is based upon the deep learning model Pointnet++ to semantically segment forest point clouds into four categories: terrain, vegetation, coarse woody debris and stems. Once

semantically segmented, the terrain, CWD and vegetation classes can be ignored when segmenting individual tree stems. The second phase of this workflow segments and quantifies individual tree stems (instance segmentation) using a hierarchical density-based spatial clustering algorithm before fitting a cylinder-orientated function to detect 'skeleton' stems and branches which are then aggregated. A similar tree level segmentation approach has also been achieved by Wilkes *et al.* (2023) through their open-source workflow TLS2trees. Tree attributes such as stem diameter, sweep and branching can then be automatically extracted. Wielgosz *et al.* (2023) improve the performance of the second phase, instance segmentation through optimizing the set of hyperparameters for different forest types. They present an automated approach based on a Bayesian strategy.

In a recent FWPA-funded study R. Jiang (in Stone & Hislop 2022), developed a method aimed at improving the accuracy of native forest tree height estimates derived from MLS Hovermap data through the application of FSCT based on tree-level-PAD profiles and was able to classify trees as either occurring in the canopy, sub canopy or as dead trees (stags) or those that had a significant dieback crown (dead top). This new workflow involved building separate tree-level PAD profiles for three categories (1) foliage only, (2) stem only and (3) foliage + stem. The plant area density at a given height (z) was estimated using the projection coverage of point clouds at that height level. Based on changes of PAD by height it was possible to identify height breaks that distinguished between upper and lower leaf density strata. Importantly, the application of this approach using dense ALS data could potentially improve the detection of dead and dying trees at both the site and landscape scale.

However, there are challenges to operationally implementing these workflows including lack of technical expertise, lack of large amounts of training data and the need for significant computational resources. For reference training data applied for the semantic and instance tree segmentation workflow, points are often just manually annotated in the software package, CloudCompare (e.g., Wilkes *et al.* 2021). However, several approaches such as synthetic data augmentation (e.g., Bryson *et al*. 2023, Perez-Carrasco *et al.* 2023) and transfer learning which fine-tunes a pre-trained model (e.g., Weinstein *et al.* 2020) are now being applied to reduce these impediments. In addition, several automated software programs have become available (e.g., Weinstein *et al.* 2020 - DeepForest open-source Python package for delineating tree crowns in RGB imagery, https://github.com/weecology/DeepForest or PyCrown for individual tree crown segmentation for LiDAR data) while Puliti *et al.* (2023) have developed an open source, benchmark dataset for semantic and instance segmentation of individual trees from dense airborne LiDAR data.

Adapting and improving these packages specifically for NSW native forests would significantly improve both the accuracy and efficiency of both ground-based and dense ALS LiDAR data collection compared to current manual methods. As with all supervised deep learning models, they require large training datasets and significant computing capacity, hence are likely only to be applied as area- or tree-based samples for supporting inference modelling with satellite data covering a much larger area of interest.

2.6 Application of smart phone LiDAR and camera sensors

Very recently, applications have been written for LiDAR-equipped mobile phones designed for tree stem detection and DBH estimates. Holcomb *et al.* 2023, for example, using an approach of raw depth imaging (i.e., stereo, dense image matching) that integrates stereo photogrammetry with the LiDAR data. Bobrowski *et al.* (2023) tested the LiDAR sensor in the iPad Pro 2020 which has been integrated high resolution cameras and a precise inertial measurement unit. Their results indicated that selected stems should be > 10 cm and distances < 2.0m from the stem is recommended. In addition, as with other LiDAR sensors, rough bark and irregular stem shapes also increased errors.

Interestingly, Zhao, *et al*. (2023) mentions that very recent published research shows one-stage models have started to overtake two-stage models in some computer vision tasks. Cao *et al.* (2023) for example, successfully applied modified YOLO v7 algorithm, within the deep learning framework PyTorch, to photos of trees located in varied and complex environments acquired by a Xiaomi smart phone. In this study YOLO v7 outperformed five other deep learning models.

In addition, the Swedish company Katam Technologies now provides a service that analyses data acquired by either sub-canopy UAVs or hand-held smart phones to provide measurements of tree stem diameters. While these phone applications have been shown to accurately estimate tree stem diameters, the sensors have a short range of only 3 – 5m.

2.7 Virtual Reality

Finally, current research is being undertaken to incorporate tree segmented MLS point clouds into a virtual reality (VR) environment for visual and on-screen measurements associated with tree inventory in native eucalypt forests (W. Chinthammit, University of Tasmania, & M. Bryson, University of Sydney, *pers comm*.). While this approach has been successfully achieved for plantations (D. Herries, Interpine Innovation NZ, *pers. comm*.) application in native forests is more challenging with increased densities of trees having irregular stem features and the presence of dense understorey vegetation. Preliminary analysis of Hovermap derived point cloud data collected in dense native eucalypt forest resulted in the successful detection of tree stems and estimation of DBH. It is hoped that this research will progress the accuracy and the operational adoption of MLS instruments such as the Hovermap for inventory assessment of monitoring plots in native forests.

References

Aalto I., Aalto, J., Hancock, S. *et al.* (2023) Quantifying the impact of management on the three-dimensional structure of boreal forests. *Forest Ecology and Management* **535:** Article 120885.

Arkin, J., Coops, N.C., Daniels, L.D. & Plowright, A. (2023) Canopy and surface estimations using RPAS and ground-point clouds. *Forestry: An International Journal of Forest Research* cpad020.

Atkins, J.W., Bohrer, G., Fahey, R. *et al*. (2018) Quantifying vegetation and canopy structural complexity from terrestrial LiDAR data using the Forestr R package. *Methods in Ecology and Evolution* **9:** 2057-2066.

Bakx, T.R.M., Koma, Z., Seijmonsbergen, A.C. & Kissling, W.D. (2019) Use and categorization of light detection and ranging metrics in avian diversity and species distribution research. *Diversity and Distributions* **25:** 1045-1059.

Banskota, A., Kayastha, N., Falkowski, M.J. *et al.* (2014) Forest monitoring using Landsat time series data: A review. *Canadian Journal of Remote Sensing* **40:** 362-384.

Bartels, S.F., Chen, H.Y.H., Wulder, M.A., White, J.C. (2016) Trends in post-disturbance recovery rates of Canada's forests following wildfire and harvest. *Forest Ecology & Management* **361:** 194-207.

Besl, P.J. & McKay, N.D. (1992) A method for registration of 3-D shapes. *IEEE Transactions on Pattern Analysis and Machine Intelligence* **14:** 239-256.

Bobrowski, R., Winczek, M., Zieba-Kulawik, K. & Wezyk, P. (2023) Best practices to use the iPad Pro LiDAR for some procedures of data acquisition in the urban forest. *Urban Forestry & Urban Greening* **79:** Article 127815.

Bolton, D.K., Coops, N.C. & Wulder, M.A. (2015) Characterizing residual structure and forest structure following high-severity fire in the western boreal of Canada using Landsat time series and airborne LiDAR data. *Remote Sensing of Environment* **163:** 48-60.

Braga, J.R.G., Peripato, V., Dal'Agnol da Silva, R. & Ferreira, M.P. (2020) Tree crown delineation algorithm based on a convolutional neural network. *Remote Sensing* **12:** Article 1288.

Bryson, M., Wang, F. & Allworth, J. (2023) Using synthetic tree data in deep learning-based tree segmentation using LiDAR point clouds. *Remote Sensing* **15:** Article 2380.

Campbell, M.J., Dennison, P.E., Hudak, A.T. *et al.* (2018) Quantifying understorey vegetation density using small-footprint airborne LiDAR. *Remote Sensing of Environment* **215:** 330-342.

Cao, L., Zheng, X. & Fang, L. (2023) The semantic segmentation of standing tree images based on the Yolo v7 deep learning algorithm. E*lectronics* **12:** Article 929.

Carrasco, L., Giam, X., Papes, M. & Kimberly, S.S. (2019) Metrics of LiDAR-derived 3D vegetation structure reveal contrasting effects of horizontal and vertical forest heterogeneity on bird species richness. *Remote Sensing* **11:** Article 743.

Casas, A., Garcia, M., Siegal, R.B. *et al.* (2016) Burned forest characterization at single-tree level with airborne laser scanning for assessing wildlife habitat. *Remote Sensing of Environment* **175:** 231-241.

Cessna, J., Alonzo, M.G., Foster, A.C. (2021) Mapping boreal forest spruce beetle health status at individual crown scale using fused spectral and structural data. *Forests* **12:** Article 1145.

Chang, L., Fan, H., Zhu, N. & Dong, Z. (2022) A two-stage approach for individual tree segmentation from TLS point clouds. *IEEE Journal of Selected Topics in Applied Earth Observation and Remote Sensing* **15:** 8682 – 8693.

Chen, Q., Baldocchi, D., Gong, P. & Kelly, M. (2006) Isolating individual trees in savanna woodland using small footprint LiDAR data. *Photogrammetric Engineering & Remote Sensing* **72:** 923-932.

Chirici, G., Giannetti, F., Mazza, E. *et al.* (2020) Monitoring clearcutting and subsequent rapid recovery in Mediterranean coppice forests with Landsat time series. *Annals of Forest Science* **77:** Article 40.

Clawges, R., Vierling, K., Vierling, L. & Rowell, E. (2008) The use of airborne LiDAR to assess avian species diversity, density, and occurrence in a pine/aspen forest. *Remote Sensing of Environment* **112:** 2064 – 2073.

de Almeida, D.R., Stark, S.C., Shao, G. *et al*. (2019) Optimizing the remote detection of tropical rainforest structure with airborne LiDAR: leaf area profile sensitivity to pulse density and spatial sampling. *Remote Sensing* **11:** Article 92.

de Almeida, D.R., Zambrano, A.M., Broadbent, E.N. *et al.* (2020) Detecting successional changes in tropical forest structure using GatorEye drone-borne LiDAR. *Biotropica* **52:** 1155-1167.

de Conto, T., Olofsson, K., Bastos Gorgens, E. *et al.* (2017) Performance of stem denoising and stem modelling algorithms on single tree point clouds from terrestrial laser scanning. *Computers and Electronics in Agriculture* **143:** 165-176.

de Conto, T. (2019) TreeLS: Terrestrial point cloud processing of forest data. R package version 1.0 https://github.com/tiagodc/TreeLS.

de Paula Pires, R., Olofsson, K., Persson, H.J. *et al.* (2022) Individual tree detection and estimation of stem attributes with mobile laser scanning along boreal forest roads. *ISPRS Journal of Photogrammetry and Remote Sensing* **187:** 211-224.

Ehbrecht, M., Schall, P., Juchheim, J. *et al.* (2016) Effective number of layers: A new measure for quantifying three-dimensional stand structure based on sampling with terrestrial LiDAR. *Forest Ecology and Management* **380:** 212-223.

Estrada, J.S., Fuentes, A. Reszka, P. & Cheein, F.A. (2023) Machine learning assisted remote forestry health assessment: a comprehensive state of the art review. *Frontiers in Plant Science* **14:** Article 1139232.

Fassnacht, F.E., Mullerova, J., Conti, L. *et al.* (2022) About the link between biodiversity and spectral variation. (2022) *Applied Vegetation Science* **22:** Article 12643.

Feret, J.-B., & de Boissieu, F. (2019) biodivMapr: An r package for α- and β-diversity mapping using remotely sensed images. *Methods in Ecology and Evolution* **11:** 64-70.

Fernandez-Guisuraga, J.M., Suarez-Seoane, S, & Calvo, L. (2022) Radar and multispectral remote sensing data accurately estimate vegetation vertical structure diversity as a fire resilience indicator. *Remote Sensing in Ecology and Conservation* **9:** 117-132.

Ferrara, C., Puletti, N., Guasti, M. & Scotti, R. (2023) Mapping understorey vegetation density in Mediterranean forests: Insights from airborne and terrestrial laser scanning integration. *Sensors* **23:** Article 511.

Ferreira, M.P., Wagner, F.H., Aragao, L.E.O.C., *et al.* (2019) Tree species classification in tropical forests using visible to shortwave infrared WorldView-3 images and textural analysis. *ISPRS Journal of Photogrammetry and Remote Sensing* **149:** 119-131.

Fisher, A., Armstron, J., Goodwin, N. & Scarth, P. (2020) Modelling canopy gap probability, foliage projective cover and crown projective cover from airborne LiDAR metrics in Australian forests and woodlands. *Remote Sensing of Environment* **237:** Article 111520.

Froidevaux, J., Jones, G. & Bollman, K. (2016) From field surveys to LiDAR: Shining a light on how bats respond to forest structure. *Remote Sensing of Environment* **175:** 242-250.

Gelabert, P.J., Montealegre, A.L., Lamelas, M.T. & Domingo, D. (2020) Forest structural diversity characterization in Mediterranean landscapes affected by fires using Airborne Laser Scanning data. *GIScience & Remote Sensing* **57:** 497-509.

Gibson, R., Danaher, T., Hehir, W. & Collins, L. (2020) A remote sensing approach to mapping fire severity in south-eastern Australia using sentinel-2 and random forest. *Remote Sensing of Environment* **240:** Article 111702.

Gibson, R.K. & Hislop, S. (2022) Signs of resilience in resprouting *Eucalyptus* forests, but areas of concern: 1 year of post-fire recovery from Australia's Black Summer of 2019-2020. *International Journal of Wildland Fire* **31:** 545-557.

Gibson, R. K., White, L. A., Hislop, S., Nolan, R., and Dorrough, J. 2022. The Post-Fire Stability Index; a New Approach to Monitoring Post-Fire Recovery by Satellite Imagery. *Remote Sensing of Environment* 280 (October): 113151. https://doi.org/10.1016/j.rse.2022.113151.

Grondin, V., Pomerleau, F. & Giguere, P. (2022) *Training deep learning algorithms on synthetic forest images for tree detection*. ICRA 2022 Workshop in Innovation in Forestry Robotics: Research and Industry Adoption.

Haywood, A. & Stone, C. (2011a) Using airborne laser scanning data to estimate structural attributes of natural eucalypt regrowth forests. *Australian Forestry* **74:** 4-12.

Haywood, A. & Stone, C. (2011b) Mapping eucalypt forest susceptible to dieback associated with bell miners (*Manorina melanophys*) using laser scanning SPOT 5 and ancillary topographical data. *Ecological Modelling* **222:** 1174-1184

Hislop, S., Stone, C., Gibson, R.K. et al. (2023) Using dense Sentinel-2 time series to explore combined fire and drought impacts in eucalypt forests. *Frontiers in Forests and Global Change* **6:** Article 1018936.

Hislop, S., Stone, C., Samuel, J., Kathuria, A., Alaibakhsh, M. and Nguyen, T.H., (2024) Estimating the extent of selective timber harvesting in private native eucalypt forests with multi-temporal LiDAR. *Australian Forestry* **86**:3-4, 152-160

Hermosilla, T., Wulder, M.A., White, J.C. *et al*. (2015) Regional detection, characterization, and attribution of annual forest change from 1984 to 2012 using Landsat-derived time-series metrics. *Remote Sensing* of *Environment* **170:** 121 – 132.

Hillman, S., Wallace, L., Lucieer, A., *et al.* (2021) A comparison of terrestrial and UAS sensors for measuring fuel hazard in a dry sclerophyll forest. *International Journal of Applied Earth Observations and Geoinformation* **95:** Article 102261.

Hirschmugl, M., Lippl, F. & Sobe, C. (2023) Assessing the vertical structure of forests using airborne and spaceborne LiDAR data in the Austrian Alps. *Remote Sensing* **15:** Article 664.

Holcomb, A., Tong, L. & Srinivasan, K. (2023) Robust single-image tree diameter estimation with mobile phones. *Remote Sensing* **15:** Article 772.

Hyyppä, E., Kukko A., Kaijaluoto, R. *et al.* (2020) Accurate derivation of stem curve and volume using backpack mobile laser scanning. *ISPRS Journal of Photogrammetry and Remote Sensing* **161:** 246-262.

Ireland, A.W., Smith, F.G.F., Jaffe, B.D. *et al*. (2021) Field experiment demonstrates the potential utility of satellite-derived reflectance indices for monitoring regeneration of boreal forest communities. *Trees, Forests and People* **6:** Article 100145.

Isenburg, M. (2013). LASzip: lossless compression of LiDAR data. *Photogrammetric engineering and remote sensing*, *79*(2), 209-217.

Iqbal, I.A., Osborn, J., Stone, C. & Lucieer, A. (2021) A comparison of ALS and dense photogrammetric point clouds for individual tree detection in Radiata pine plantations. *Remote Sensing* **13:** Article 3536.

Jarron, L.R., Coops, N.C., MacKenzie, W.H. *et al.* (2020) Detection of sub-canopy forest structure using airborne LiDAR. *Remote Sensing of Environment* **244:** Article 111770.

Jaskierniak, D., Lane, N.J., Robinson, A. & Lucieer, A. (2011) Extracting LiDAR indices to characterise multilayered forest structure using mixture distribution functions. *Remote Sensing of Environment* **115:** 573-583.

Jiang, R. (2020) *Using LiDAR for landscape mapping of potential habitat for the critically endangered Leadbeaters possum*. PhD Thesis. University of Melbourne.

Jiang, X., Wu, Z., Han, S. *et al.* (2023) A multi-scale approach to detecting standing dead trees in UAV RGB images based on improved faster R-CNN. *PLoS ONE* **18:** Article 0281084.

Jutras-Perreault, M.-C., Gobakken, T., Naesset, E. & Orka, H.O. (2023) Comparison of different remotely sensed data sources for detection of presence of standing dead trees using a tree-based approach. *Remote Sensing* **15:** Article 2223.

Kamoske, A.G., Dahlin, K.M., Stark, S.C., & Serbin, S.P. (2019) Leaf area density from airborne LiDAR: Comparing sensors and resolutions in a forest ecosystem. *Forest Ecology and Management* **433:** 364-375.

Karna, Y.K., Penman, T.D., Aponte, C. *et al.* (2020) Persistent changes in the horizontal and vertical canopy structure of fire-tolerant forests after severe fire as Quantified using multi-temporal airborne LiDAR data. *Forest Ecology and Management* **472:** Article 118255.

Kane, V.R., McGaughey, R.J., Bakker, J.D. (2010) Comparisons between field- and LiDAR-based measures of stand structural complexity. *Canadian Journal of Forest Research* **40:** 761-773.

Kanerva, H., Honkavaara, E., Nasi, R. *et al.* (2022) Estimating tree health decline caused by Ips typographus L. from UAS RGB images using a deep one-stage object detection neural network. *Remote Sensing* **14:** Article 6257.

Kathuria, A. (2023) Sampling design for forest resource assessment of private native forest, Northern NSW. Technical report for NSW Local Land Services. Available at https://dx.doi.org/10.13140/RG.2.2.17698.20166

Ke, Y. & Quackenbush, L.J. (2011) A comparison of three methods for automatic tree detection and delineation from high spatial resolution imagery. *International Journal of Remote Sensing* **32:** 3625-3647.

Kennedy, R.E., Yang, Z., & Cohen, W.B. (2010) Detecting trends in forest disturbance and recovery using yearly Landsat time series 1. LandTrendr – temporal segmentation algorithms. *Remote Sensing of Environment* **114:** 2897-2910.

Krisanski, S., Taskhiri, M.S. & Gonzalez Aracil, S. (2021a) Sensor agnostic semantic segmentation of structurally diverse and complex forest point clouds using deep learning. *Remote Sensing* **13:** Article 1413.

Krisanski, S., Taskhiri, M.S., Gonzalez Aracil, S. *et al.* (2021b) Forest structural complexity tool – An open source, fully-automated tool for measuring forest point clouds. *Remote Sensing* **13:** Article 4677.

Lee, Y., Woo, H. & Lee J-S. (2022) Forest inventory assessment using integrated light detection and ranging (LiDAR) systems: Merged point cloud of airborne and mobile laser scanning systems. *Sensors and Materials* **34:** Article 4583.

Listopad, C.M., Masters, R.E., Drake, j., *et al.* (2015) Structural diversity indices based on airborne LiDAR as ecological indicators for managing highly dynamic landscapes. *Ecological Indicators* **57:** 268-279.

Mathes, T., Seidel, D., Haberie, K-H., *et al.* (2023) What are we missing? Occlusion in laser scanning point clouds and its impact on detection of single-tree morphologies and stand structure variables. *Remote Sensing* **15:** Article 450.

Mäyra, J., Keski-Saari, S., Kivinen, S. *et al.* (2021) Tree species classification from airborne hyperspectral and LiDAR data using 3D convolutional neural networks. *Remote Sensing of Environment* **256:** Article 112322

McGaughey, R. (2021) FUSION/LDV: *Software for LiDAR data analysis and visualization.* Version 4.40. Seattle, W.A.: U.S. department of Agriculture, Forest Service, Pacific Northwest Research Station.

Meiforth, J.J., Buddenbaum, H., Hill, J. *et al*. (2020) Stress detection in New Zealand Kauri canopies with WorldView-2 satellite and LiDAR data*. Remote Sensing* **12:** Article 1906.

Mellor A, Boukir S, Haywood A, Jones S. 2015. Exploring issues of training data imbalance and mislabelling on random forest performance for large area land cover classification using the ensemble margin. *ISPRS Journal of Photogrammetry and Remote Sensing*. **105:** 155–168.

Miltiadou, M., Campbell, N.D.F., Gonzalez Aracil, S., *et al.* (2018) Detection of dead standing *Eucalyptus camaldulensis* without tree delineation for managing biodiversity in native Australian forest. *International Journal of Applied Earth Observation & Geoinformation* **67:** 135-147.

Miltiadou, M., Agapiou, A., Gonzalez Aracil, S. & Hadjimitsis, D.G. (2020) Detecting dead standing eucalypt trees from voxelised full-waveform LiDAR using multi-scale 3D windows for tackling height and size variations. *Forests* **11:** Article 161.

Moran, C.J., Rowell, E.M. & Seielstad, C.A. (2018) A data-driven framework to identify and compare forest structure classes using LiDAR. *Remote Sensing of Environment* **211:** 154-166.

Moudry, V., Cord, A.F., Gabor, L., *et al.* (2023) Vegetation structure derived from airborne laser scanning to assess species distribution and habitat suitability: The way forward. *Diversity and Distribution* **29:** 39-50.

Murfitt, J., He, Y., Yang, J. *et al.* (2016) Ash decline assessment in Emerald Ash Borer infested natural forests using high spatial resolution images. *Remote Sensing* **8:** Article 256.

Olofsson, K., Holmgren, J. & Olsson, H. (2014) Tree stem and height measurements using terrestrial laser scanning and the RANSAC algorithm. *Remote Sensing* **6:** 4323-4344.

Owens, C.J., Kavanagh, R.P., & Bruce, E. (2014) Remote sensing can locate and assess the changing abundance of hollow-bearing trees for wildlife in Australian native forests. *Wildlife Research* **41:** 703-716.

Pearse, G.D., Watt, M.S., Dash, J.P., *et al.* (2018) Comparison of models describing forest inventory attributes using standard and voxel-based LiDAR predictors across a range of pulse densities. *International Journal of Applied Earth Observation Geoinformation* **78:** 341-351.

Perez-Carrasco, M., Karelovic, B. & Molina, R. (2023) Precision silviculture: use of UAVs and comparison of deep learning models for the identification and segmentation of crowns in pine crops. *International Journal of Digital Earth* **15:** 2223-2238.

Petras, V., Petrasova, A., McCarter, J.B., *et al.* (2023) Point density variations in airborne LiDAR point clouds. *Sensors* **23:** Article 1593.

Puletti, N., Galluzzi, M., Grotti, M. & Ferrara, C. (2021) Characterizing subcanopy structure of Mediterranean forests by terrestrial laser scanning data. *Remote Sensing Applications: Society and Environment*. **24:** Article 100620.

Puletti, N., Castronuovo, R. & Ferrara, C. (2023) Crossing 3D Forest: An R package for evaluating empty space structure in forest ecosystems. *Research & Reviews: Journal of Ecology and Environmental Sciences* **11**: 001.

Puliti, S., Pearce, G., Surovy, P. *et al.* (2023) FOR-instance: a UAV laser scanning benchmark dataset for semantic and instance segmentation of individual trees. https://doi.org/10.5281/zenodo.8287792).

Raumonen, P., Kaasalainen, M., Akerblom, M. *et al.* (2013) Fast automatic precision tree models from terrestrial laser scanner data. *Remote Sensing* **5:** 491-520.

Roussel, J-R., Auty, D. Coops, N.C., *et al.* (2020) lidR: An R package for analysis of airborne laser scanning (ALS) data. *Remote Sensing of Environment* **251:** Article 112061.

Sani-Mohammed, A., Yao, W. & Heurich, M. (2022) Instance segmentation of standing dead trees in dense forest from imagery using deep learning. *ISPRS Open Journal of Photogrammetry and Remote Sensing***. 6:** Article 100024.

Shang, X. & Chisholm, L.A. (2013) Classification of Australian native forest species using hyperspectral remote sensing and machine-learning classification algorithms. *IEEE Journal of Selected Topics in Applied Earth Observations and Remote Sensing* **7:** 2481-2489.

Silva, C.A., Hudak, A.T. & Vierling, L.A. (2021) TREETOP: A Shiny-based application and R package for extracting forest information from LiDAR data for ecologists and conservationists. *Methos in Ecology and Evolution* **13:** 1164-1176.

Silver, M.J. & Carnegie, A.J. (2017) *An independent review of Bell Miner Associated Dieback*. Final Report. NSW Office of Environment and Heritage.

Sothe, C., De Almeida, C.M., Schimalski, M.B., *et al.* (2020) Comparative performance of convolutional neural network, weighted and conventional support vector machine and random forest for classifying tree species using hyperspectral and photogrammetric data. *GIScience & Remote Sensing* **57:** 369-394.

Stone, C. & Hislop, S. (Editors) (2022) Characterising native forest structure from co-incident terrestrial and airborne LiDAR. FWPA PNC546-2021 Final Report. https://fwpa.com.au/characterising-native-forest-structure-from-co-incident-terrestrial-and-airborne-LiDAR

Straker, A., Puliti, S., Breidenbach, J., *et al.* (2023) Instance segmentation of individual tree crowns with YOLOv5: A comparison of approaches using ForInstance benchmark LiDAR dataset. *ISPRS Open Journal of Photogrammetry and Remote Sensing* **9:** Article 100045.

Sylain, J.-D., Droplet, G. & Brown, N. (2019) Mapping dead forest cover using a deep convolutional neural network and digital aerial photography. *ISPRS Journal of Photogrammetry and Remote Sensing* **156:** 14-26.

Tang, J., Chen, Y., Kukko, A., *et al.* (2015) SLAM-aided stem mapping for forest inventory with small-footprint mobile LiDAR. *Forests* **6:** 4588-4606.

Torresan, C., Corona, P., Scrinzi, G. & Marsal, J.V. (2016) Using classification trees to predict forest structure types from LiDAR data. *Annals of Forest Research* **59:** 281-298.

Van Ewijk, K.Y., Treitz, P.M., & Scott, N.A. (2011) Characterising forest succession in Central Ontario using LiDAR-derived indices. *Photogrammetric Engineering & Remote Sensing* **77:** 261 – 269.

Van Lier, O.R., Luther, J.E., White, J.C., *et al.* (2021) Effect of scan angle on ALS metrics and area-based predictions of forest attributes for balsam fir dominated stands. *Forestry: An International Journal of Forest Research* **6:** 1-24.

Vatandaslar, C., Seki, M. & Zeybek, M. (2023) Assessing the potential of mobile laser scanning for stand-level forest inventories in near-natural forests. *Forestry: An International Journal of Forest Research* **96:** 448-464.

Verbesselt, J., Hyndman, R., Newham, G. & Culvenor, D. (2020) Detecting trend and seasonal changes in satellites image time series. *Remote Sensing of Environment* **114:** 106-115.

Vogeler, J.C., Hudak, A.T., Vierling, L.A., *et al.* (2014) Terrain and vegetation structural influences on local avian species richness in two-mixed-conifer forests. *Remote Sensing of Environment* **147:** 13-22.

Weinstein, B.G., Marconi, S., Aubry-Kientz, M., *et al.* (2020) DeepForest: A Python package for RGB deep learning tree crown delineation. *Methods in Ecology and Evolution* **11:** 1743-1751.

White, J.C., Wulder, M.A., Varhola, A., *et al*. (2013) Best Practices Guide for Generating Forest Inventory Attributes from Airborne Laser Scanning Data Using the Area-based Approach. *Information Report FI0-X-10*. Victoria, BC, Canada: Canadian Forest Service.

White, J.C., Wulder, M.A., Hermosilla, T. *et al.* (2017) A nationwide annual characterization of 25 years of forest disturbance and recovery for Canada using Landsat time series. *Remote Sensing Environment* **194:** 303-321.

White, J.C., Saarinen, N., Wulder, M.A. *et al.* (2019) Assessing spectral measures of post-harvest forest recovery with field plot data. *International Journal of Applied Earth Observation & Geoinformation* **80:** 102-114.

White, J.C., Hermosilla, T., Wulder, M.A. & Coops, N.C. (2022) Mapping, validating, and interpreting spatio-temporal trends in post-disturbance forest recovery. *Remote Sensing of Environment* **271:** Article 112904.

Wielgosz, M., Puliti, S., Wilkes, P. & Astrup, R. (2023) Point2Tree(P2T) – Framework for parameter tuning of semantic and instance segmentation used with mobile laser scanning data in coniferous forest. *Remote Sensing* **15:** Article 3737.

Wilkes, P., Jones, S.D., Suarez, L., *et al.* (2016) Using discrete-return airborne laser scanning to quantify number of canopy strata across diverse forest types. *Methods in Ecology and Evolution* **7:** 700-712.

Wilkes, P., Disney, M., Armston, J., *et al.* (2023) TLS2trees: A scalable tree segmentation pipeline for TLS data. *Methods in Ecology and Evolution*.

Windrim, L. & Bryson, M. (2020) Detection, segmentation, and model fitting of individual tree stems from airborne laser scanning of forests using deep learning. *Remote Sensing* **12:** Article 1469.

Yel, S.G. & Gormus, E.T. (2023) Exploiting hyperspectral and multispectral images in the detection of tree species: A review. *Frontiers in Remote Sensing* DOI 10.3389/frsen.2023.1136289.

Zhang, J., Zhao, X., Chen, Z. & Lu, Z. (2019) A review of deep learning-based semantic segmentation for point cloud. *IEEE Access* **7:** 179118-179133.

Zhang, Z., Cao, L. & She, G. (2017) Estimating forest structural parameters using canopy metrics derived from airborne LiDAR data in subtropical forests. *Remote Sensing* **9:** Article 990.

Zhao, H., Morgenroth, J., Pearse, G. & Schindler, J. (2023) A systematic review of individual tree crown detection and delineation with convolutional Neural Networks. *Current Forestry Reports* **9:** 149-170.